

RI 9581

RI 9581

REPORT OF INVESTIGATIONS/1996

For Reference

Not to be taken from this room

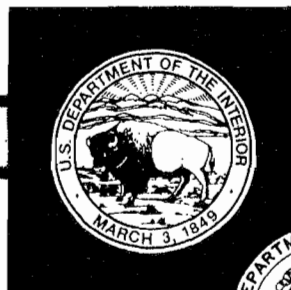
LIBRARY
SPOKANE RESEARCH CENTER
RECEIVED

JAN 25 1996

U.S. BUREAU OF MINES
E. 315 MONTGOMERY AVE.
SPOKANE, WA 99207

Using a Computer Spreadsheet To Characterize Rock Masses Prior to Subsidence Prediction and Numerical Analysis

UNITED STATES DEPARTMENT OF THE INTERIOR



BUREAU OF MINES

*U.S. Department of the Interior
Mission Statement*

As the Nation's principal conservation agency, the Department of the Interior has responsibility for most of our nationally-owned public lands and natural resources. This includes fostering sound use of our land and water resources; protecting our fish, wildlife, and biological diversity; preserving the environmental and cultural values of our national parks and historical places; and providing for the enjoyment of life through outdoor recreation. The Department assesses our energy and mineral resources and works to ensure that their development is in the best interests of all our people by encouraging stewardship and citizen participation in their care. The Department also has a major responsibility for American Indian reservation communities and for people who live in island territories under U.S. administration.

Report of Investigations 9581

**Using a Computer Spreadsheet
To Characterize Rock Masses
Prior to Subsidence Prediction
and Numerical Analysis**

By K. M. O'Connor, J. A. Siekmeier, and L. R. Powell

**UNITED STATES DEPARTMENT OF THE INTERIOR
Bruce Babbitt, Secretary**

**BUREAU OF MINES
Rhea Lydia Graham, Director**

International Standard Serial Number
ISSN 1066-5552

CONTENTS

	<i>Page</i>
Abstract	1
Introduction	2
Rock mass classification applied to high-extraction coal mines	3
Selection of a classification system	4
Classification of individual beds	4
Bending stiffness of individual beds	4
Definition of a geostructural element	4
Bending stiffness of a laminated beam	5
Bridging potential of a laminated beam	6
Validation of stiffness discontinuities	6
Rock mass classification spreadsheet	6
Laboratory properties database	7
Rock mass rating criteria	10
Rock mass stiffness and deflection calculation	10
Assumptions and interactive parameters	10
Stratigraphy and rock mass stiffness	10
Bending stiffness and deflection of individual beds	11
Transformed section and average deformation modulus	11
Bending stiffness and bridging potential of laminated beam	12
Laminated beam analysis macro	12
Parameter studies for the laminated beam deflection model	12
Effect of assumed laminated beam thickness	12
Effect of mined panel width	12
Effect of assumed span angle	13
Effect of changing overburden geology	13
Comparison of monitored mine sites	13
Strata identification	14
Comparison with conventional subsidence parameters	14
Observations based on comparisons	15
Conclusions	15
Summary	16
References	16
Appendix A.—Data and analysis of instrumented sites	37
Appendix B.—Rationale for utilizing simple beam model	62
Appendix C.—Abbreviations and symbols used in the report	69

ILLUSTRATIONS

1. Horizontal discontinuities defined by bending stiffness profile	20
2. Horizontal discontinuities compared with TDR measurements	20
3. Boundaries of geostructural elements defined by predicted horizontal discontinuities	21
4. Transformed cross section of equivalent elastic beam	21
5. Conceptual model of overburden response to high-extraction coal mining	22
6. Flowchart for spreadsheet	22
7. Rock properties lookup table	23
8. Rock mass rating criteria	24
9. Core description of individual beds	25
10. Adjusted rock mass rating of individual beds	26
11. Stiffness and deflection of individual beds	27
12. Transformed section and modulus of laminated beam	28
13. Stiffness and bridging potential of laminated beam	29

ILLUSTRATIONS—Continued

	<i>Page</i>
14. Logic of beam analysis macro	30
15. Implementation of beam analysis macro	31
16. Maximum beam deflection for all possible beam thicknesses	31
17. Effect of panel width on maximum beam deflection	32
18. Maximum deflection as a function of panel width to panel depth for a beam of maximum possible thickness	32
19. Effect of span angle on maximum beam deflection	33
20. Effect of stratigraphy on maximum beam deflection	33
21. Map showing site locations	34
22. Summary of number of strata identified in core logs	35
23. Empirical subsidence ratio versus panel width to panel depth	35
24. Analytical bridging potential versus panel width to panel depth	36
A-1. Consol Rend Lake Mine	39
A-2. Old Ben No. 21 Mine	42
A-3. Old Ben No. 24 Mine panel 1 site	45
A-4. Old Ben No. 24 Mine panel 2 site	48
A-5. Old Ben No. 24 Mine North Marcum site	51
A-6. Old Ben No. 25 Mine	54
A-7. Galatia Mine	57
A-8. Freeman Orient Mine	60
B-1. Elastic beam	66
B-2. Elastic beam on Winkler foundation	66
B-3. Elastic half-space	67
B-4. Comparison of beam deflection profiles	68

TABLES

1. Parameters for rock mass rating	4
2. Angles of internal friction and break, from literature	5
3. Laboratory rock properties	7
4. Summary of instrumented panels	13
5. Laminated beam data	14

UNIT OF MEASURE ABBREVIATIONS USED IN THIS REPORT

deg	degree	MN	meganewton
kg/m ³	kilogram per cubic meter	MN•m	meganewton meter
km	kilometer	MPa	megapascal
m	meter	MPa•m ⁴	megapascal quartic meter
m ²	square meter	MPa•m ⁴ /m	megapascal quartic meter per meter
m ⁴	quartic meter	N•m	newton meter
m/d	meter per day	N/m	newton per meter
m/m	meter per meter	(N/m)/m	newton per meter per meter
m/s ²	meter per second squared		

U.S. Customary Units

lb/ft ³	pound per cubic foot	psi	pound per square inch
--------------------	----------------------	-----	-----------------------

Reference to specific products does not imply endorsement by the U.S. Bureau of Mines.

Disclaimer of Liability

The U.S. Bureau of Mines expressly declares that there are no warranties expressed or implied that apply to the software described herein. By acceptance and use of said software, which is conveyed to the user without consideration by the Bureau of Mines, the user hereof expressly waives any and all claims for damage and/or suits for or by reason of personal injury, or property damage, including special, consequential, or similar damages arising out of or in any way connected with the use of the software described herein.

USING A COMPUTER SPREADSHEET TO CHARACTERIZE ROCK MASSES PRIOR TO SUBSIDENCE PREDICTION AND NUMERICAL ANALYSIS

By K. M. O'Connor,¹ J. A. Siekmeier,¹ and L. R. Powell²

ABSTRACT

Variations in overburden geology must be considered in applying subsidence prediction methodologies developed by the U.S. Bureau of Mines (USBM). To characterize rock mass overlying high-extraction coal mines, the USBM utilizes a computer spreadsheet program and modified Rock Mass Rating (RMR) system. The spreadsheet calculates an RMR based on a bed's engineering properties determined from core logs and laboratory tests. An in situ deformation modulus and a bending stiffness are computed for each bed. Stiffness-versus-depth plots identify groups of beds with similar stiffness. Large variations in stiffness between adjacent beds are considered significant horizontal discontinuities where slip is likely. Time domain reflectometry (TDR) is used to verify this hypothesis by measuring shear displacement along such discontinuities. A model of the overburden is built by assuming that a near-surface laminated beam exists above a transition zone in which large plastic slip occurs along horizontal discontinuities. Increasingly thicker groups of beds are modeled to determine the most probable beam thickness based on a comparison with measured deflection profiles. The inverse of maximum beam deflection is an index parameter known as "bridging potential," a single value that incorporates both overburden geology and mine geometry.

¹Civil engineer.

²Supervisory geologist.

Twin Cities Research Center, U.S. Bureau of Mines, Minneapolis, MN.

INTRODUCTION

The U.S. Bureau of Mines (USBM) undertook the work described in this report as part of an effort to better quantify rock mass parameters that influence subsidence caused by past and current mine development. Consideration of the consequences of mining is becoming increasingly important as the need for more energy and minerals conflicts with the land use needs of an expanding, environmentally conscious population. Accurate subsidence prediction methods have been developed that allow greater resource utilization by predicting impacts and allowing appropriate land uses to be found or mining plans to be adjusted under sensitive surface areas. The surface effects of subsidence can be minimized on natural and constructed facilities by implementing proper land use planning and mitigation measures.

Generally, the knowledge for selecting the proper mitigation measures is gained from precalculation of ground movements using empirical models. To be truly predictive, these empirical models cannot rely exclusively on the backcalculation of the input variables based on subsidence profile measurements at nearby sites. Rather, it should be possible to relate the input parameters of these models to the geologic structure and properties of the overburden. This is important because distinct geologic differences can be identified between and within the major coalfields of the United States (30, 56).³ Site-specific data are important, and just as important is a method to systematically and quantitatively relate the data to an empirical model. Thus, the methodology described in this report was developed to provide a tool for quantifying geologic differences that affect overburden response to mining and to promote the evolution of prediction techniques beyond empirical models.

Stratigraphic variation in the coal measure rocks of the United States is the result of depositional environments of ancient coal-forming swamps. Conditions were constantly changing in the ancient fluvial-deltaic system in response to tectonic downwarping and differential compaction of sediments, causing vertical and lateral facies changes. This controlled the thickness and distribution of units with similar lithologic composition. The boundary between such areas is often a zone of abrupt lithologic change occurring over a relatively short distance.

Such depositional and structural conditions influence the mechanical characteristics of the overburden, which subsequently dictate the characteristics of the subsidence trough developed on the surface over high-extraction mines. The geotechnical properties of rock masses that

influence their behavior during subsidence events are density; compressive, tensile, cohesive, and shear strength; bulk, Young's, and shear modulus; Poisson's ratio; and slake durability (25). These properties are controlled by the composition, texture, cement, and structure of the rock mass. In addition, rock masses derive much of their strength from confining stresses and the attendant increases in the frictional resistance across bedding, stratification, joints, and faults (26).

A review of the literature indicates that many geological factors have been identified as influencing ground movements associated with subsidence (33, 41, 70). The overall rock mass strength has been shown to influence the rate, duration, magnitude, and extent of subsidence. Analytical, graphical, empirical, and numerical subsidence models contain variables that require rock mass conditions to be characterized. Allen (2) suggested that the effect of geological differences should be determined by collecting data in different geological settings, then characterizing subsidence mechanisms based on geological and surface movement data. Recently, a number of field measurement programs were conducted as part of the Illinois Mine Subsidence Research Program (59) to characterize the process of subsurface caving, fracturing, and surface subsidence over high-extraction coal mines.

Subsidence is a process in which bending, fracturing, shearing, and caving occur above a mined-out panel and progress to the surface. The creation of an underground void by mining disturbs the natural equilibrium of the rock strata, which results in a redistribution of rock stresses. Strata immediately overlying the void collapse into the void either as slabs or blocks with dimensions controlled by preexisting and mining induced fractures. The height and geometry of collapse are controlled by the mechanism of block formation, which is controlled by the lithology, macrostructure, and tensile and shear strengths of the rock strata and preexisting fractures (26, 33, 35, 57, 60, 70, 89). At some height above the void, caving stops because of bulking of the caved material that begins to accept the weight of the overburden and is recompacted. Strata above the caved zone bend rather than cave, causing fracturing, bed shearing, and bed separation. The result is a combination of bending, fracturing, shearing, separating, caving, and heaving, all of which are controlled by the overburden rock mass characteristics as well as the void's original width, height, and depth.

Existing mine subsidence models can be divided into two broad categories: empirical and phenomenological (68). "Empirical" implies the method is derived by correlating experiences and observations of previously mined areas. "Phenomenological" implies that the actual physical

³Italic numbers in parentheses refer to items in the list of references preceding the appendixes.

behavior of the Earth materials is modeled. Field and laboratory studies have been cited to support both approaches.

Several empirical subsidence prediction techniques, such as the profile and influence function methods, have been developed to describe the subsidence trough. Brauner (14) points out that one basic assumption of both these empirical methods is the law of equivalence. Hypothetically, all mined voids having the same width-to-depth ratio will produce the same amount of subsidence. However, this assumption is valid only if the rock properties do not substantially vary with depth and do not vary from site to site.

The National Coal Board (NCB) graphical method (51) inherently assumes that all coal mining regions that apply this method have a uniform geology, since this allows a complex set of geologic variables to be removed. Unfortunately, this simplification is only successful if the geology does in fact remain constant. In reality this is seldom the case, which means that the NCB method can be less than 90% accurate even for the area in Great Britain where data were collected when the method was developed (88). Attempting to transplant this method directly to other coal basins can produce much less satisfactory results depending on the geologic conditions.

Physical models have been utilized to simulate caving and subsidence (71, 91, 96, 97), but it is not known how well these models simulate actual rock mass behavior. Numerical models have also been used to simulate caving induced by high-extraction mining (7, 17, 18, 34, 50, 53, 67, 69, 72, 86). Lithologic variability, structural discontinuities, and complicated topography can be simulated by these numerical models, and they provide valuable insights into rock mass behavior. Unfortunately, both the physical and numerical models are limited to intensive study of only one site because of the effort required to obtain and adjust the input parameters and boundary conditions.

It is difficult to appropriately characterize rock mass properties to the detail required by numerical models, and therefore the empirical profile function and influence function methods continue to be widely used for subsidence

prediction. For both methods, the arbitrary constraints and coefficients characterizing the rock mass must be back-calculated from field measurements. Local geological influences can be quantified by the values of functional parameters, such as the subsidence factor, angle of break, angle of draw, critical radius, influence factor, and zone factors. Brauner (14) cautions that the angle of draw is inadequate as a material parameter because it is not a pure rock characteristic and, therefore, fails to meet the requirements of a material parameter, namely measurability and sole material dependence. Until recently, the only practical guidance that existed for choosing an appropriate profile or influence function was to select a function used previously for a region of similar geology.

This report documents efforts to develop a procedure to use core log descriptions as input to enhanced empirical subsidence prediction methods (79-80). These methods overcome the limitations of earlier efforts (48, 73-75), which used coarse measures of overburden stratigraphy. The current investigation explores the use of a rock mass classification scheme, core log descriptions, and a commercially available spreadsheet to provide a more refined description of the overburden. This allows use of an engineering mechanics approach to explicitly consider rock mass stiffness. An index parameter known as "bridging potential" is defined, which will allow rock mass structure and properties to be incorporated into the empirical subsidence prediction capabilities being developed. A profile or influence function can then be chosen in which the input variables can be related to this index parameter. Bridging potential is an index parameter only and cannot be used to predict subsidence directly.

This methodology provides a procedure for comparing the response of different overburdens to high-extraction mining by quantifying core log descriptions and developing a site-specific bridging potential that is based on principles of engineering mechanics. The methodology also provides a rational measure of a laminated beam's capacity to resist deflection based on overburden geology and the width and depth of the mined-out panel.

ROCK MASS CLASSIFICATION APPLIED TO HIGH-EXTRACTION COAL MINES

Since there are many factors that control rock mass response to underground excavations, researchers have developed empirical rock mass classification procedures as a practical means of incorporating observed rock mass characteristics and case histories into the design of underground excavations (9). Although early efforts were restricted to developing empirical procedures for designing roof support and tunnel liners, these techniques have been extended to predict rock mass caving behavior (28, 44, 55, 56, 81, 83).

Classification systems are used by engineers and geologists as communication and evaluation tools to describe rock masses. Six major classification systems have evolved in the last half century (5, 8, 10, 19, 47, 77, 92-93). Among these, the Rock Mass Rating (RMR) system (8, 10) and the Q-System (5) have been adopted as the basis for modified classification systems utilized in coal and hard-rock underground mining (20, 29, 43, 45-46, 66, 82).

SELECTION OF A CLASSIFICATION SYSTEM

For this study, the RMR system was chosen for several reasons. The RMR scale is intuitive and straightforward, and it incorporates significant parameters. It requires only a moderate level of detail, which is of practical importance since the RMR is often determined using core logs with few engineering property data. Furthermore, Golder Associates (29) had already adapted two of the rating parameters (i.e., spacing of discontinuities and condition of discontinuities) to account for the specific character of coal measure strata.

CLASSIFICATION OF INDIVIDUAL BEDS

The RMR system requires the input of six basic parameters plus adjustments described by three additional parameters (table 1) (10). These parameters and adjustments are combined to arrive at the RMR using equation 1.

$$\text{RMR} = [R_{\text{IRS}} + R_{\text{ROD}} + R_{\text{JS}} + R_{\text{JC}} + R_{\text{JW}} + R_{\text{JO}}] \\ \times A_{\text{B}} \times A_{\text{S}} \times A_{\text{F}}. \quad (1)$$

These parameters are determined directly from core logs or inferred using other site data and engineering judgment. The adjustments must be determined from other field test data in conjunction with core logs. The need for subjective engineering judgment and interpretation is due to the fact that data have not been collected in a form that can be directly equated to the parameters listed in equation 1. Future exploration and field testing would be focused on quantifying these specific parameters.

BENDING STIFFNESS OF INDIVIDUAL BEDS

The in situ deformation modulus, E , of each bed is estimated using the correlation proposed by Serafim and Pereira (65). These researchers found that the existing empirical relationship between the RMR and modulus should be modified for rock masses with an RMR less than 50.

$$E = 10 [(RMR - 10) / 40] \times 1,000 \text{ (MPa)}. \quad (2)$$

For the current study, it is assumed that E is the same in tension as in compression and no adjustment is made for the effect of increased stiffness due to increased confinement with depth. The moment of inertia, I , can be determined for each lithologic bed based on its thickness, t , if plane strain conditions are assumed. The moment of inertia is calculated per 1-m width.

$$I = \frac{t^3 \times 1}{12} \text{ (m}^4\text{)}. \quad (3)$$

Then, bending stiffness of each bed per 1-m width is

$$\text{Bending Stiffness} = E I \text{ (MPa} \cdot \text{m}^4\text{)}. \quad (4)$$

Example histograms of the RMR, modulus, moment of inertia, and bending stiffness versus depth for a single core log are shown in figure 1. Bed thicknesses are indicated by the distances between the horizontal steps in the histograms. Note that the bending stiffness is heavily dependent on the bed thickness so that thin beds appear as narrow spikes of low stiffness. A logarithmic scale prevents the low stiffness of thin beds from becoming overshadowed by the relatively large stiffness of thick beds. The histograms are used to identify large differences in the bending stiffnesses of adjacent lithologic beds. The contacts between these very different lithologic beds have been found to be the locations of the most significant horizontal discontinuities in a horizontally bedded rock mass (33, 70). Figure 2 shows the relationship between the horizontal discontinuities identified in figure 1 and the actual displacements measured in the field using time domain reflectometry (TDR).

Table 1.—Parameters for rock mass rating

Parameter	Parameter symbol	Spreadsheet symbol	Range of values
Basic:			
Intact rock strength	R_{IRS}	RMR1	0 -15
Drill core quality	R_{ROD}	RMR2	0 -20
Spacing of discontinuities	R_{JS}	RMR3	0 -20
Condition of discontinuities . . .	R_{JC}	RMR4	0 -30
Groundwater conditions	R_{JW}	RMR5	0 -15
Orientation of discontinuities . .	R_{JO}	RMR6	-12 - 0
Adjustments:			
Blasting damage	A_{B}	NAp	0.8- 1.0
In situ stress or stress change . .	A_{S}	NAp	0.6- 1.2
Major fault or fracture presence	A_{F}	NAp	0.7- 1.0
NAp Not applicable.			

DEFINITION OF A GEOSTRUCTURAL ELEMENT

The identified horizontal discontinuities separate groups of beds that have similar bending stiffnesses (figure 3). These groups of beds are defined as geostructural elements. In reality these elements are large three-dimensional plates overlying a mined-out panel. For high-extraction coal mines where the panel width and length are equal to, or greater than, the panel depth, it is assumed that the element can be modeled as a two-dimensional beam (48). For all cases considered in this report, the geostructural elements are viewed in a transverse cross section.

The effective span of each geostructural element is assumed to increase linearly with distance above the high-extraction panel (figure 3). Lines are projected up from the panel ribs at an angle of 80° from horizontal, which is consistent with values for angle of break found in the literature (table 2). For the response of strata near the surface, the simplifying assumption of span increasing with distance above the coal seam can be justified based on physical models (71, 91, 96-97).

BENDING STIFFNESS OF A LAMINATED BEAM

Several geostructural elements in coal measure strata may act together to form a laminated beam. Marino (48) used a laminated beam model to investigate the maximum probable span that could develop before initial collapse over longwall panels, but this was restricted to estimates of the height to which immediate roof caving would occur before a stratum was reached that could support itself. This observation has prompted researchers (62) to use the concept of an equivalent elastic beam (figure 4) and model the overburden as a laminated medium (4, 63). The equivalent elastic beam model is consistent with previous studies (73-76) that found that there is a direct correlation between the tilt and horizontal displacement of the surface during subsidence. This is known to be true for elastic beam bending. The use of the simplest possible model to describe the mechanics of subsidence is appealing because it provides analytic equations that can easily be incorporated into a spreadsheet. The justification for such a simple model is discussed in appendix B.

The weighted rock mass modulus E^* of the laminated beam is

$$E^* = \frac{\sum_{i=1}^n [E_i t_i]}{\sum_{i=1}^n t_i} \quad (\text{MPa}), \quad (5)$$

where n is the number of beds in the laminated beam, E_i is the deformation modulus of a bed, and t_i is its thickness as shown in figure 4.

To calculate the moment of inertia (I) of the laminated beam or transformed section, the following quantities are calculated. A transformed width ($(E_i/E^*) t_i$) is calculated for each stratum proportional to its modulus. The distance from the top of the transformed section to the neutral axis is then computed as

$$y^* = \frac{\sum_{i=1}^n \left[\frac{E_i}{E^*} (1) t_i y_i \right]}{\sum_{i=1}^n \left[\frac{E_i}{E^*} (1) t_i \right]} \quad (\text{m}) \quad (6)$$

for a cross-sectional width of unity and a distance from the top of the transformed section to the midpoint of each bed of y_i . The distance from the neutral axis (na) of the transformed section to the midpoint of each bed (figure 4) is computed as

$$d_i = y^* - y_i \quad (\text{m}), \quad (7)$$

and moment of inertia of the transformed section is

$$I^* = \sum_{i=1}^n \left[\frac{t_i^3 \left(\frac{E_i}{E^*} (1) \right)}{12} + t_i \left(\frac{E_i}{E^*} (1) \right) d_i^2 \right] \quad (\text{m}^4). \quad (8)$$

For a laminated beam then,

$$\text{Bending Stiffness} = E^* I^* \quad (\text{MPa} \cdot \text{m}^4). \quad (9)$$

Table 2.—Angles of internal friction and break, from literature

Stratum	Angle of internal friction, deg	Angle of break, deg		References
		Calculated	Observed	
Clay	15-20	52.5-55	NAp	1, 52
Clay and shale	NAp	NAp	60	52
Coal	45	67.5	NAp	1, 52
Limestone	NAp	NAp	85	52
Plastic	NAp	NAp	60-80	52
Rocky	NAp	NAp	80-90	52
Sand	35-45	62.5-67.5	NAp	1, 52
Sand	NAp	NAp	45	52
Sandstone:				
Hard	NAp	NAp	85	52
Moderate	50-70	70 -80	NAp	1, 52
Shale:				
Hard	45	67.5	NAp	1, 52
Moderate	37	63.5	NAp	1, 52
Unconsolidated	NAp	NAp	40-60	52

NAp Not applicable.

BRIDGING POTENTIAL OF A LAMINATED BEAM

The bridging potential of a laminated beam represents its capacity to resist bending under the influence of its own weight. Bridging potential is defined as

$$\text{Bridging Potential} = \frac{1}{\Delta_{\max}} \quad (\text{m}^{-1}), \quad (10)$$

where

$$\Delta_{\max} = \frac{1}{K} \times \frac{w L^4}{E^* I^*} \quad (\text{m}) \quad (11)$$

is the maximum deflection of a simple beam, L is the effective span in meters (figure 5), and

$$w = \sum_{i=1}^n \frac{[\rho_i g t_i (1)]}{1000} \quad (\text{MN/m}) \quad (12)$$

is the self weight of the beam, where ρ_i is the mass density of each bed in kilograms per cubic meter, and g is acceleration due to gravity in meters per second squared.

The constant, K , in equation 11 is equal to 77 for pinned end conditions and equal to 384 for fixed end conditions. For this study, it was assumed that the end conditions were fixed, as discussed in appendix B.

VALIDATION OF STIFFNESS DISCONTINUITIES

Rock mass displacements over eight high-extraction panels in southern Illinois were monitored using the principle of TDR (6, 23). A coaxial cable was grouted into a borehole drilled from the surface through the soil and rock mass over the panel prior to mining. A cable tester was connected to the cable at the surface and a voltage pulse sent down the cable. At every location where there was a change in cable geometry, a reflection was sent back to the tester, where the waveform was displayed and recorded. The shape and magnitude of the waveform are directly related to the type and magnitude of cable damage. Based on laboratory correlations, it is possible to distinguish shear deformation

from tensile deformation and to quantify shear displacement (23).

TDR signatures for one instrumented borehole, shown in figure 2, were used to verify that shear displacements tended to occur along the horizontal discontinuities identified by the classification and bending stiffness analysis and shown in figure 1. The signatures were recorded as the longwall face approached and advanced past the borehole. The regularly spaced TDR spikes, indicated with asterisks in figure 2, are associated with crimps made in the cable prior to placement in the borehole and are used as reference points. The other spikes show the locations where movement along discontinuities caused cable deformation.

Localized shear is measured at locations where large changes in the bending stiffness occur. On May 11, the TDR cable was being sheared at depths of 71.4, 77.3, and 103.0 m. These localized displacements correspond to thin beds at these depths. The drill core showed a coal from 71.4 to 71.9 m, a limestone from 76.7 to 77.2 m, a shale from 102.6 to 103.0 m, and a sandstone from 103.0 to 103.8 m. The increased spike magnitudes on the May 15 TDR signature show that shearing continued at these locations, and ultimately the cable was sheared at a depth of 103.0 m. By May 21, additional shear deformations become visible on the TDR signature at depths of 28.7, 44.0, 49.4, 55.7, and 61.7 m. The drill core showed a limestone from 27.3 to 27.6 m, a dark gray shale from 50.3 to 50.4 m, and a coal from 56.2 m to 56.4 m.

Of the 14 horizontal discontinuities identified by the bending stiffness profile in figure 1, 9 of the predicted discontinuities (64%) were found to be locations where measurable displacement actually occurred (figure 2). Only three displacements were measured at locations where discontinuities had not been predicted. The authors believe that the agreement between predicted displacement locations and actual measured movements is representative of the current state of the art of TDR technology and demonstrates the potential accuracy of this technique. Based on the correlation between the lithology determined from the core log and shear displacements measured with TDR, it seems reasonable to divide the overburden into geostructural elements separated by significant horizontal discontinuities identified by large differences in bending stiffness.

ROCK MASS CLASSIFICATION SPREADSHEET

A spreadsheet program is used to calculate an RMR for each bed based on the lithology, thickness, and engineering properties, which are determined from core logs and laboratory tests. Once the RMR is calculated, the spreadsheet has two major functions (figure 6). First, the spreadsheet calculates values used to graphically represent the character of each lithologic bed in the overburden. It calculates an in situ deformation modulus for each bed using the empirical relationship between the modulus and the RMR and then uses

this modulus along with additional parameters that are based on mine geometry to calculate the bending stiffness and bridging potential for each bed. Second, the spreadsheet creates a transformed section that allows groups of beds to be modeled as an elastic beam. It then calculates a bridging potential for the entire rock mass.

In this section, the various components of the spreadsheet will be explained along with input parameters needed to determine the RMR. An example from the Illinois Coal Basin

will be used to demonstrate how the spreadsheet is applied at a specific site. The program was developed using Quattro Pro for Windows, Version 5.0.

LABORATORY PROPERTIES DATABASE

The spreadsheet ROCKPRP.WQ1 contains a lookup table that provides a convenient format for compiling engineering properties of coal measure strata (figure 7). The values are estimates for the Illinois Coal Basin based on data from

various references (11-12, 16, 38-39, 94-95). For purposes of this report, the properties were grouped by rock type and color. The database (table 3) is being expanded to include the geologic formation and member name according to conventions established by the Illinois State Geological Survey (78), which will allow for a more sophisticated lookup table. The formulas used in figure 7 are

$$D16: +C16/145 \quad (\text{repeated down to row 67})$$

$$F16: +E16*(1/2.2)*(1/0.3048)^3 \quad (\text{repeated down to row 67})$$

Table 3.—Laboratory rock properties

Material ¹	Description	Strength		Density		Site name	Locality	State	Reference
		psi	MPa	lb/ft ³	kg/m ³				
Dolomite	Gray, medium-grained	47,600	328	175	2,800	-	-	TN	94
	Gray	52,000	359	172	2,760	-	-	TN	94
	Siliceous	35,600	246	173	2,770	-	-	TN	94
Limestone	Dolomitic-marlston	10,000	69	131	2,100	-	-	CO	11
	Limonitic	24,900	172	182	2,920	-	-	AL	94
	Coarse white	24,000	166	177	2,830	-	-	AL	94
	Metamorphic	24,000	166	170	2,720	-	-	CA	11
	Kerogenaceous magnesian	-	-	136	2,180	-	-	CO	94
	. . do.	16,600	114	140	2,250	-	-	CO	94
	Calcareous	22,300	154	167	2,680	-	-	IL	11
	Dark gray to gray	5,812	40	-	-	Heron Road	West Frankfort	IL	38
	Light gray	31,416	217	-	-	. . do. do.	IL	38
	. . do.	16,335	113	-	-	North Marcum	Benton	IL	39
	Dark gray	25,327	175	-	-	. . do. do.	IL	39
	Gray to green	8,773	61	-	-	. . do. do.	IL	39
	Fossiliferous	10,200	70	-	-	-	-	IN	94
	. . do.	10,900	75	148	2,370	-	-	IN	94
	Unknown	5,300	37	137	2,190	-	-	IN	12
	Fossiliferous	9,700	67	-	-	-	-	IN	94
	Dolomitic-unmileral	23,900	165	175	2,800	-	-	MO	11
	Dolomitic-galena	13,400	92	206	3,300	-	-	MO	11
	Dolomitic-unmileral	37,800	261	170	2,730	-	-	MO	11
	Dolomitic-galena	16,100	111	275	4,410	-	-	MO	11
	Fossiliferous	20,700	143	165	2,650	-	-	MO	12
	. . do.	23,800	164	167	2,670	-	-	MO	12
	Oolitic, fossiliferous	16,800	116	160	2,560	-	-	MO	12
	Dolomitic	25,400	175	166	2,660	-	-	MO	11
	Oolitic, fossiliferous	18,200	126	154	2,460	-	-	MO	12
	Dolomitic-glaucanit	21,200	146	167	2,670	-	-	MO	11
Sandy, dolomitic	29,800	206	167	2,680	-	-	MO	11	
Dolomitic	28,800	199	168	2,690	-	-	MO	11	
. . do.	28,700	198	173	2,780	-	-	MO	11	
Limestone	Dolomitic	28,400	196	169	2,710	-	-	MO	11
	Fossiliferous	21,300	147	170	2,730	-	-	OH	12
	. . do.	26,100	180	175	2,810	-	-	OH	12
	Dolomitic	8,000	55	162	2,600	-	-	OH	95
	Unknown	28,500	197	168	2,690	-	-	OH	94
	Fossiliferous	20,400	141	175	2,800	-	-	OH	12
	Fine-grained	15,800	109	150	2,410	-	-	OH	12
	Unknown	17,900	123	162	2,600	-	-	OH	12
	Fossiliferous	21,600	149	168	2,690	-	-	OH	12
	Sandy	22,600	156	162	2,590	-	-	OH	12
	Dolomitic	13,000	90	156	2,500	-	-	OH	95

See footnotes at end of table.

Table 3.—Laboratory rock properties—Continued

Material ¹	Description	Strength		Density		Site name	Locality	State	Reference	
		psi	MPa	lb/ft ³	kg/m ³					
Limestone	Dolomitic—Cont'd.									
	.do.	26,000	179	175	2,800	-	-	OH	95	
	.do.	12,000	83	156	2,500	-	-	OH	95	
	Unknown	18,900	130	167	2,670	-	-	OK	11	
	Siliceous	22,000	152	154	2,470	-	-	OK	11	
	Chalky	2,400	17	-	-	-	-	SD	11	
	.do.	3,700	26	113	1,810	-	-	SD	11	
	.do.	4,200	29	118	1,890	-	-	SD	11	
	.do.	1,500	10	134	2,150	-	-	SD	11	
	.do.	1,800	12	125	2,000	-	-	SD	11	
	.do.	1,300	9	82	1,310	-	-	SD	11	
	.do.	700	5	-	-	-	-	SD	11	
	.do.	1,200	8	88	1,410	-	-	SD	11	
	.do.	1,400	10	122	1,960	-	-	SD	11	
	.do.	2,400	17	107	1,710	-	-	SD	11	
	.do.	700	5	111	1,780	-	-	SD	11	
	Unknown	25,100	173	170	2,730	-	-	TN	12	
	.do.	25,100	173	171	2,740	-	-	TN	12	
	Gray	37,600	259	-	-	-	-	TN	94	
	Contact	23,600	163	-	-	-	-	UT	95	
	Unknown	28,000	193	173	2,780	-	-	UT	95	
	.do.	23,000	159	167	2,680	-	-	WV	95	
	.do.	29,500	203	-	-	-	-	WV	95	
	Sandstone	Fossiliferous	22,400	154	203	3,260	-	-	AL	94
		Ferruginous	34,100	235	183	2,930	-	-	AL	94
		.do.	24,200	167	196	3,140	-	-	AL	94
		Unknown	9,063	63	-	-	Heron Road	West Frankfort	IL	38
		Light gray	8,892	61	-	-	.do.	.do.	IL	38
		.do.	6,514	45	-	-	.do.	.do.	IL	38
		.do.	5,564	38	-	-	.do.	.do.	IL	38
.do.		6,242	43	-	-	.do.	.do.	IL	38	
.do.		7,550	52	-	-	.do.	.do.	IL	38	
Gray		9,431	65	-	-	.do.	.do.	IL	38	
Light gray		-	-	-	-	North Marcum	Benton	IL	39	
Gray to green		6,281	43	-	-	.do.	.do.	IL	39	
.do.		6,316	44	-	-	.do.	.do.	IL	39	
Light gray		6,700	46	-	-	.do.	.do.	IL	39	
Gray to green		5,958	41	-	-	.do.	.do.	IL	39	
Light gray		-	-	-	-	.do.	.do.	IL	39	
.do.		8,097	56	-	-	.do.	.do.	IL	39	
Coarse-grained		6,100	42	135	2,170	-	-	OH	94	
Unknown		10,400	72	129	2,060	-	-	OH	94	
.do.		8,000	55	-	-	-	-	OH	94	
Coarse-grained		5,100	35	-	-	-	-	OH	94	
Unknown		7,700	53	-	-	-	-	OH	94	
Coarse-grained		5,200	36	-	-	-	-	OH	94	
Unknown		10,900	75	134	2,140	-	-	OK	12	
.do.		6,300	43	135	2,170	-	-	OK	12	
Friable		7,600	52	141	2,260	-	-	OK	12	
Silty		10,800	74	156	2,500	-	-	OK	12	
.do.		8,600	59	-	-	-	-	OK	12	
Unknown		9,400	65	134	2,150	-	-	PA	11	
.do.		9,500	66	134	2,150	-	-	PA	11	
.do.	8,300	57	135	2,170	-	-	PA	11		
.do.	9,700	67	134	2,150	-	-	PA	11		
.do.	9,700	67	133	2,130	-	-	PA	11		
Sandstone	Unknown	9,900	68	135	2,170	-	-	PA	11	
	.do.	14,800	102	152	2,430	-	-	PA	11	

See footnotes at end of table.

Table 3.—Laboratory rock properties—Continued

Material ¹	Description	Strength		Density		Site name	Locality	State	Reference
		psi	MPa	lb/ft ³	kg/m ³				
Sandstone	Unknown—Cont'd.								
	.do.	9,700	67	138	2,210	-	-	PA	12
	.do.	17,800	123	155	2,490	-	-	PA	11
	.do.	11,100	77	135	2,160	-	-	PA	11
	.do.	11,100	77	134	2,150	-	-	PA	11
	.do.	12,600	87	137	2,200	-	-	PA	12
	Fine-grained	23,000	159	168	2,700	-	-	PA	12
	Unknown	15,600	108	153	2,450	-	-	PA	12
	.do.	11,500	79	135	2,170	-	-	UT	95
	.do.	15,500	107	137	2,200	-	-	UT	95
	.do.	32,400	223	147	2,350	-	-	UT	95
	.do.	27,700	191	145	2,330	-	-	UT	95
	.do.	14,200	98	134	2,140	-	-	UT	95
	.do.	13,100	90	144	2,310	-	-	UT	11
	.do.	7,100	49	-	-	-	-	UT	11
	.do.	18,000	124	142	2,280	-	-	UT	11
	.do.	13,800	95	143	2,290	-	-	UT	11
	.do.	20,300	140	148	2,370	-	-	UT	11
	.do.	8,600	59	139	2,220	-	-	UT	11
	.do.	12,600	87	134	2,150	-	-	UT	11
	.do.	8,100	56	133	2,130	-	-	UT	11
	.do.	4,800	33	133	2,130	-	-	UT	11
	Argillaceous	15,300	106	175	2,800	-	-	WV	11
	Graywacke	20,500	141	162	2,600	-	-	WV	11
	Unknown	21,900	151	156	2,500	-	-	WV	95
	.do.	19,400	134	156	2,500	-	-	WV	95
	.do.	16,200	112	162	2,600	-	-	WV	95
Shale	Calcareous	22,700	157	-	-	-	-	CO	94
	Green	-	-	-	-	Heron Road	West Frankfort	IL	38
	Dark gray to green	4,195	29	-	-	.do.	.do.	IL	38
	Black	8,475	58	-	-	.do.	.do.	IL	38
	Gray to green	8,271	57	-	-	.do.	.do.	IL	38
	Gray to dark gray	-	-	-	-	.do.	.do.	IL	38
	Gray	8,506	59	-	-	.do.	.do.	IL	38
	.do.	10,236	71	-	-	.do.	.do.	IL	38
	.do.	-	-	-	-	.do.	.do.	IL	38
	.do.	-	-	-	-	.do.	.do.	IL	38
	Dark gray	7,950	55	-	-	.do.	.do.	IL	38
	.do.	2,942	20	-	-	.do.	.do.	IL	38
	.do.	-	-	-	-	.do.	.do.	IL	38
	Gray	5,285	36	-	-	North Marcum	Benton	IL	39
	.do.	7,390	51	-	-	.do.	.do.	IL	39
	.do.	6,333	44	-	-	.do.	.do.	IL	39
	.do.	7,063	49	-	-	.do.	.do.	IL	39
	Gray to green	5,168	36	-	-	.do.	.do.	IL	39
	.do.	4,498	31	-	-	.do.	.do.	IL	39
	.do.	6,531	45	-	-	.do.	.do.	IL	39
	.do.	8,832	61	-	-	.do.	.do.	IL	39
	Gray	8,422	58	-	-	.do.	.do.	IL	39
	.do.	-	-	-	-	.do.	.do.	IL	39
	.do.	7,482	52	-	-	.do.	.do.	IL	39
	.do.	7,980	55	-	-	.do.	.do.	IL	39
	.do.	8,306	57	-	-	.do.	.do.	IL	39
	.do.	7,099	49	-	-	.do.	.do.	IL	39
	.do.	4,446	31	-	-	.do.	.do.	IL	39
	.do.	6,842	47	-	-	.do.	.do.	IL	39
	.do.	7,958	55	-	-	.do.	.do.	IL	39
.do.	6,841	47	-	-	.do.	.do.	IL	39	

See footnotes at end of table.

Table 3.—Laboratory rock properties—Continued

Material ¹	Description	Strength		Density		Site name	Locality	State	Reference
		psi	MPa	lb/ft ³	kg/m ³				
Shale	Unknown	10,900	75	160	2,560	-	-	OH	12
	.do.	15,600	108	-	-	-	-	OH	94
	Silty	12,300	85	-	-	-	-	TN	12
	.do.	12,100	83	158	2,530	-	-	TN	12
	Carbonaceous	16,300	112	144	2,300	-	-	TN	12
	.do.	16,000	110	144	2,300	-	-	TN	12
	Unknown	31,300	216	175	2,810	-	-	UT	95
	Silicified	33,500	231	175	2,800	-	-	UT	95
	Unknown	18,500	128	150	2,400	-	-	WV	95
	Siderite banded	16,300	112	172	2,760	-	-	WV	11
	Unknown	11,600	80	162	2,600	-	-	WV	95
	.do.	15,000	103	-	-	-	-	WV	95
	Carbonaceous	14,500	100	171	2,740	-	-	WV	11
	SH-SLTST	Siliceous	28,600	197	173	2,780	-	-	MI
.do.		28,400	196	170	2,730	-	-	MI	11
SH-SLT-MS	Unknown	14,700	101	170	2,720	-	-	PA	12
Siltstone	Gray	6,374	44	-	-	Heron Road	West Frankfort	IL	38
	.do.	9,075	63	-	-	.do.	.do.	IL	38
	.do.	9,227	64	-	-	.do.	.do.	IL	38
	.do.	9,830	68	-	-	.do.	.do.	IL	38
	Gray to green	9,841	68	-	-	.do.	.do.	IL	38
	Medium gray	6,844	47	-	-	.do.	.do.	IL	38
	Dark gray	10,007	69	-	-	.do.	.do.	IL	38
	Gray to green	4,453	31	-	-	North Marcum	Benton	IL	39
	Unknown	5,300	37	166	2,660	.do.	.do.	OH	12
	.do.	5,000	34	167	2,680	.do.	.do.	OH	12
	Argillaceous	8,100	56	-	-	.do.	.do.	OK	12
	Unknown	16,400	113	172	2,760	.do.	.do.	PA	12
	SLT-SS-SH	Unknown	26,800	185	172	2,760	.do.	.do.	AL
SLTST-SH	.do.	37,200	257	172	2,760	.do.	.do.	AL	94
	.do.	45,800	316	173	2,770	.do.	.do.	AL	94

¹MS = mudstone; SH = shale; SLTST = siltstone; SLT = slate; SS = sandstone.

NOTE.—Dashes indicate no data.

ROCK MASS RATING CRITERIA

The spreadsheet RMR-TBLS.WQ1 (figure 8) contains lookup tables that provide a convenient format for summarizing the criteria and values established by Bieniawski (8, 10) for the RMR and modified by Golder Associates (29) for use with coal measure strata. RMR1 corresponds with R_{IRS} in equation 1 and is a measure of intact rock strength. RMR2 corresponds with R_{ROD} and is a measure of drill core quality in terms of the rock quality designation. RMR3 corresponds with R_{JS} and is a measure of joint spacing, which is reinterpreted as the distance between bedding planes (i.e., bed thickness). RMR4 corresponds with R_{JC} and is a measure of joint condition in terms of roughness, which is reinterpreted as the condition of bedding planes. RMR5 corresponds with R_{JW} and is a measure of the presence of water along joints or bedding planes. RMR6 corresponds with R_{JO} and is a measure of joint orientation with respect to the mine opening. For

this study the adjustment factors A_B (blast damage), A_S (in situ stress), and A_F (presence of major faults or fractures) were assumed to have a values of 1, 0.75, and 0.75, respectively.

ROCK MASS STIFFNESS AND DEFLECTION CALCULATION

TEMPLATE.WQ1 is the main spreadsheet for calculation of the rock mass stiffness and bridging potential. For purposes of discussion, the North Marcum Branch site is used. The coal seam is at a depth of 181.4 m, and the panel width is 304.8 m.

Assumptions and Interactive Parameters

This portion of the spreadsheet (figure 9) summarizes assumptions and parameters that can be altered to perform a sensitivity analysis.

Stratigraphy and Rock Mass Stiffness

This portion of the spreadsheet, columns A to N (figure 9), is where a user inputs core information. The RMR for each stratum is computed automatically in columns U to AA (figure 10), based on laboratory properties and the rating criteria in the supporting spreadsheets (ROCKPRP.WQ1 and RMR-TBLS.WQ1). For purposes of illustration, only the first eleven strata are included. There are 103 strata in the complete spreadsheet. The formulas used in figure 10 are repeated down to row 151:

P49: +A49*@SIN(\$J\$18/180*@PI)
 Q49: +A50*@SIN(\$J\$18/180*@PI)
 R49: +P49*0.3048
 S49: +Q49*0.3048
 T49: @VLOOKUP(B49,[ROCKPRP]\$A\$16..\$D\$76,3)
 U49: @VLOOKUP(T49,[RMR-TBLS]\$B\$13..\$D\$19,2)
 V49: @VLOOKUP(F49,[RMR-TBLS]\$F\$13..\$H\$19,2)
 W49: @VLOOKUP(H49,[RMR-TBLS]\$J\$11..\$L\$17,2)
 X49: @VLOOKUP(I49,[RMR-TBLS]\$B\$25..\$D\$35,2)
 Y49: @VLOOKUP(J49,[RMR-TBLS]\$F\$25..\$H\$31,2)
 Z49: @VLOOKUP(K49,[RMR-TBLS]\$J\$25..\$L\$31,2)
 AA49: @SUM(U49..Z49)*L49*M49

Bending Stiffness and Deflection of Individual Beds

This portion of the spreadsheet, columns AC to AK (figure 11), calculates the bending stiffness of individual beds. The deflection of each bed due to self-weight is also computed. The formulas used in figure 11 are

AC49: $10^{((AA49-10)/40)*1000}$
 AD49: +S49-R49
 AE49: +AD49³/12
 AF49: +AC49*AE49
 AG44: 0 (scaling factor)
 AG49: @LOG(AF49)+\$AG\$44
 AH49: +AF49*\$J\$20/(BA49-BA48)
 AI49: 1/AH49*BC49⁴
 AJ44: 10⁷ (scaling factor)
 AJ49: 1/AI49*\$AJ\$44
 AK44: 10 (scaling factor)
 AK49: @LOG(1/AI49)+\$AK\$44

Transformed Section and Average Deformation Modulus

This portion of the spreadsheet, columns AM to AY (figure 12), computes the transformed section and deformation modulus for a selected laminated beam thickness. To compute this value for a selected beam the user must input a valid beam thickness (i.e., one of the values in column S) and use the beam analysis macro "_initialize" or "_reset" (see below). The formulas used in figure 12 are

AM49: +AC49*AD49
 AN49: @SUM(\$AM\$49..AM49)/S49
 AO49: +AC49/\$J\$24
 AP49: +AO49
 AQ49: +AD49*1*AO49
 AR49: (S49+R49)/2
 AS49: +AQ49*AR49
 AT49: @SUM(\$AS\$49..AS49)/@SUM(\$AQ\$49..AQ49)
 (valid only for row corresponding to selected thickness of laminated beam)
 AU49: ((AR49-\$J\$26)^2)^0.5

AV49: $(AP49 \cdot AD49^3) / 12$
 AW49: $+AQ49 \cdot AU49^2$
 AX49: $@SUM(\$AV\$49..AV49) + @SUM(\$AW\$49..AW49)$
 AY49: $+AN49 \cdot AX49$
 (valid only for row corresponding to selected thickness laminated beam)

Bending Stiffness and Bridging Potential of Laminated Beam

This portion of the spreadsheet, columns AZ to BE (figure 13), computes the bending stiffness and bridging potential of the selected laminated beam. The formulas used in figure 13 are:

AZ49: $@VLOOKUP(B49, [ROCKPRP] \$A\$16.. \$F\$67, 5) \cdot 9.81 / 10^6$
 BA49: $+BA48 + (AZ49 \cdot AD49)$
 BB49: $+AY49 \cdot \$A:\$J\$20 / BA49$
 BC49: $\$A:\$J\$28 + (2 \cdot ((\$J\$22 \cdot @TAN(\$J\$30 / 180 \cdot @PI)) - 49 \cdot @TAN(\$J\$30 / 180 \cdot @PI)))$
 BD49: $1 / BB49 \cdot (BC49^4)$
 BE49: $1 / BD49$

Laminated Beam Analysis Macro

To facilitate use of the spreadsheet, a macro was developed. The logic is documented in figure 14, and the actual spreadsheet implementation is shown in figure 15. Results of the analysis are stored in columns BH to BM. The macros "_initialize" and "_reset" can be used to compute values for a selected valid beam thickness (i.e., one of the values in column S as shown in figure 10). The macro "_analyze" is used to compute values for all possible beam thickness (i.e., all values in column S).

PARAMETER STUDIES FOR THE LAMINATED BEAM DEFLECTION MODEL

The current model hypothesized for the overburden includes a zone of block caving near the mine, which is overlain by a zone of strata separation and fracturing that eventually transitions to a near-surface zone of laminated beam bending (figure 5). This response has been illustrated by physical modeling (91, 96). Based on an analysis of 65 case histories, Kendorski (42) concluded that the transition zone upper limit is 24 to 60 times the mined thickness (figure 5). This is consistent with the cases in appendix A.

EFFECT OF ASSUMED LAMINATED BEAM THICKNESS

To demonstrate the significance of assumed beam thickness, data from the Old Ben No. 24 Mine (panel 1) were used (40, 87). Maximum deflection values were computed for all possible beam thicknesses based on all the bedding contacts identified in the core log (i.e., not just the significant horizontal discontinuities identified in the stiffness-versus-depth profile). As shown in figure 16, the maximum deflection decreases as the beam thickness increases, but there is only a limited range of maximum deflection values that are physically possible.

The upper limit on beam deflection in the Illinois Coal Basin is considered to be 70% of the mined thickness

based on measured subsidence data for all longwall panels (table 4). The maximum subsidence must be some value greater than zero, and it seems reasonable to assume a lower limit equal to one-half the upper limit (i.e., 35% of the mined thickness) for most high-extraction mines in Illinois.

Working with the hypothesis that a near-surface laminated beam can support its own weight only by fixed end supports, the maximum and minimum deflection limits in figure 16 indicate the range of possible beam thickness. Based on the data and profiles presented in appendix A, this hypothesis is considered valid over a range of panel widths. The limits and range of beam thickness should be regarded as index values. These values are indices that are controlled by rock mass properties and mine geometry.

EFFECT OF MINED PANEL WIDTH

Assume that the laminated beam has fixed end supports and that the hypothetical beam thickness is 50 m. If the panel width is increased from 72 m (subcritical) to 288 m (supercritical), mathematically the maximum deflection of this hypothetical beam would increase from 0.01 m to 3.00 m (figure 17). This upper value is not even physically possible because the mined thickness is only 2.4 m. Conversely, if the panel width is increased from 77 to 288 m, the

Table 4.—Summary of instrumented panels

Site	Depth, m	Panel width, m	Mined thickness, m	Face advance rate, m/d	Maximum measured subsidence, m	Subsidence ratio	Bridging potential of entire overburden m^{-1}
Consol Rend Lake Mine, Jefferson County	224.7	183	2.9	5.2	1.89	0.65	122
Freeman Orient No. 4 Mine (retreat), Williamson County.	75.7	117	1.8	3.7	0.96	0.52	73
Kerr-McGee Galatia Mine, Saline County	122.5	204	1.8	16.8	1.37	0.72	18
Old Ben No. 21 Mine (retreat), Franklin County . . .	199.6	91	2.1	0.9	0.52	0.24	1,475
Old Ben No. 24 Mine, Marcum Branch, Franklin County.	181.4	305	1.83	9.1	1.32	0.72	11
Old Ben No. 24 Mine, panel 1, Franklin County . . .	188.7	144	2.4	2.1	1.43	0.59	212
Old Ben No. 24 Mine, panel 2, Franklin County . . .	188.4	144	2.4	1.5	1.59	0.65	142
Old Ben No. 25 Mine, Franklin County	159.1	259	1.8	8.5	1.31	0.73]15

laminated beam thickness would have to increase from 18 to 70 m in order to limit the maximum deflection to 70% of the mined thickness. This simple example demonstrates that, as a panel width increases from subcritical to supercritical, the hypothesis of a near-surface laminated beam supported only at its ends becomes invalid. Therefore, the beam must be supported by underlying caved strata for supercritical panel widths.

The range of panel widths over which the working hypothesis is valid can be shown by assuming that the laminated beam is 188.8 m thick (i.e., equal to the entire thickness of overburden) and then incrementally increasing the width from 77 to 400 m. When maximum deflection is plotted versus the width-depth ratio (figure 18), there is a significant increase in the slope of this curve as the width-depth ratio increases above 1.0. This is consistent with width-depth ratios of 1.0 to 1.4 required for the maximum subsidence ratio (37, 51, 90) and may be considered an upper limit for the working hypothesis. When the span-thickness (i.e., width-depth) ratio of a beam is smaller than 0.2 (58), the behavior of the beam is governed more by shear than bending, and this may be considered a lower limit for the working hypothesis.

EFFECT OF ASSUMED SPAN ANGLE

The span angle is the angle from a vertical line above the panel edge to an assumed break line (52). The

complementary angle has been referred to as "the angle of break" (figure 5). The span angle is

$$\text{span } \angle = 90^\circ - \text{break } \angle \quad (13)$$

Values from the literature are listed in table 2, where the range of break angles for coal measure strata is 60° to 80°. So the range of span angles would be 30° to 10°.

Increasing the span angle is similar to increasing panel width. If the span angle is increased from 10° to 30° (figure 19) the beam thickness (required to limit the maximum deflection to 70% of mined thickness) increases from 27 to 55 m. A value of 10° is the default span angle used in the spreadsheet.

EFFECT OF CHANGING OVERBURDEN GEOLOGY

The same parameter study was performed for two sites. The variation of overburden within the Illinois Coal Basin does not produce a significant variation in the curves of maximum deflection versus hypothetical beam thickness (figure 20). This may partially explain why the current empirical techniques for subsidence prediction are reasonably accurate in large parts of the Illinois Coal Basin even though most of the techniques do not account for geologic characteristics directly.

COMPARISON OF MONITORED MINE SITES

The rock mass classification and beam deflection spreadsheet was used to interpret overburden behavior at eight panels in southern Illinois (figure 21 and appendix A). The mine geometries, measured maximum subsidence, and computed maximum deflections for a range of beam thicknesses are summarized in tables 4 and 5. It must be

emphasized again that this methodology is not intended to be used to predict maximum subsidence. Rather, it is intended to provide a straightforward procedure to use core log descriptions as input for existing empirical predictive techniques and for other types of analysis capable of simulating the overburden response to high-extraction coal

Table 5.—Laminated beam data

Site and model	Assumed thickness, m	Span, m	Weight, MPa	EI, 10 ⁶ MPa·m ⁴	Maximum deflection, m
Consol Rend Lake Mine, Jefferson County:					
1	32.2	250.8	0.74	4.27	1.79
2	46.7	245.7	1.05	13.61	0.73
3	57.8	241.8	1.31	28.01	0.42
Freeman Orient No. 4 Mine, (retreat), Williamson County:					
1	11.9	139.5	0.23	0.09	2.61
2	15.2	138.3	0.29	0.18	1.55
3	27.3	134.1	0.57	1.86	0.26
Kerr-McGee Galatia Mine, Saline County:					
1	31.5	236.1	0.62	2.66	1.89
2	46.3	230.9	0.97	8.78	0.82
3	52.9	228.5	1.12	13.34	0.60
4	64.9	224.3	1.39	25.65	0.36
Old Ben No. 21 Mine (retreat), Franklin County:					
1	20.1	154.3	0.41	0.69	0.87
2	29.0	151.2	0.59	2.23	0.36
3	42.7	146.4	0.90	8.78	0.12
4	61.0	139.9	1.34	28.16	0.05
Old Ben No. 24 Mine, Marcum Branch, Franklin County:					
1	66.8	345.4	1.52	39.32	1.43
2	76.7	341.9	1.75	61.01	1.02
3	98.3	334.3	2.25	140.97	0.52
Old Ben No. 24 Mine, panel 1, Franklin County					
1	21.5	203.0	0.43	0.69	2.74
2	30.8	199.7	0.64	2.69	0.99
3	51.2	192.5	1.13	13.31	0.30
Old Ben No. 24 Mine, panel 2, Franklin County					
1	18.9	203.8	0.36	0.34	4.75
2	32.6	198.9	0.68	2.56	1.08
3	57.6	190.1	1.27	13.85	0.31
Old Ben No. 25 Mine, Franklin County					
1	43.7	299.7	1.00	9.92	2.13
2	55.9	295.4	1.31	24.62	1.06
3	66.6	291.6	1.56	41.86	0.70
4	70.5	290.3	1.66	45.46	0.67

mining. Similar to the subsidence ratio, the bridging potential is an index value that incorporates both overburden geology and mine geometry. These index values allow ratio comparisons to be made using data available from 90 sites in Illinois.

STRATA IDENTIFICATION

The number of strata identified in each core log used in this study is plotted versus total hole depth in figure 22. The plot is intended to convey the variability in core-logging procedures by different individuals with respect to identifying different lithologic beds. Differentiation can become quite subjective in bedded coal measure rocks where color and material may grade back and forth. This is important because the moment of inertia of each bed is dependent on the cube of the thickness (equations 3 and 8), and therefore, core interpretation has a major impact on the values of

bending stiffness and bridging potential that are calculated. Thickness is determined subjectively by the person logging core, and it is not an objective and repeatable measurement. The USBM is currently developing a database to identify each stratum according to geological formation and member name using standards developed by the Illinois State Geological Survey (78) to rationally explain the variation in number of strata among these sites.

COMPARISON WITH CONVENTIONAL SUBSIDENCE PARAMETERS

A conventional approach for summation of subsidence data is a plot of subsidence ratio versus the width-depth ratio, such as shown in figure 23. The working hypothesis of a near-surface laminated beam supported only by fixed ends is considered valid for $0.2 < \text{width-depth ratio} < 1.0$, and over this range the data for longwall and retreat mines

are clustered in bands. The trend is a nonlinear increase in subsidence ratio, which approaches an asymptotic value of 0.8 as the width-depth ratio exceeds 1.4.

Bridging potential is defined as the inverse of maximum deflection, so figure 24 simply restates figure 18. The bridging potential shows a nonlinear decrease as the width-depth ratio increases, and it asymptotically approaches 0 as the width-depth ratio exceeds 1.4. The similarity between figures 23 and 24 suggests that the simple model of a laminated beam supported by fixed ends, and the associated analytical relationships, is valid for longwall and retreat mines within the range $0.2 < \text{width-depth ratio} < 1.0$. For a width-depth ratio greater than 1.4, the laminated beam must be supported by caved material.

The scatter for room-and-pillar mines in figure 23 is due to variations in extraction and, therefore, pillar support. The variability of pillar support did not allow the overburden to deform in a mode consistent with the laminated beam bending model except for the few cases that fall within the band for retreat mines. In fact, sinkhole-type subsidence is more common over shallow room-and-pillar mines (37).

Bridging potential cannot be used to directly predict subsidence. Typical values of maximum subsidence are 1 to 2 m for longwall panels in Illinois (table 4). This corresponds to a bridging potential of 1 to 0.5. In figure 24, the bridging potential is calculated for an assumed beam thickness equal to the entire overburden thickness, which produces a maximum bridging potential of about 1,000 (i.e., a deflection of 0.001 m). Bridging potential must therefore be regarded only as an index parameter of rock mass properties and mine geometry. The deflection equation of a simple beam is used because it incorporates gross parameters of the behavior such as material properties, flexural stiffness, and span. The deflection value calculated is not physically meaningful, and bridging potential is not intended to be an indicator of failure conditions. It cannot be used to predict subsidence because the deflection of a simple elastic beam supported by fixed ends cannot accurately predict the subsidence of a nonelastic nonhomogeneous rock mass. In addition, the panel width is not typically the critical unsupported span of a particular overburden. Caving begins when the face reaches some critical distance from the start of the panel, and Marino (48) presents a technique for estimating the

span at first cave. Finally, the depth of mining is not the thickness of the equivalent elastic laminated beam at failure. To reiterate, bridging potential cannot be used to predict subsidence, but it does provide a single index value that indicates potential overburden response over a range of mine geometries and thus may be a useful input parameter for other empirical subsidence prediction techniques.

OBSERVATIONS BASED ON COMPARISONS

This method is useful for rock mass characterization since it objectively quantifies the character of any site based on geology and mine geometry. The major advantages of the method are—

1. The RMR is a quantifiable method of describing the geology of a specific site.
2. The empirical relation used to calculate a deformation modulus from the RMR is simple, repeatable, and based on case histories.
3. The bending stiffness is based on the principles of engineering mechanics.
4. The bridging potential incorporates mine geometry and is similarly based on principles of engineering mechanics. It provides a rational measure of the laminated beam's capacity to resist deflection.

The discrepancy between the deflection of the laminated beam model and the measured subsidence profile is an expected result since—

1. The simple model of a laminated beam deflecting over previously failed beds without support from the failed beds is valid only over a limited range of panel widths ($0.2 < \text{width-depth ratio} < 1.0$),
2. The laminated beam thickness is unknown and may be greater or less than that inferred from the bending stiffness and TDR measurements.
3. The assumption of a constant beam thickness may not be valid.
4. The unsupported span could only be estimated since the transverse panel dimension is not necessarily the critical span at failure.
5. The rock mass is nonelastic and nonhomogeneous.

CONCLUSIONS

The research documented in this report was motivated by a need to classify and describe overburden over high-extraction coal mines. This evolved into development of

a laminated beam model for coal measure strata using data available for the Illinois Coal Basin. These rock masses are transected by discontinuities such as fractures,

joints, and bedding planes, which normally control rock mass behavior (54). The measurements and analysis presented in this report indicate that shearing and separation tend to localize between beds of differing bending stiffness, and the methodology described in this report can be used to locate discontinuities with the greatest potential for slip and separation. It is reasonable to expect that such discontinuities at specific locations must be incorporated within numerical models (67). It is further concluded from the TDR field data that development of a laminated beam over high-extraction panels involves momentary bridging by individual beds or groups of beds.

It is hypothesized that the response of strata near the surface can be modeled as a laminated beam with a (1) fixed end support only, (2) a span that increases linearly with distance above the coal seam, and (3) a constant thickness. Based on data from eight mine sites in the Illinois Coal Basin, the laminated beam is required to have a thickness such that the maximum deflection is no greater than 70% of the mined thickness. The laminated beam thickness is unknown and may be greater, or less, than

that inferred from the bending stiffness and TDR measurements. The assumption of an unsupported span is only valid when panel widths are less than supercritical and when the span at first roof fall can be determined with certainty. For these reasons, bridging potential cannot be used to predict subsidence. Despite these limitations, the laminated beam model provides simple relations that can be implemented in a spreadsheet to objectively compare overburden behavior based on core logs and any number of possible mine geometries.

Empirical correlations between a subsidence factor and overburden geology have been developed by other researchers, but those are valid only for limited areas in which there is little variation in overburden geology. The spreadsheet developed in this study allows a user to determine a site-specific index parameter defined as the bridging potential, which is based on principles of engineering mechanics, provides a rational measure of a laminated beam's capacity to resist deflection, and is controlled by overburden geology as well as by the width and depth of the panel.

SUMMARY

This report focuses on the relationship between the bending stiffness of individual beds and subsurface displacements measured using TDR. Displacements measured over eight high-extraction coal mine panels in southern Illinois are compared with the bed stiffness profiles. Based on these comparisons it is hypothesized that, as the face approached and passed through a transverse cross section, the process of caving and subsidence over these high-extraction mines involved (1) shearing ahead of the face along horizontal discontinuities located far up into the overburden, (2) momentary bridging by individual beds or groups of beds, followed by (3) bed separation and vertical displacement, and (4) ultimate development of a laminated beam near the surface that rests on caved material. The thickness of the hypothesized laminated beam is based on mine geometry and significant differences in the bending stiffness of individual beds that coincide with horizontal discontinuities along which shearing occurred. The deflected profile of this near-surface laminated beam is

compared with the measured surface subsidence profile. Although it has been shown that a simple beam model is not appropriate for predicting subsidence over high-extraction mines, the spreadsheet provides a rational technique to graphically display the character of the overburden based on measured rock mass characteristics and a proposed mine plan.

The process documented in this report can be summarized as follows: (1) assemble core log in the TEMPLATE.WQ1 spreadsheet, (2) compute modified RMR for each bed identified in core log, (3) compute in situ modulus and bending stiffness for each bed, (4) compute maximum deflection for all possible laminated beam thicknesses, (5) determine the probable range of beam thicknesses required to limit the maximum deflection to a value between 70% and 35% of the mined thickness, (6) identify significant horizontal discontinuities within this range of beam thicknesses, and (7) compare TDR measurements with the predicted horizontal discontinuities.

REFERENCES

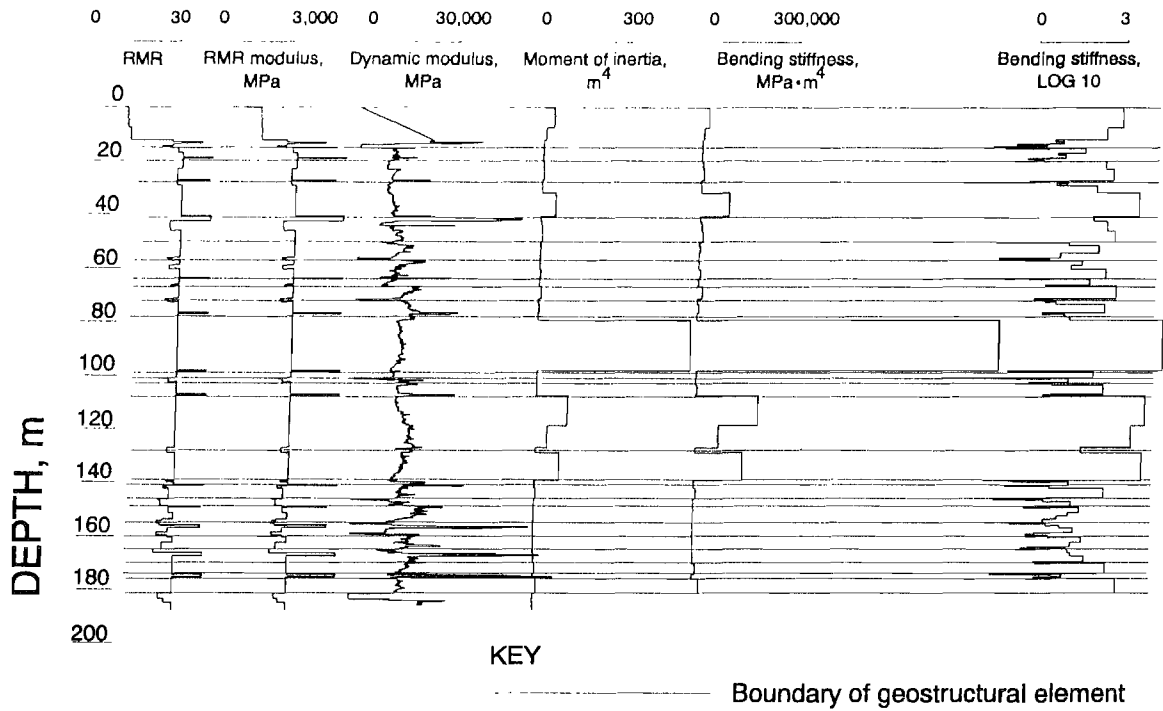
1. Adler, L. and M. C. Sun. Ground Control in Bedded Formations. Bulletin 28, Research Division, Virginia Polytechnic Institute, Blacksburg, December, 1968, 266 pp.
2. Allen, A. S. Basic Questions Concerning Mine Subsidence in the United States. Bull. Amer. Assoc. Eng. Geol., v. 15, No. 2, 1978, pp. 147-161.
3. American Institute of Steel Construction, Inc., Chicago, IL. Manual of Steel Construction. 7th edition, 1973.
4. Bai, M., D. Elsworth, Z. Li, and N. Tomlin. Evaluation of Stresses and Displacements Induced in Discretely Layered Media. Int. J. Rock Mech. Min. Sci. & Geomech. Abstr., Vol. 27, No. 1, 1990, pp. 23-31.

5. Barton, N., R. Lien, and J. Lunde. Engineering Classification of Rock Masses for the Design of Tunnel Support. *Rock Mechanics*, Vol. 6, No. 4, 1974, pp. 189-236.
6. Bauer, R. A., C. H. Dowding, D. J. Van Rosendaal, B. B. Mehnert, M. B. Su, and K. M. O'Connor. Application of Time Domain Reflectometry to Subsidence Monitoring. Final Report, Office of Surface Mining, Assistance Agreement No. HQ51-CT6-01537, Pittsburgh, PA, 1991, 48 pp.; NTIS PB 91-22841.
7. Benzley, S. E. and R. D. Krieg. A Continuum Finite Element Approach for Rock Failure and Rubble Formation. Sandia National Laboratories, Report SAND80-0227, Albuquerque, NM, 1980, 24 pp.
8. Bieniawski, Z. T. Engineering Classification of Jointed Rock Masses. *Transactions, South African Institution of Civil Engineers*, Vol. 15, No. 12, 1973, pp. 335-344.
9. _____. The Geomechanics Classification in Rock Engineering Applications. Paper in Proceedings of the 4th International Congress Rock Mechanics (Montreux, 1979), A. A. Balkema, Rotterdam, Vol. 2, 1979, pp. 41-48.
10. _____. Engineering Rock Mass Classifications. John Wiley and Sons, New York, NY, 1989, pp. 137-175.
11. Blair, B. E. Physical Properties of Mine Rock, Part 3. BuMines, RI 5130, Washington, D.C., 1955, 66 pp.
12. _____. Physical Properties of Mine Rock, Part 4. BuMines, RI 5244, Washington, D.C., 1956, 72 pp.
13. Booth, C. J. and E. D. Spande. Response of Groundwater Hydrology to Subsidence Above a Longwall Mine in Illinois. Paper in Proceedings of Session on Mine Subsidence - Prediction and Control, (Pittsburgh, October 1990), 33rd Annual Meeting, Assoc. of Eng. Geologists, 1990, pp. 113-118.
14. Brauner, G. Subsidence Due to Underground Mining - 1. Theory and Practices in Predicting Surface Deformation. BuMines IC 8571, 1973, 56 pp.
15. Brucher, D. F., B. B. Mehnert, D. J. Van Rosendaal, and R. A. Bauer. Rock Strength and Overburden Changes Due to Subsidence Over a Longwall Coal Mining Operation in Illinois. Paper in Rock Mechanics Contributions and Challenges (Proc. 31st U.S. Symp. on Rock Mechanics, Golden, CO), Balkema, 1990, pp. 563-570.
16. Carmichael, R. S. CRC Handbook of Physical Properties of Rocks. Volume II, CRC Press, Boca Raton, 1982, pp. 321-322.
17. Coulthard, M. A. and A. J. Dutton. Numerical Modelling of Subsidence Induced by Underground Coal Mining. Paper in Key Questions in Rock Mechanics (Proc. 29th U.S. Symp. on Rock Mechanics, Minneapolis, MN), Balkema, 1988, pp. 529-536.
18. Daemen, J. J. K. and M. Hood. Subsidence Profile Functions Derived from Mechanistic Rock Mass Models. Paper in the Proceedings of the Workshop on Surface Subsidence Due to Underground Mining, (Morgantown, WV, Nov. 30-Dec.2, 1981), West Virginia Univ., 1982, pp. 124-141.
19. Deere, D. U., A. J. Hendron, F. D. Patton, and E. J. Cording. Design of Surface and Near Surface Construction in Rock. Paper in Failure of Breakage of Rock (Proceedings of the 8th U.S. Symp. on Rock Mechanics, Minneapolis, MN), Am. Institute of Min., Met. and Petrol. Eng., New York, 1967, pp. 237-302.
20. Dhar, B. B., N. C. Saxena, and U. K. Singh. Rock Mass Characterization for Estimation of Support Load in Underground Galleries and for Prediction of Surface Subsidence in Indian Coalfields. Paper in Eurock '92 (Proceedings of Symp., Chester, U.K., September 1992), Int'l Soc. for Rock Mech., 1992, pp. 348-353.
21. Doney, E. D. and S. S. Peng. Subsidence Prediction in the Illinois Basin. Paper in the Proceedings of the 10th Conference on Ground Control in Mining, (Morgantown, June 10-12, 1991), West Virginia Univ., 1991, pp. 212-219.
22. Dowding, C. H. and F. C. Huang. Telemetric Monitoring for Early Detection of Rock Movement with Time Domain Reflectometry. *J. Geo. Eng., Am. Soc. Civ. Eng.*, v. 120, no. 8, 1994, pp. 1413-1427.
23. Dowding, C. H., M. B. Su, and K. M. O'Connor. Principles of Time Domain Reflectometry Applied to Measurement of Rock Mass Deformation. *Int. J. Rock Mechanics and Mining Sciences*, Vol. 25, No. 5, 1988, pp. 287-297.
24. Drumm, E. C. and R. M. Bennett. Subsidence Effects on Structures, Volume III: Reduced Data. Institute for Geotechnology, Report No. 92-01, University of Tennessee, Knoxville, September, 1992, pp. A-1 to A-22; available for inspection at the Bureau of Mines Twin Cities Research Center, Minneapolis, MN.
25. Dunrud, C. R. Coal Mine Subsidence - Western United States. Paper in Man-Induced Subsidence, ed. by T. L. Holzer, *Reviews in Eng. Geol.*, v. 6, *Geol. Soc. Amer.*, 1984, pp. 151-194.
26. Dunrud, C. R. and F. W. Osterwald. Effects of Coal Mine Subsidence in the Sheridan, Wyoming Area. USGS Prof. Paper 1164, 1980, 49 pp.
27. Fekete, S. Mathematical Models of Composite Structures. Chapter 4 and Chapter 7 in *Soil Settlement Effects on Buildings*, E. Dulácska, ed., Elsevier Science Publishing Co., New York, NY, 1992, pp.157-220 and pp.359-443.
28. Ghose, A. H. and D. Gupta. A Rock Mass Classification Model for Caving Roofs. *International Journal of Mining and Engineering Geology*, Vol. 5, 1988, pp. 257-271.
29. Golder Associates. Geotechnical Study of Rock Mass Classification Parameters for Sydney Coal Field, Nova Scotia. Report to CANMET, DSS Contract No. 09SQ.23440-8-9002, Ottawa, Ontario, Canada, Aug. 1989, 111 pp., 91 figs., 15 tables.
30. Gray, R. E. and R. W. Bruhn. Coal Mine Subsidence - Eastern United States. Paper in Man-Induced Land Subsidence, ed. by T.L. Holzer, *Reviews in Eng. Geol.*, v. 6, *Geol. Soc. Amer.*, 1984, pp. 123-149.
31. Griffel, W. Handbook of Formulas for Stress and Strain. Frederick Ungar Publishing Company, New York, 1966, pp. 24-51.
32. Harmel, R. M. North-South, East-West Movement and Surface Subsidence, Old Ben 21, Sesser, Illinois. Memo to L. A. Panek, BuMines, Denver, September 13, 1972, 15 pp.; available for inspection at the Bureau of Mines, Twin Cities Research Center, Minneapolis, MN.
33. Hasenfus, G. J., K. L. Johnson, and D. W. H. Su. A Hydrogeomechanical Study of Overburden Aquifer Response to Longwall Mining. Paper in the Proceedings of the 7th International Conference on Ground Control in Mining, (Morgantown, WV, August 3-5, 1988), West Virginia University, 1988, pp. 149-161.
34. Hasenfus, G. J. and D. W. H. Su. Comprehensive Integrated Approach for Longwall Development Design. Paper in the Proceedings of the Workshop on Coal Pillar Mechanics and Design, BuMines IC 9315, 1992, pp. 225-237.
35. Haycocks, C. and C. D. Breeds. Ground Control Simulation During Longwall Mining. Paper in the Proceedings of the 16th Symposium on Application of Computers and Operations Research in the Mineral Industry, AIME, New York, 1979, pp. 528-536.
36. Hetényi, M. Series Solutions for Beams on Elastic Foundations. *Journal of Applied Mechanics*, *Transactions of the Am. Soc. of Mech. Eng.*, June, 1971, pp. 507-514.
37. Hunt, S. R. Surface Subsidence Due to Coal Mining in Illinois. Ph.D. dissertation, Univ. of Illinois, Urbana-Champaign, 1980, 129 pp.
38. Illinois State Geological Survey. Rock Mechanics Laboratory Test Results, Heron Road Subsidence Research Site (Contract PO 213293), March, 1993, 35 pp.; available for inspection at the Bureau of Mines, Twin Cities Research Center, Minneapolis, MN.
39. _____. Rock Mechanics Laboratory Test Results, North Marcum Subsidence Research Site (Contract PO 233118), October, 1993, 38 pp.; available for inspection at the Bureau of Mines, Twin Cities Research Center, Minneapolis, MN.
40. Dames and Moore. A Demonstration of Longwall Mining - Appendix (Contract JO 3339-9, Old Ben Coal Co.), BuMines OFR 86(2)-85, 1983, 371 pp.

41. Kane, W. F. and L. R. Powell. The Effects of Geology on Coal Mine-Induced Subsidence in the United States. Paper in Geology in Coal Resource Utilization, ed. by D. C. Peters, TechBooks, Fairfax, VA, 1991, pp. 335-355.
42. Kendorski, F. S. Effect of High-Extraction Coal Mining on Surface and Ground Waters. Paper in the Proceedings of the 12th International Conference on Ground Control in Mining, (Morgantown, August 3-5, 1993), West Virginia Univ., 1993, pp. 412-425.
43. Kendorski, F. S., R. A. Cummings, Z. T. Bieniawski, and E. H. Skinner. Rock Mass Classification for Block Caving Drift Support. Paper in the Proceedings of the International Congress on Rock Mechanics, (Melbourne, Australia, 1983), Balkema, Vol. B, 1983, pp. 51-63.
44. Kidybinski, A. Classification of Rocks for Longwall Cavability. Paper in State-of-the-Art of Ground Control in Longwall Mining and Mining Subsidence, (Proc. of Symposium SME-AIME Meeting, September, 1982), Soc. Min. Eng., New York, 1982, pp. 31-37.
45. Laubscher, D. H. A Geomechanics Classification System for the Rating of Rock Mass in Mine Design. J. South African Inst. of Mining and Metallurgy, Vol. 90, No. 10, 1990, pp. 257-273.
46. Laubscher, D. H., and H. W. Taylor. The Importance of Geomechanics Classification of Jointed Rock Masses in Mining Operations. Paper in the Proceedings of the Symposium on Exploration for Rock Engineering (Johannesburg, South Africa, 1976), Int. Soc. for Rock Mech., 1976, pp. 119-128.
47. Lauffer, H. Gebirgsklassifizierung für den Stollendau. Geologie und Bauwesen, Vol. 24, No. 1, 1958, pp. 46-51.
48. Marino, G. G. Analysis of Initial Collapse of the Overburden Over Longwall Panels Using Subsidence Data. Paper in the Proceedings of the 7th International Conference on Ground Control in Mining (Morgantown, August, 1988), West Virginia Univ., 1988, pp. 234-246.
49. Mehnert, B. B., D. J. VanRoosendaal, R. A. Bauer, D. Barkley, and E. Gefell. Final Report of Subsidence Investigations Over a High-Extraction Retreat Mine in Williamson County, Illinois. Illinois Mine Subsidence Research Program, Illinois State Geological Survey, Champaign, Illinois, September, 1992, 92 pp.
50. Munson, D. E. and S. E. Benzley. Analytical Subsidence Model using Void-Volume Distribution Functions. Paper in the State of the Art in Rock Mechanics (Proc. 21st U.S. Symp. on Rock Mech., Rolla, MO), Univ. of Missouri-Rolla, 1980, pp. 299-307.
51. National Coal Board. Subsidence Engineers' Handbook, Camgate Litho Ltd, London, 1975, 111 pp.
52. Obert, L., and W. I. Duvall. Rock Mechanics and the Design of Structures in Rock. John Wiley & Sons, New York, NY, 1967, pp. 561-562.
53. O'Connor, K. M., and C. H. Dowding. Distinct Element Modeling and Analysis of Mining-Induced Subsidence. Rock Mechanics and Rock Engineering, Vol. 25, 1992, pp. 1-24.
54. O'Connor, K. M., J. E. O'Rourke, and J. Carr. Influence of Rock Discontinuities on Coal Mine Subsidence (Contract No. J0100087), BuMines OFR 30-84, 1983, 129 pp; NTIS PB84-166370.
55. Peng, S. S. and H. S. Chiang. Longwall Mining. John Wiley & Sons, New York, 1984, 708 pp.
56. Piciacchia, L., M. C. Betourney and D. Labrie. Rock Mechanics Investigation and Assessment of Near Surface Crown Pillar Stability at Four Ontario and Quebec Mines. Paper in the Proceedings of the International Conference on Surface Crown Evaluation for Active and Abandoned Mines, (Timmons, Ontario, 1989), CANMET, Ottawa, 1989, pp. 47-56.
57. Piggott, R. J. and P. Eynon. Ground Movements Arising from the Presence of Shallow Abandoned Mine Workings. Paper in Large Ground Movements and Structures (Proc. of Conference, Cardiff, Wales, July 4-7, 1977), Halsted Press, London, 1978, pp. 749-780.
58. Popov, E. P. Introduction to Mechanics of Solids. Prentice-Hall, Englewood Cliffs, NJ, 1968, pp.486-487.
59. Powell, L. R. and P. B. DuMontelle. The Illinois-Bureau of Mines Cooperative Mine Subsidence Research Program. Paper in the Proceedings of the Second Conference on Ground Control Problems in the Illinois Coal Basin (Carbondale, May, 1985), Southern IL Univ., 1985, pp. 13-17.
60. Price, D. G., A. B. Malkin and J. L. Knill. Foundations of Multi-story Blocks on the Coal Measures with Special Reference to Old Mine Workings. Quart. Jour. Engng. Geol., v. 1, 1969, pp. 271-322.
61. Pulse, R. R. Results of the Subsidence Study at Old Ben No. 21; (OCT. 68 - JULY 70) Settlement Probe, BPC & TDR Monitoring Methods. In-house report, BuMines, Denver, July, 1970, 4 pp.; available for inspection at the Bureau of Mines, Twin Cities Research Center, Minneapolis, MN.
62. Pytel, W. M., and Y. P. Chugh. Subsidence Prediction in Longwall Mining Using a Beam Theory Based Simplified Analytical Model. Paper in the Proceedings of the 3rd Workshop on Surface Subsidence Due to Underground Mining (Morgantown, June 1-4, 1992), West Virginia Univ., 1992, pp. 66-75.
63. Salamon, M. D. G. and G. Yang. The Seam Element Method: Prediction of Subsidence Due to Coal Mining. Paper in the Proceedings of the 3rd Workshop on Surface Subsidence Due to Underground Mining, (Morgantown, June 1-4, 1992), West Virginia Univ., 1992, pp. 47-55.
64. Scott, R. F. Foundation Analysis. Prentice-Hall, Inc., Englewood Cliffs, NJ, 1981, pp. 62-67.
65. Serafim, J. L., and J. P. Pereira. Considerations of the Geomechanics Classification of Bieniawski. Paper in the Proceedings of the International Symposium on Engineering Geology and Underground Construction (Boston, MA, 1983), Balkema, 1983, pp. 33-34.
66. Sheorey, P. R. Experiences with Application of the NGI Classification to Coal Measures. Int. J. Rock Mech. Min. Sci. & Geomech. Abstr., Vol. 28, No. 1, 1991, pp. 27-33.
67. Siekmeier, J. A. and K. M. O'Connor. Modeling Overburden Response to Longwall Mining. Paper in the Proceedings of the First Canadian Symposium on Numerical Modelling Applications in Mining and Geomechanics (Montreal, Quebec, March 27-30, 1993), McGill Univ., 1993, pp. 110-118.
68. Singh, M. M. Experience with Subsidence due to Mining. Paper in Evaluation and Prediction of Subsidence (Int'l Conf., Pensacola, FL, January 1978), ASCE, New York, 1978, pp. 92-112.
69. Siriwandane, H. J. and J. Amanat. Prediction of Subsidence in Hilly Ground Terrain Using Finite Element Method. Paper in the Proceedings of the 2nd International Conference on Stability in Underground Mining (Lexington, Kentucky, August 1984), AIME, New York, 1984, pp. 554-575.
70. Su, D. W. H. Finite Element Modeling of Subsidence Induced by Underground Coal Mining: The Influence of Material Nonlinearity and Shearing Along Existing Planes of Weakness. Paper in the Proceedings of the 10th International Conference on Ground Control in Mining (Morgantown, June, 1991), West Virginia Univ., 1991, pp. 287-300.
71. Sutherland, H. J., K. W. Schuler, and S. E. Benzley. Numerical and Physical Simulations of Strata Movement Above Idealized Mine Structures. In Situ, Vol. 7, No. 1, 1983, pp. 87-113.
72. Szostak-Chrzanowski, A. An interactive Modeling of Ground Subsidence using Nonlinear Elastic Finite Element Analysis. Paper in the Proceedings of the 5th Canadian Symposium on Mining Surveying and Rock Deformation Measurements, (Fredericton, New Brunswick, 1988), Univ. New Brunswick, 1988, pp. 524-535.
73. Tandanand, S. and L. R. Powell. Assessment of Subsidence Data from the Northern Appalachian Basin for Subsidence Prediction. BuMines RI 8630, 1982, 14 pp.
74. _____. Consideration of Overburden Lithology for Subsidence Prediction. Paper in the Proceedings of the Workshop on Surface Subsidence Due to Underground Mining (Morgantown, WV, 1981), West Virginia Univ., 1981, pp. 17-29.
75. _____. Influence of Lithology on Longwall Mining Subsidence. Mining Engineering, v. 36, 1984, pp. 1666-1671.
76. Tandanand, S., and T. Triplett. New Approach for Determining Ground Tilt and Strain Due to Subsidence. Paper in the Proceedings of the National Symposium on Mining, Hydrology, Sedimentology, and

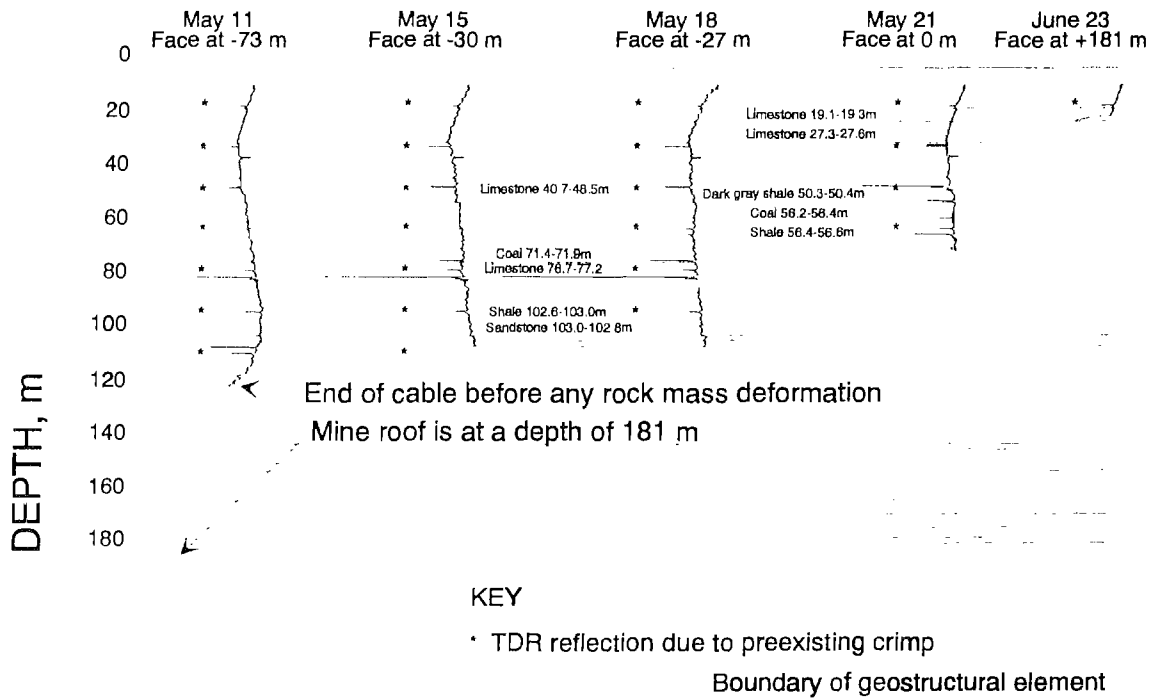
- Reclamation (Lexington, KY, 1987), Univ. of Kentucky, 1987, pp. 217-221.
77. Terzaghi, K. Rock Defects and Loads on Tunnel Support. Rock Tunneling with Steel Supports, eds. Proctor and White, Commercial Shearing Co., Youngstown, OH, 1946, pp. 15-99.
78. Treworgy, C. Designing a Stratigraphic Database: An Example from the Coal Section of the Illinois State Geological Survey. *Geobyte*, April, 1992, pp. 33-37.
79. Triplett, T. L. and D. W. Yurchak. Determination of an Intensity Function for Subsidence Prediction. Paper in Rock Mechanics Contributions and Challenges (Proc. 31st U.S. Symp. on Rock Mech., Golden, CO), Balkema, 1990, pp. 169-175.
80. _____. Predicting the Effects of Subsidence from High Extraction Mining in Illinois. Paper in the Proceedings of the Symposium on Mine Subsidence - Prediction and Control (Pittsburgh, October, 1990), Assoc. Eng. Geo., 1990, pp. 71-77.
81. Unal, E. Development of Design Guidelines and Roof Control Standards for Coal Mine Roofs. Ph.D. Dissertation, Pennsylvania State University, August, 1983, 355 pp.
82. Unal, E., and I. Ozkan. Characterization of Weak, Stratified and Clay-Bearing Rock Masses. Paper in Eurock '92 (Proc. of Symposium, Chester, U.K., September 1992), Int'l. Soc. for Rock Mech., 1992, pp. 330-335.
83. Unrug, K. and T. B. Szwiłski. Strata Cavability in Longwall Mining. Paper in the Proceedings of the First International Conference on Stability in Underground Mining (Lexington, KY, August 1983), AIME, New York, 1984, pp. 131-147.
84. Van Roosendaal, D. J., D. F. Bratcher, B. B. Mehnert, J. T. Kelleher, and R. Bauer. Overburden Deformation and Hydrologic Changes Due to Longwall Mine Subsidence in Illinois. Paper in the Proceedings of the 3rd Conference on Ground Control Problems in the Illinois Coal Basin (Carbondale, June, 1990), Southern Illinois Univ., 1990, pp. 73-82.
85. Van Roosendaal, D. J., B. B. Mehnert, and R. A. Bauer. Three-Dimensional Ground Movements During Dynamic Subsidence of a Longwall Mine in Illinois. Paper in the Third Workshop on Surface Subsidence Due to Underground Mining (Morgantown, WV, June 1-4, 1992) West Virginia Univ., 1992, pp. 290-298.
86. Vogeles, M. D. A Rational Design of Tunnel Supports: An Interactive Graphics Based Analysis of Support Requirements of Excavations in Jointed Rock Masses. U.S. Army, W.E.S. Technical Report GL-79-15, September, 1979, 525 pp.
87. Wade, L. V. and P. J. Conroy. Rock Mechanics Study of a Longwall Panel. Mining Engineering (Littleton, CO), December, 1980, pp. 1728-1734.
88. Wardell, K. World Wide Approaches to Subsidence Prediction. Section in Environmental and Geotechnical Considerations in Subsidence Engineering, Short Course, (Pittsburgh, PA, May 31-June 3, 1983), Univ. Missouri-Rolla, 1983, 13 pp.
89. Wardell, K. and J. C. Wood. Ground Instability Problems Arising from the Presence of Old Shallow Mine Workings. Proceedings of the Midland Soil Mechanics and Foundation Engineering Society, v. 7, 1966, Paper No. 36, pp. 5-30.
90. Webb, B. A Study of Longwall Subsidence in the Appalachian Coal Field. M. S. Thesis, Virginia Polytechnic Institute and State University, Blacksburg, 1982, 204 pp.
91. Whittaker, B. N., P. Gaskell, and D. J. Reddish. Subsurface Ground Strain and Fracture Development Associated with Longwall Mining. Mining Science and Technology, Vol. 10, 1990, pp. 71-80.
92. Wickham, G. E., H. R. Tiedemann, and E. H. Skinner. Ground Support Prediction Model - RSR Concept. Paper in the Proceedings of the 2nd Rapid Excavation and Tunneling Conference (San Francisco, 1974), AIME, New York, 1974, pp. 691-707.
93. _____. Support Determination Based on Geologic Predictions. Paper in the Proceedings of the Rapid Excavation and Tunneling Conference (New York, 1972), AIME, New York, 1972, pp. 43-64.
94. Windes, S. L. Physical Properties of Mine Rock, Part 1. BuMines, RI 4459, Washington, D.C., 1949, 79 pp.
95. _____. Physical Properties of Mine Rock, Part 2. BuMines, RI 4727, Washington, D.C., 1950, 40 pp.
96. Wold, M. B. Physical Model Study of Caving Under Massive Sandstone Roof Conditions at Moura, Queensland. CSIRO, Division of Geomechanics, Report No. 57, 1984, 63 pp.
97. Yenge, L. I. Analysis of Bulk Flow of Materials Under Gravity Caving Process. Part 2: Theoretical and Physical Modeling of Gravity Flow of Broken Rock. Colorado School of Mines Quarterly, Vol., 76, No. 3, July, 1981, 67 pp.

Figure 1



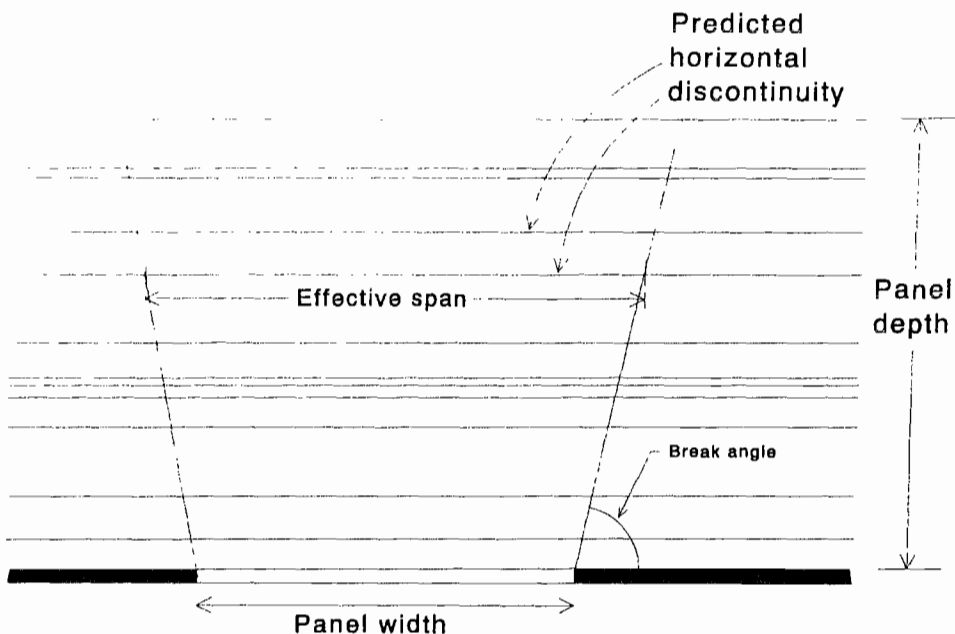
Horizontal discontinuities defined by bending stiffness profile.

Figure 2



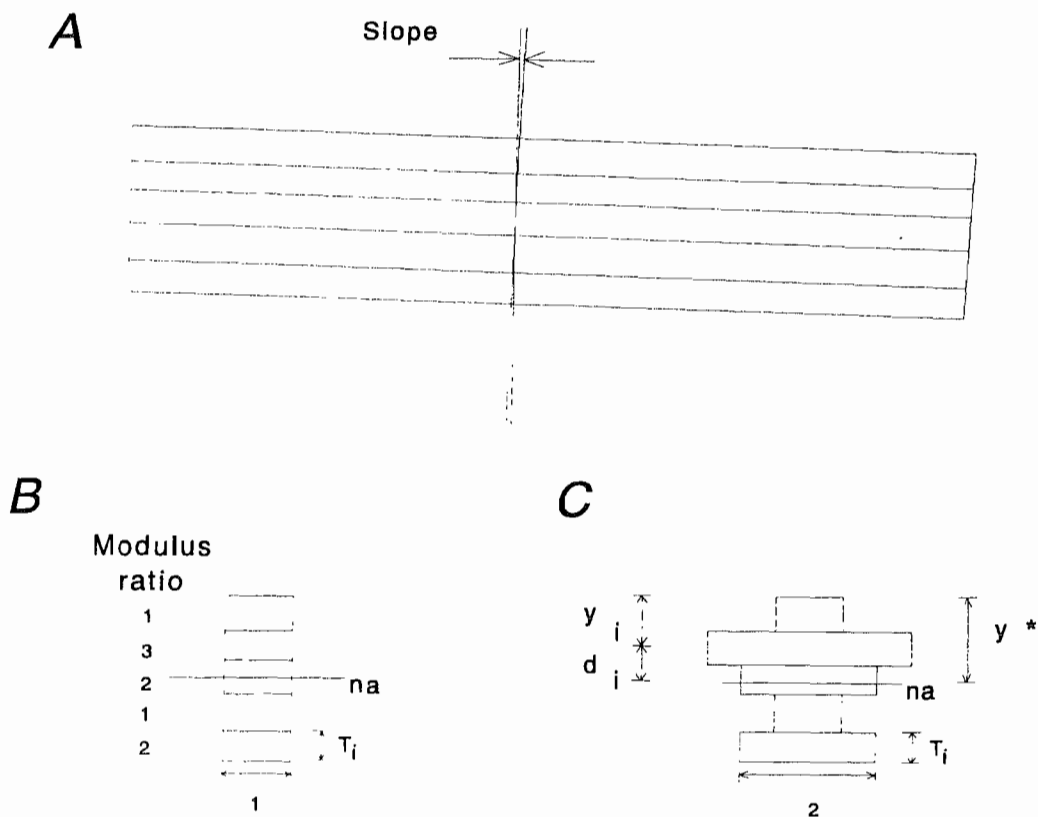
Horizontal discontinuities compared with TDR measurements.

Figure 3



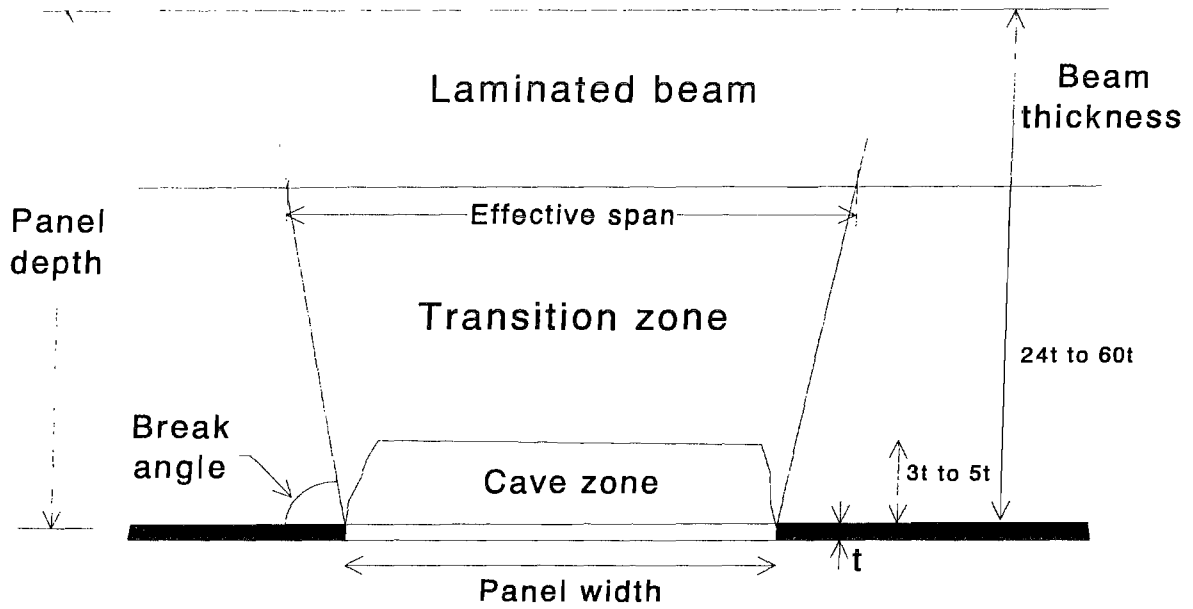
Boundaries of geostructural elements defined by predicted horizontal discontinuities.

Figure 4



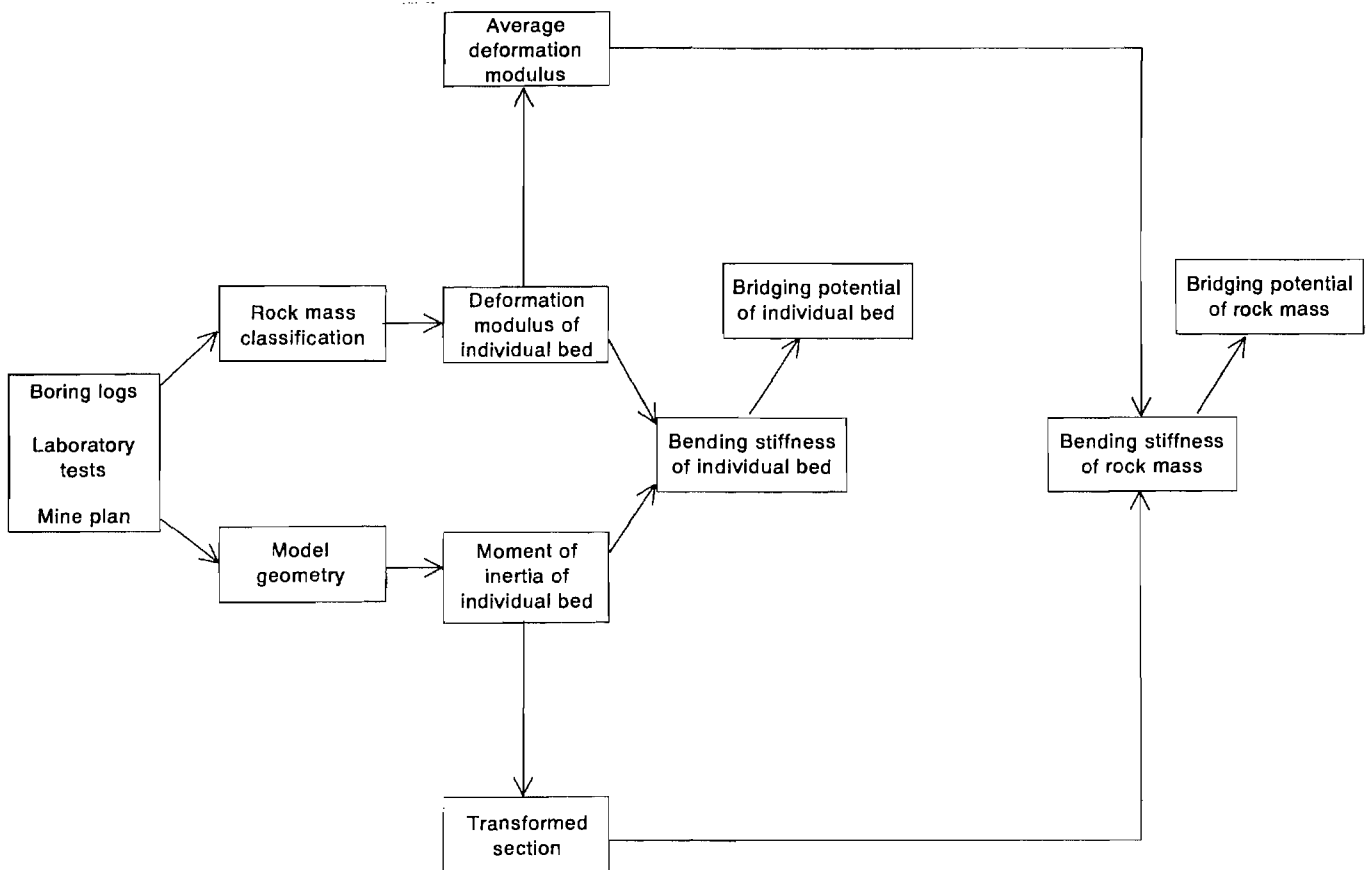
Transformed cross section of equivalent elastic beam. A, Bending deflection of laminated beam. B, Original unit width cross section and modulus ratio. C, Width of laminae transformed in proportion to modulus.

Figure 5



Conceptual model of overburden response to high-extraction coal mining.

Figure 6



Flowchart for spreadsheet.

Figure 7

A	B	C	D	E	F	
1	FILENAME	ROCKPRP.QW1				
2	FLOPPY	F104				
3	DATE	1-6-94				
4						
5	THIS SPREADSHEET PROVIDES THE STRENGTH AND DENSITY					
6	OF THE ROCK TYPES USED IN THE TEMPLT SPREADSHEET					
7						
8						
9	STRENGTH AND DENSITY ESTIMATED BASED ON DATA IN					
10	REFERENCES LISTED IN CELLS H1 TO H16					
11						
12						
13	MATERIAL	COLOR	STRENGTH	DENSITY		
14			PSI	MPa	lb/# ³	
15					kg/m ³	
16	CLAYSTONE	GRAY	9000	62	150	2408
17	CLAYSTONE	LT GRAY	9000	62	150	2408
18	CLAYSTONE	MED GRAY	9000	62	150	2408
19	CLAYSTONE	DK GRAY	9000	62	150	2408
20	CLAYSTONE	GRAY TO GREEN	9000	62	150	2408
21						
22	COAL		1200	8	130	2087
23						
24	CONGLOMERATE		11000	76	150	2408
25						
26	LIMESTONE	GRAY	20000	138	150	2408
27	LIMESTONE	LT GRAY	20000	138	150	2408
28	LIMESTONE	MED GRAY	20000	138	150	2408
29	LIMESTONE	DK GRAY	20000	138	150	2408
30	LIMESTONE	GRAY TO BROWN	20000	138	150	2408
31	LIMESTONE	BROWN	20000	138	150	2408
32						
33	MUDSTONE	GRAY	4800	33	140	2247
34						
35	SANDSTONE	GRAY	6000	41	135	2167
36	SANDSTONE	LT GRAY	6000	41	135	2167
37	SANDSTONE	MED GRAY	6000	41	135	2167
38	SANDSTONE	DK GRAY	6000	41	135	2167
39						
40	SHALE	GRAY	8000	55	150	2408
41	SHALE	LT GRAY	8000	55	150	2408
42	SHALE	MED GRAY	8000	55	150	2408
43	SHALE	DK GRAY	8000	55	150	2408
44	SHALE	GRAY TO GREEN	8000	55	150	2408
45	SHALE	BLACK	8000	55	150	2408
46						
47	SILTSTONE	GRAY	9000	62	160	2568
48	SILTSTONE	LT GRAY	9000	62	160	2568
49	SILTSTONE	MED GRAY	9000	62	160	2568
50	SILTSTONE	DK GRAY	9000	62	160	2568
51	SILTSTONE	GRAY TO GREEN	9000	62	160	2568
52	SILTSTONE	GRAY TO BROWN	9000	62	160	2568
53	SILTSTONE	GREEN	9000	62	160	2568
54	SILTSTONE	BROWN	9000	62	160	2568
55						
56	CLAY BEAM		20	0	120	1926
57						
58	SIDERITE		10000	69	160	2568
59						
60	PYRITE		8000	55	160	2568
61						
62	BONE		1100	8	130	2087
63						
64	SOIL		20	0	120	1926
65	CLAYEY SOIL		20	0	120	1926
66	SILTY SOIL		20	0	120	1926
67	SANDY SOIL		20	0	120	1926

Rock properties lookup table.

Figure 8

	A	B	C	D	E	F	G	H	I	J	K	L
1		FILENAME	RMR-TBLS QW1									
2		FLOPPY										
3		DATE	05-24-93									
4												
5												
6												
7												
8												
9												
10												
11												
12												
13												
14												
15												
16												
17												
18												
19												
20												
21												
22												
23												
24												
25												
26												
27												
28												
29												
30												
31												
32												
33												
34												
35												
36												

RMR1 FROM UNIAXIAL			
STRENGTH			
LOW	HIGH		RMR1
MPa	MPa		
0	1		0
1	4		1
5	24		2
25	49		4
50	99		7
100	249		12
250			15

RMR2 FROM RQD			
RQD	RQD		RMR2
LOW	HIGH		
%	%		
NA			ERR
			ERR
0	24		3
25	49		8
50	74		13
75	89		17
90	100		20

RMR3 FROM BEDDING THICKNESS		
THICKNESS	m	RMR3
NA		ERR
		ERR
VERY THIN	<0.06	5
THIN	0.06-0.20	8
MEDIUM	0.20-0.60	10
THICK	0.60-2.00	15
VERY THICK	>2.0	20

RMR4 FROM BED CONTACT	
CONDITION	RMR4
NA	ERR
	ERR
GOUGE FILLED	0
MUDDY	2
SLICKEN INT	3
SLICKEN SIM	5
PLA SMO INT	10
PLA SMO SIM	15
SL ROUGH INT	20
SL ROUGH SIM	25
VERY ROUGH	30

RMR5 FROM GROUNDWATER	
CONDITION	RMR5
NA	ERR
	ERR
FLOWING	0
DRIPPING	4
WET	7
DAMP	10
DRY	15

RMR6 JOINT ORIENTATION	
ORIENTATION	RMR6
NA	ERR
	ERR
V UNFAVORABLE	-12
UNFAVORABLE	-10
FAIR	-5
FAVORABLE	-2
V FAVORABLE	0

Rock mass rating criteria.

Figure 9

TEMPLATE	A	B	C	D	E	F	G	H	I	J	K	L	M	N
1	filename		TEMPLATE.WB1											
2	datefile		RJ-NM.WQ1											
3	date		06-26-95											
4														
5														
6														
7														
8														
9														
10														
11														
12														
13														
14														
15														
16														
17														
18										90.00	DEG			
19														
20										384.00				
21										181.4	METERS			
22										98.33	METERS			
23														
24										2108.13	MPa			
25														
26														
27										53.54	METERS			
28										305.00	METERS			
29										334.08	METERS	334.08		
30										10.00	DEGREES			
31														
32														
33														
34														
35														
36														
37														
38														
39														
40														
41														
42														
43														
44														
45														
46														
47														
48														
49														
50														
51														
52														
53														

FOOTAG START OF BED	ROCK TYPE	COLOR	RECOVERY		RQD		BEDDING PLANE THICKNESS	BED CONTACT COND	GROUND WATER CONDITION	ADJUST FOR JOINT ORIENTATION	ADJUST FOR FAULTS	ADJUST FOR STRESS	MEASURED MODULUS
			LOW	HIGH	LOW	HIGH							
ft			%	%	%	%	m						MPa
0.00	SOIL	CLAYEY			0.00	0.00	NA		WET	FAIR		0.75	0.75
25.00	SHALE	NA			0.00	0.00	NA		WET	FAIR		0.75	0.75
40.00	SANDSTONE	LT GRAY	100.00	100.00	57.00	57.00	VERY THIN	PLA SMO INT	WET	FAIR		0.75	0.75
42.00	LMESTONE	LT GRAY	100.00	100.00	57.00	57.00	MEDIUM	SL ROUGH INT	WET	FAIR		0.75	0.75
45.20	CONGLOMERAT	LT GRAY	100.00	100.00	57.00	57.00	VERY THIN	PLA SMO INT	WET	FAIR		0.75	0.75
46.00	SHALE	DK GRAY	100.00	100.00	57.00	75.00	VERY THIN	PLA SMO INT	WET	FAIR		0.75	0.75
48.00	COAL	BLACK	100.00	100.00	75.00	75.00	VERY THIN	MUDDY	WET	FAIR		0.75	0.75
48.50	CLAYSTONE	OF Y TO GREEN	100.00	100.00	89.00	89.00	VERY THIN	SLICKEN INT	WET	FAIR		0.75	0.75
50.50	LMESTONE	GR Y TO GREEN	100.00	100.00	89.00	89.00	MEDIUM	SL ROUGH INT	WET	FAIR		0.75	0.75
51.00	SHALE	GR Y TO GREEN	100.00	100.00	89.00	89.00	VERY THIN	PLA SMO INT	WET	FAIR		0.75	0.75
56.00	SHALE	DK GRAY	100.00	100.00	100.00	****	VERY THIN	PLA SMO INT	WET	FAIR		0.75	0.75

Core description of individual beds.

Figure 10

TEMPLATE	P	Q	R	S	T	U	V	W	X	Y	Z	AA
1												
2												
3												
4												
5												
6												
7												
8												
9												
10												
11												
12												
13												
14												
15												
16												
17												
18												
19												
20												
21												
22												
23												
24												
25												
26												
27												
28												
29												
30												
31												
32												
33	START DEPTH OF BED	END DEPTH OF BED	START DEPTH OF BED	END DEPTH OF BED	UNI	RMR1	RMR2	RMR3	RMR4	RMR5	RMR6	ADJUSTED RMR
34	ft	ft	m	m	MPa							
35												
36												
37												
38												
39												
40												
41												
42												
43	0.00	25.00	0.00	7.62	0.14	0.00	ERR	ERR	ERR	7.00	-5.00	1.13
44	25.00	40.00	7.62	12.19	55.17	7.00	ERR	ERR	ERR	7.00	-5.00	5.06
45	40.00	42.60	12.19	12.98	41.38	4.00	13.00	5.00	10.00	7.00	-5.00	19.13
46	42.60	45.20	12.98	13.78	137.93	12.00	13.00	10.00	20.00	7.00	-5.00	32.06
47	45.20	46.00	13.78	14.02	75.86	7.00	13.00	5.00	10.00	7.00	-5.00	20.81
48	46.00	48.00	14.02	14.63	55.17	7.00	13.00	5.00	10.00	7.00	-5.00	20.81
49	48.00	48.50	14.63	14.78	8.28	2.00	17.00	5.00	2.00	7.00	-5.00	15.75
50	48.50	50.50	14.78	15.39	62.07	7.00	17.00	5.00	3.00	7.00	-5.00	19.13
51	50.50	51.00	15.39	15.54	137.93	12.00	17.00	10.00	20.00	7.00	-5.00	34.31
52	51.00	56.60	15.54	17.25	55.17	7.00	17.00	5.00	10.00	7.00	-5.00	23.06
53	56.60	59.20	17.25	18.04	55.17	7.00	20.00	5.00	10.00	7.00	-5.00	24.75

BIENIAWSKI'S

$$RMR = RMR1 + RMR2 + RMR3 + RMR4 + RMR5$$

where

RMR1 reflects strength of intact rock material

RMR2 reflects drill core quality (RQD)

RMR3 reflects spacing of discontinuities

RMR4 reflects condition of discontinuities

RMR5 reflects ground water conditions

$$ADJUSTED RMR = (RMR1 + RMR2 + RMR3 + RMR4 + RMR5 + RMR6) \cdot$$

where:

RMR6 is a negative number

and is an adjustment for joint orientations

A is an adjustment for major faults

B is an adjustment for adjacent excavations

Adjusted rock mass rating of individual beds.

Figure 11

TEMPLATE	AC	AD	AE	AF	AG	AH	AI	AJ	AK
1									
2									
3									
4									
5									
6									
7									
8									
9									
10									
11									
12									
13									
14									
15									
16									
17									
18		B							
19									
20									
21									
22									
23									
24									
25									
26									
27									
28									
29									
30									
31									
32									
33									
34									
35									
36									
37									
38									
39									
40									
41									
42									
43									
44									
45									
46									
47									
48									
49									
50									
51									
52									
53									

ESTIMATED MODULUS BED	THICKNESS BED	MOMENT INERTIA BED	STIFFNESS UNIT WIDTH BED	LOG STIFFNESS UNIT WIDTH BED +	UNIT WIDTH SELF WEIGHT BED	DEFLECTION UNIT WIDTH SELF WEIGHT BED	INVERSE OF DEFLECTION X	LOG INVERSE OF DEFLECTION +
E	d	d ³ /12	EI	0.00	EI A w	wL ⁴ /4EI	10000000.00	10.00
MPa	m	m ⁴ /m	MPa m ³		m ³	m		
599.96	7.62	36.87	22121.20	4.34	58993238.29	304.40	32851.24	7.52
752.60	4.57	7.96	5993.77	3.78	21312393.40	827.85	12079.53	7.08
1690.93	0.79	0.04	70.13	1.85	1598513.81	11003.56	908.80	5.96
3560.92	0.79	0.04	147.69	2.17	3029677.50	5787.88	1727.75	6.24
1863.43	0.24	0.00	2.25	0.35	150099.65	116714.74	85.68	4.93
1863.43	0.61	0.02	35.18	1.55	938122.81	18630.26	536.76	5.73
1392.36	0.15	0.00	0.41	-0.39	50550.46	345538.68	28.94	4.46
1690.93	0.61	0.02	31.92	1.50	851279.54	20470.20	488.52	5.69
1053.34	0.15	0.00	1.20	0.08	127538.03	136551.83	73.23	4.86
2121.11	1.71	0.41	879.00	2.94	8371933.31	2066.48	4839.15	6.68
2337.49	0.79	0.04	96.95	1.99	1988766.99	8672.28	1153.10	6.06

Stiffness and deflection of individual beds.

Figure 12

TEMPLATE	AM	AN	AO	AP	AQ	AR	AS	AT	AU	AV	AW	AX	AY
1													
2													
3													
4													
5													
6													
7													
8													
9													
10													
11													
12													
13													
14													
15													
16													
17													
18													
19													
20													
21													
22													
23													
24													
25													
26													
27													
28													
29													
30													
31													
32													
	Ed	WEIGHTED MODULUS ROCKMASS	MODULUS RATIO	TRANSFORMED WIDTH	TRANSFORMED AREA	DEPTH CENTER OF BED	A* y	DEPTH NEUTRAL AXIS ROCKMASS	DISTANCE OF BED FROM N AXIS	MOMENT INERTIA UNIT WIDTH BED	A* Dy ²	MOMENT INERTIA UNIT WIDTH ROCKMASS	STIFFNESS UNIT WIDTH ROCKMASS
	MPa m	MPa	E/E*	b*	A*	y	m ³	m	m	m ⁴ /m	m ⁴ /m	m ⁴ /m	MPa m ³
33													
34													
35													
36													
37													
38													
39													
40													
41													
42													
43	4571.72	599.96	0.28	0.28	2.17	3.81	8.26	3.81	49.73	10.49	5363.90	5374.40	3224443.33
44	3440.87	657.20	0.36	0.36	1.63	9.91	16.17	6.43	43.64	2.84	3108.08	8483.32	5376559.65
45	1340.03	720.29	0.80	0.80	0.64	12.59	8.00	7.31	40.96	0.03	1066.19	9551.34	6879903.81
46	2821.96	883.69	1.69	1.69	1.34	13.38	17.91	8.72	40.16	0.07	2159.24	11710.85	10348783.35
47	454.38	906.73	0.88	0.88	0.22	13.90	3.00	8.90	39.64	0.00	338.76	12049.61	10833453.57
48	1135.95	940.84	0.88	0.88	0.54	14.33	7.72	9.35	39.22	0.02	828.76	12878.39	12116541.73
49	212.19	945.90	0.66	0.66	0.10	14.71	1.48	9.43	38.84	0.00	151.82	13030.21	12320032.68
50	1030.79	975.02	0.80	0.80	0.49	15.09	7.38	9.82	38.46	0.02	723.10	13753.33	13409762.91
51	617.73	1005.20	1.92	1.92	0.29	15.47	4.53	10.04	38.07	0.00	424.79	14178.12	14251835.28
52	3620.47	1115.61	1.01	1.01	1.72	16.40	28.16	11.24	37.15	0.42	2369.60	16548.14	18461220.89
53	1852.42	1169.27	1.11	1.11	0.88	17.65	15.51	11.80	35.90	0.05	1132.20	17680.39	20673160.97

Transformed section and modulus of laminated beam.

Figure 13

TEMPLATE	AZ	BA	BB	BC	BD	BE	BF
1							
2							
3							
4							
5							
6							
7							
8							
9							
10							
11							
12							
13							
14							
15							
16							
17							
18							
19							
20							
21							
22							
23							
24							
25							
26							
27							
28							
29							
30							
31							
32							
33							
34							
35							
36							
37							
38							
39							
40							
41							
42							
43	0.02	0.14	*****	366.07	2.09	0.48	
44	0.02	0.25	*****	364.46	2.08	0.48	
45	0.02	0.27	*****	364.18	1.79	0.56	
46	0.02	0.29	*****	363.90	1.27	0.79	
47	0.02	0.29	*****	363.81	1.23	0.81	
48	0.02	0.31	*****	363.60	1.16	0.87	
49	0.02	0.31	*****	363.54	1.15	0.87	
50	0.02	0.33	*****	363.33	1.10	0.91	
51	0.02	0.33	*****	363.27	1.05	0.96	
52	0.02	0.37	*****	362.67	0.90	1.11	
53	0.02	0.39	*****	362.39	0.84	1.19	

L = BED EFFECTIVE SPAN

$L = W + (2 * (D_b - D_t) * \tan(B))$

where:

W = panel width or span of bed beneath current

Dt = depth to top of bed beneath current bed

Db = depth to bottom of bed beneath current be

B = span angle

UNIT WEIGHT	LOAD		EFFECTIVE SPAN	DEFLECTION ROCKMASS	INVERSE OF DEFLECTION
BED					
	w	$E * I * A / w$	L	$wL^4 / AE * I$	BRIDGING POTENTIAL ROCKMASS
MN/m ³	MPa	m ³	m	m	

Stiffness and bridging potential of laminated beam.

Figure 14

	start row#	48	data begins in row 48
	stop row#	50	row # for immediate roof stratum
	step#	1	
	Loop#	51	loop counter
_analyze	{_check}		
	{_initialize}		
	{FOR B124,B121,B122,B123,_main}		
_check	{SelectBlock macros.C21..C29}		check that correct row # is being used in subroutine _initialize
	{Search.Find "52"}		
	{Search.ReplaceBy @string(D4,0)}		
	{Search.Next}		
_main	{_reset}		
	{_calculate}		
_initialize	{BlockValues S129,J21}		input mined seam depth
	{BlockValues S129,J22}		set initial laminated beam thickness = seam depth
	{BlockValues J27,J28}		set initial span width to mine panel width
	{BlockValues AN129,J24}		compute weighted modulus (E*) of laminated beam
	{BlockValues AT129,J26}		compute depth to neutral axis
	{BlockValues AY129,J32}		compute bending stiffness (E*I*)
	{BlockValues BA129,J34}		compute beam weight per unit length
	{BlockValues BD129,J36}		compute maximum deflection of beam
	{Search.Block BS19..BS32}		initialize cell designation in Subroutine _calculate
	{Search.Find @STRING(BO33,0)}		"
	{Search.ReplaceBy "48"}		start with row 48
	{Search.ReplaceAll}		
	{SelectBlock scrutch:B124..B124}		initialize loop #
	{PutCell "48"}		start with loop #48
_reset	{BlockValues S129,J22}		set laminated beam thickness = seam depth
	{BlockValues J27,J28}		set span width to mine panel width
	{BlockValues AN129,J24}		compute weighted modulus (E*) of laminated beam
	{BlockValues AT129,J26}		compute depth to neutral axis
	{BlockValues AY129,J32}		compute bending stiffness (E*I*)
	{BlockValues BA129,J34}		compute beam weight per unit length
	{BlockValues BD129,J36}		compute maximum deflection of beam
	{Search.Block BS19..BS32}		update cell designation in Subroutine _calculate
	{Search.Find @STRING(BO32,0)}		"
	{Search.ReplaceBy @STRING(BO33,0)}		"
	{Search.ReplaceAll}		"
	51		current row #
	52		new row #
_calculate	{BlockValues BC52,L28}		compute span for new assumed beam thickness
	{BlockValues L28,J28}		input span
	{BlockValues S52,J22}		input new beam thickness
	{BlockValues AN52,J24}		compute weighted modulus (E*) of laminated beam
	{BlockValues AT52,J26}		compute depth to neutral axis
	{BlockValues AY52,J32}		compute bending stiffness (E*I*)
	{BlockValues BA52,J34}		compute beam weight per unit length
	{BlockValues BD52,J36}		compute maximum deflection of beam
	{BlockValues J22,BH52}		store beam thickness
	{BlockValues J24,BK52}		store weighted modulus
	{BlockValues J28,BL52}		store span
	{BlockValues J32,BM52}		store bending stiffness
	{BlockValues J34,BN52}		store beam weight
	{BlockValues J36,BO52}		store maximum deflection

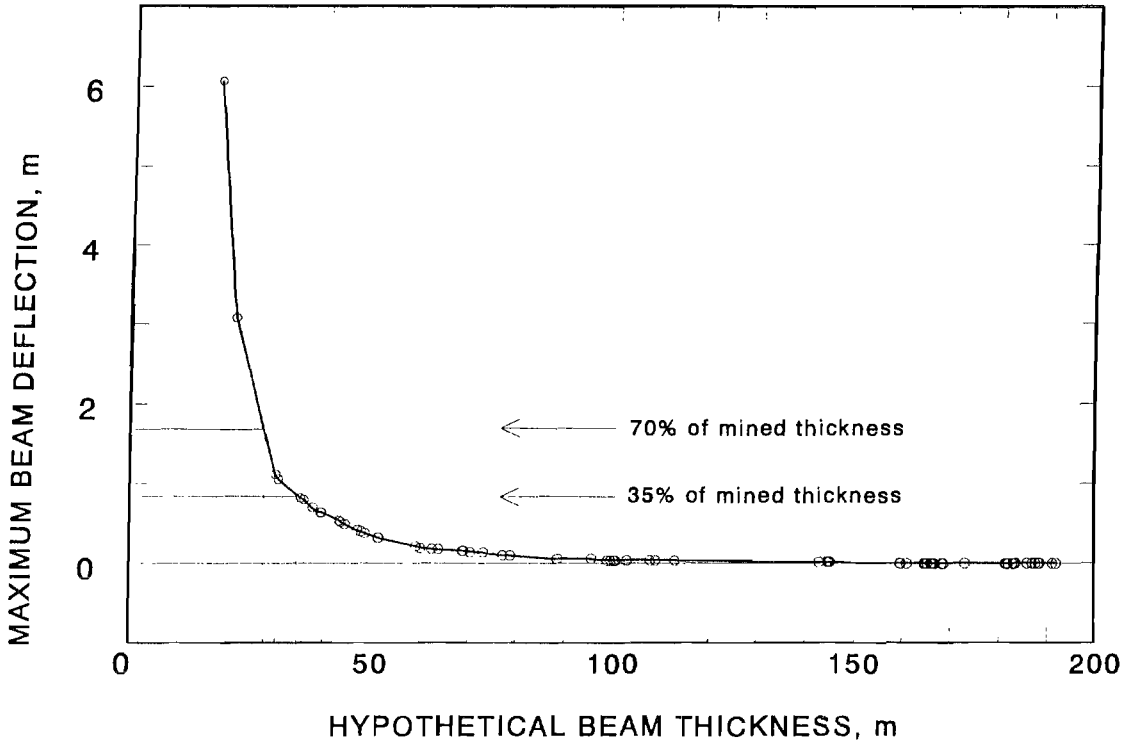
Logic of beam analysis macro.

Figure 15

Old_Ben_Panel_1	BH	BI	BJ	BK	BL	BM	BN	BO	BP	BQ	BR	BS	BT	BU
17														
18	_MAIN ROUTINE			_INITIALIZE ROUTINE				_RESET ROUTINE				_CALCULATE ROUTIN		
19				{Block Values S129,J21}			{Block Values S129,J22}		{Block Values S129,J22}			{Block Values BC52,L28}		
20				{Block Values S129,J22}			{Block Values S129,J22}		{Block Values J27,J28}			{Block Values L28,J28}		
21	start row#		48	{Block Values J27,J28}			{Block Values AN129,J24}		{Block Values AN129,J24}			{Block Values S52,J22}		
22	stop row#		50	{Block Values AN129,J24}			{Block Values AT129,J26}		{Block Values AT129,J26}			{Block Values AN52,J24}		
23	step#		1	{Block Values AT129,J26}			{Block Values AY129,J22}		{Block Values AY129,J22}			{Block Values AT52,J26}		
24	Loop#		51	{Block Values AY129,J22}			{Block Values BA129,J24}		{Block Values BA129,J24}			{Block Values AV52,J22}		
25				{Block Values BA129,J24}			{Block Values BD129,J26}		{Block Values BD129,J26}			{Block Values BA52,J24}		
26	{_INITIALIZE}			{Block Values BD129,J26}			{Search Block BS19..BS22}		{Search Block BS19..BS22}			{Block Values BD52,J26}		
27	{POR B124,B121,B122,B123..max}			{Search Block BS19..BS22}			{Search Find @STRING(BO32,0)}		{Search Find @STRING(BO32,0)}			{Block Values J22,BH52}		
28	{_RESET}			{Search Find @STRING(BO32,0)}			{Search ReplaceBy @STRING(BO32,0)}		{Search ReplaceBy @STRING(BO32,0)}			{Block Values J24,BK52}		
29	{_CALCULATE}			{Search ReplaceBy "48"}			{Search ReplaceAll}		{Search ReplaceAll}			{Block Values J28,BL52}		
30				{Search ReplaceAll}								{Block Values J22,BL52}		
31				{SelectBlock B124..B124}								{Block Values J34,BJ52}		
32				{PutCell "48"}					51			{Block Values J36,BM52}		

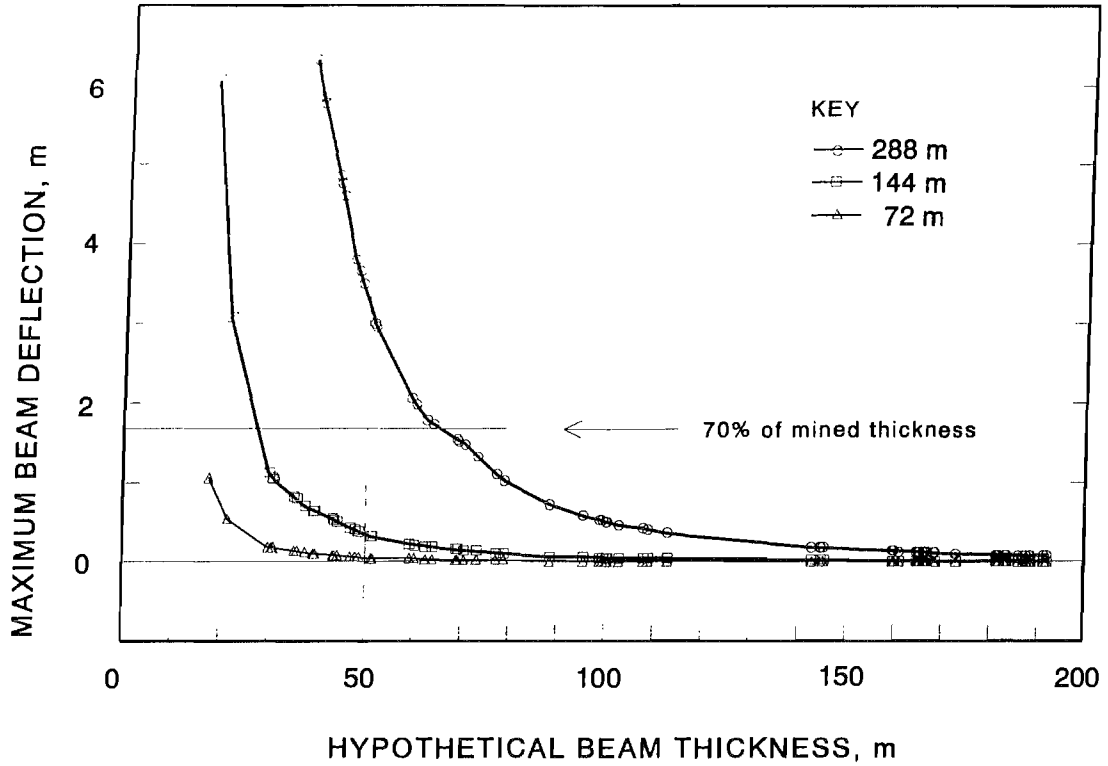
Implementation of beam analysis macro.

Figure 16



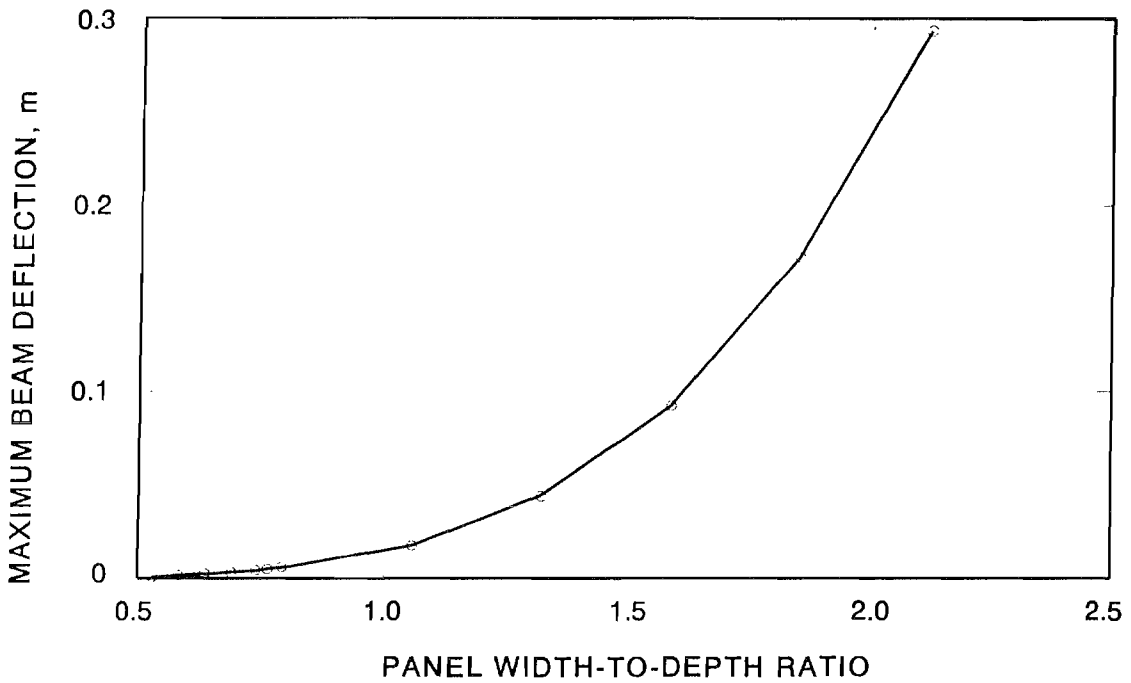
Maximum beam deflection for all possible beam thicknesses.

Figure 17



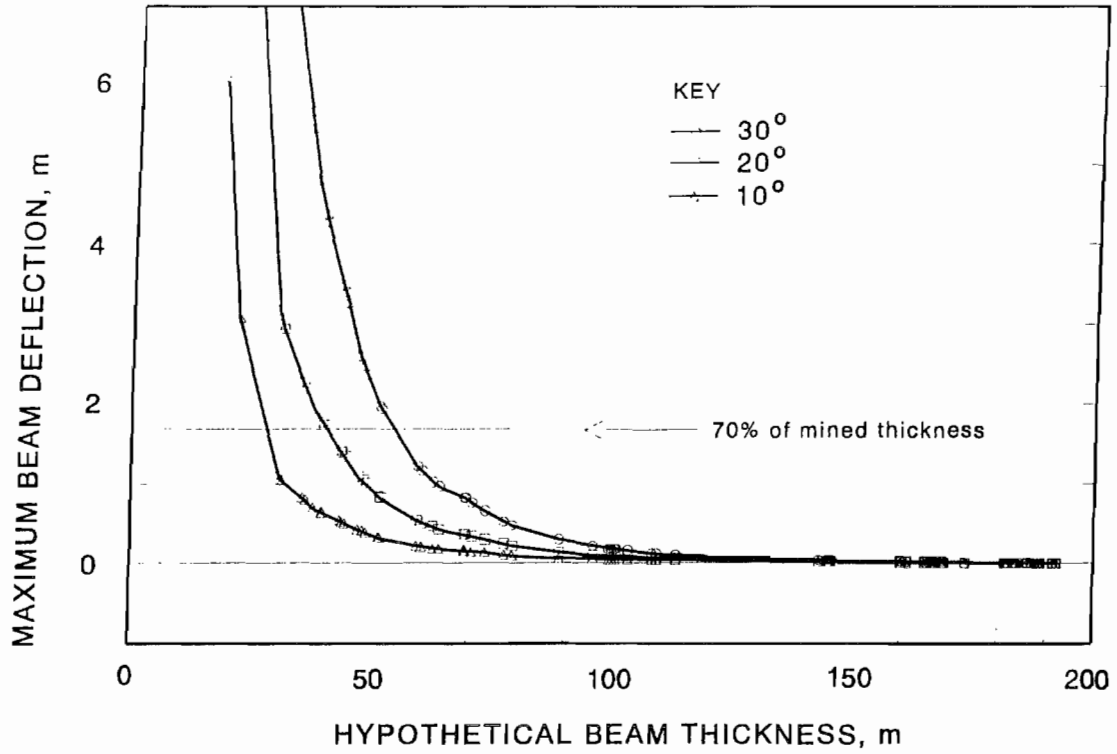
Effect of panel width on maximum beam deflection.

Figure 18



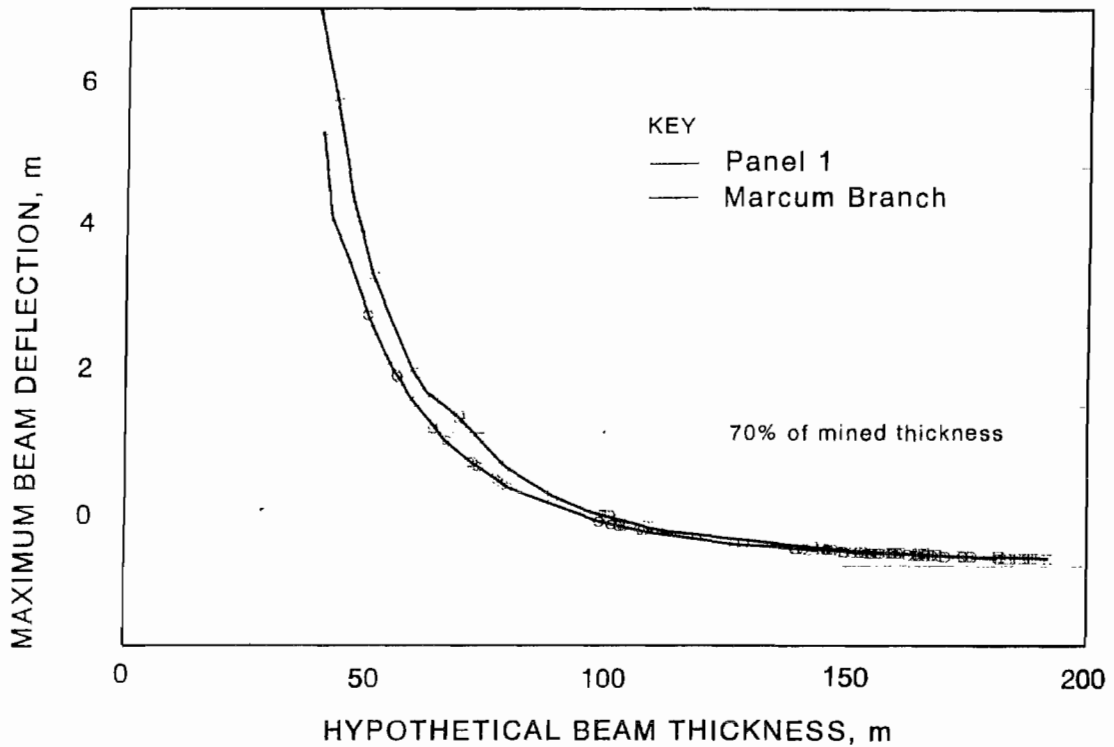
Maximum deflection as a function of panel width to panel depth for a beam of maximum possible thickness.

Figure 19



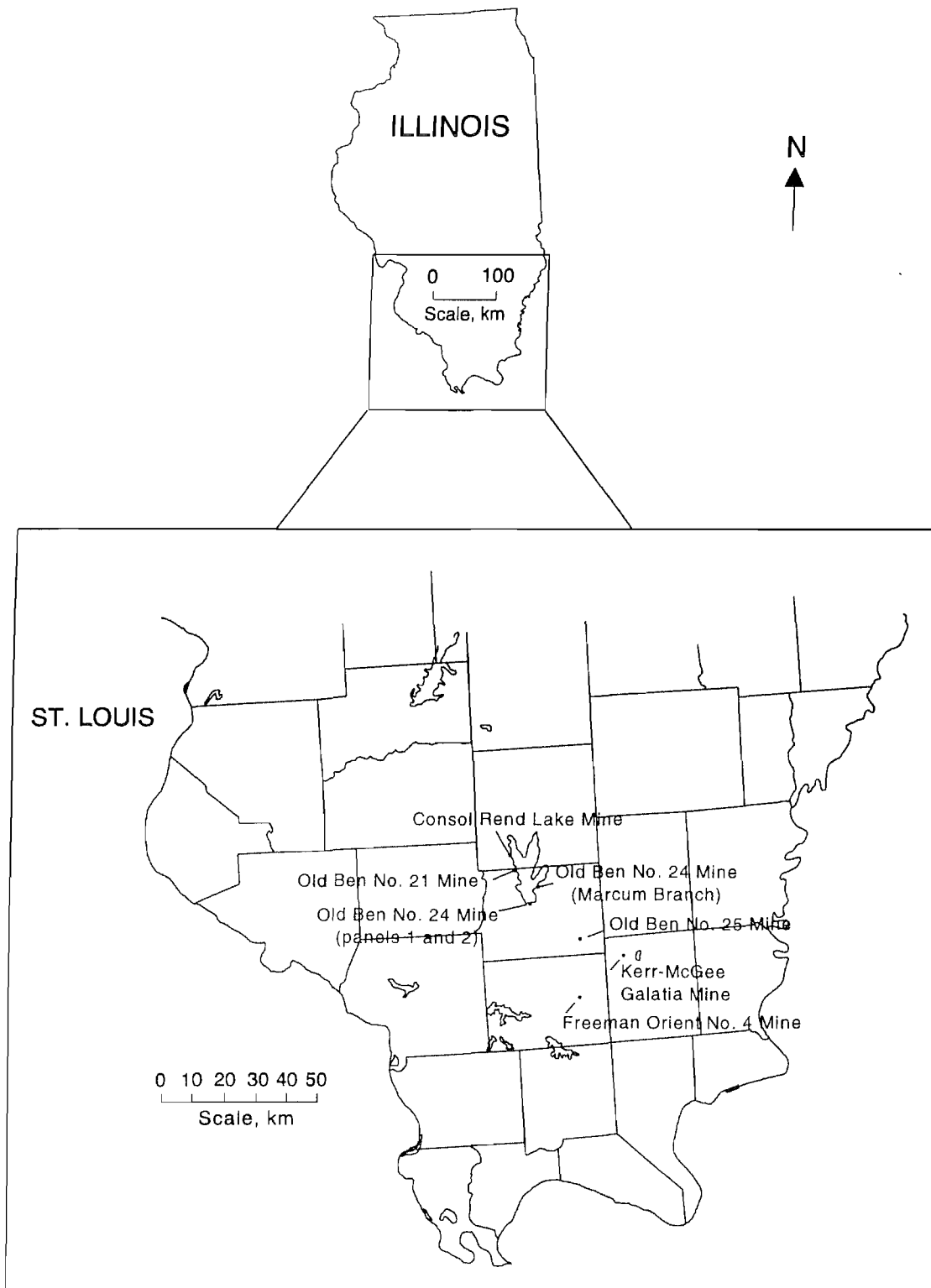
Effect of span angle on maximum beam deflection.

Figure 20



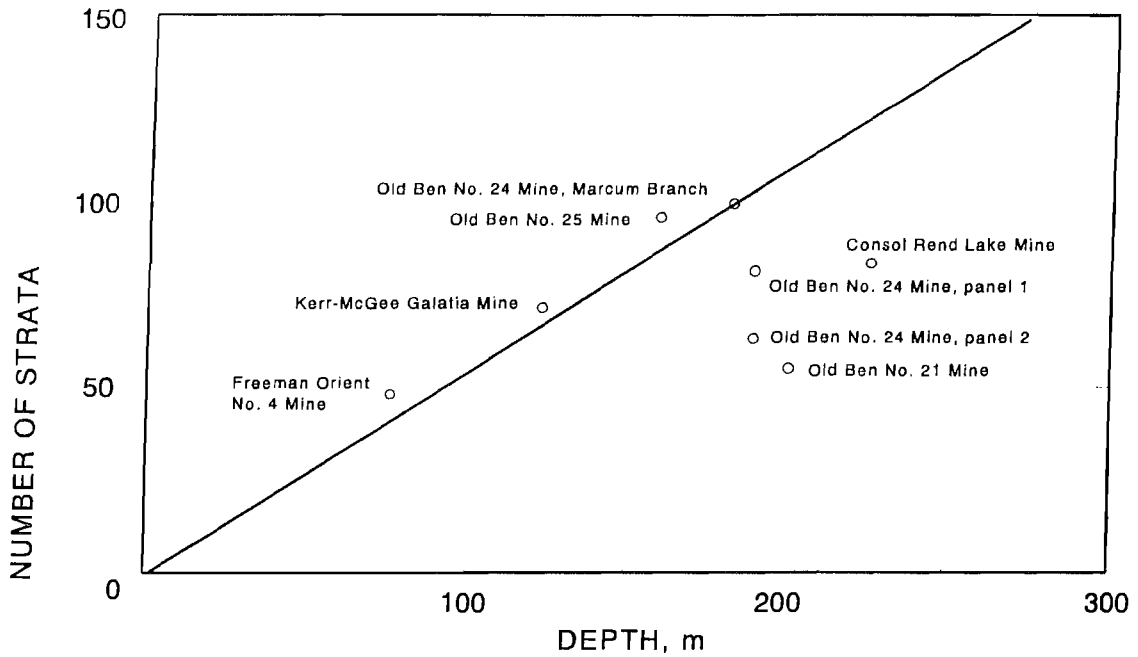
Effect of stratigraphy on maximum beam deflection.

Figure 21



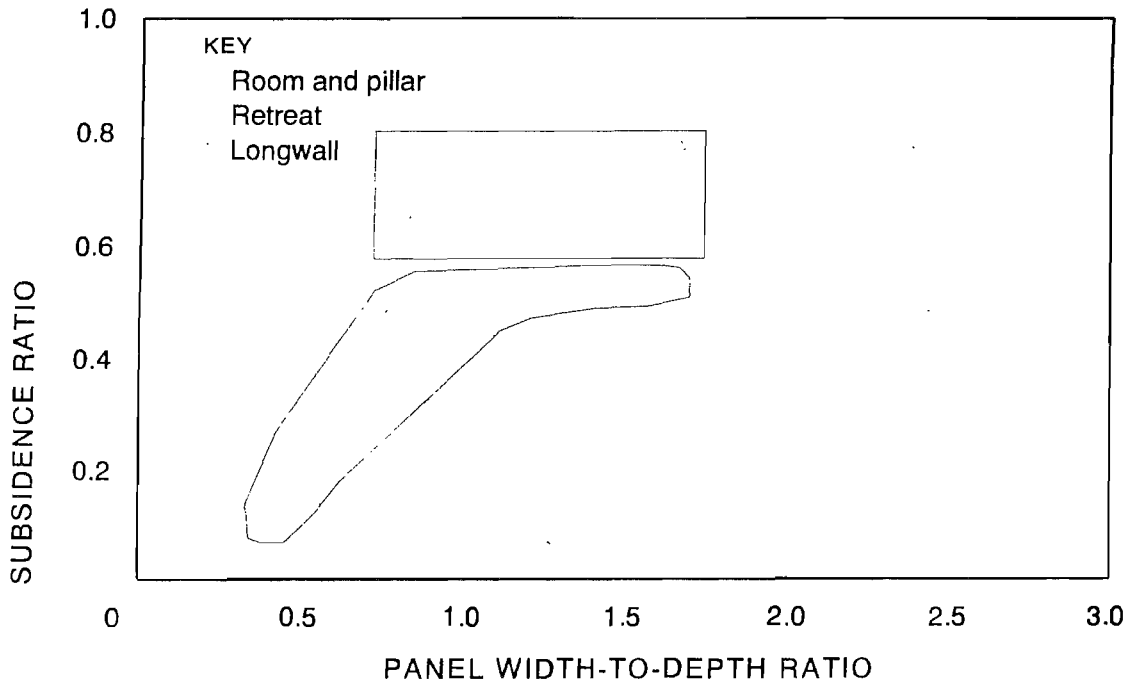
Map showing site locations.

Figure 22

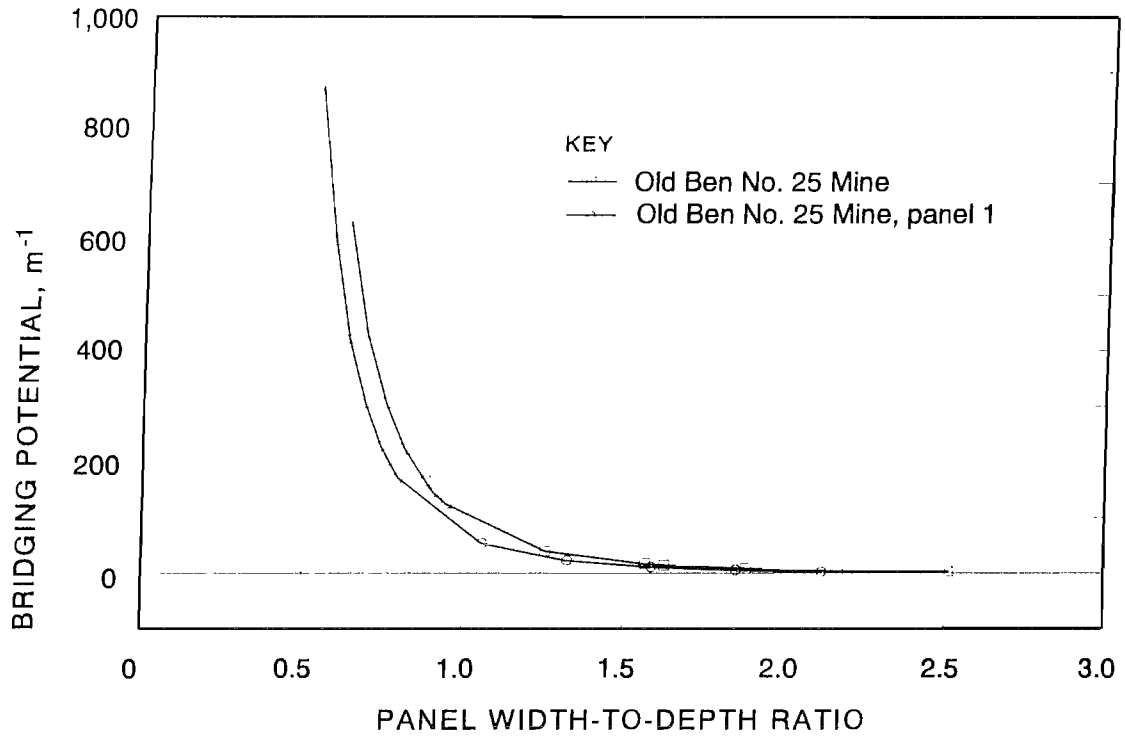


Summary of number of strata identified in core logs.

Figure 23



Empirical subsidence ratio versus panel width to panel depth.

Figure 24

Analytical bridging potential versus panel width to panel depth.

APPENDIX A.—DATA AND ANALYSIS OF INSTRUMENTED SITES

Data have been compiled, plotted, and analyzed for eight mine sites in Illinois. Six of the sites are over longwall panels and two are over high-extraction retreat panels. The sites are listed below by location, progressing from the center to the edge of the Illinois Coal Basin.

To allow comparison, mine maps, surface subsidence profiles, and overburden bending stiffness profiles have been plotted at consistent scales. The data are presented in a format that illustrates the process by which core logs and mine layouts are incorporated into the overburden classification and analysis.

Consol Rend Lake Mine

Two adjacent longwall panels were instrumented (6, 13, 15, 84). Panel 3 was mined in mid-1980, and panel 2 had been mined previously (figure A-1C). TDR cables were installed over the centerline and also over the panel rib. They were undermined in August 1980 and the TDR records for the centerline cable are shown in figure A-1B. Based on cores obtained before and after mining, the fracture frequency increases were in the range of 2 per 3-m run to 10 per 3-m run throughout the overburden. Shear wave velocities decreased by 12% to 18% at depths of 79, 88, 98, and 146 m. The general decrease of 1% to 10% throughout the rest of the overburden was attributed to wave attenuation through a fractured medium filled with fluid. TDR reflections developed at 14.3 m and 32.2 m, but no records were obtained when the face was within 40 m of the cable location. The most probable laminated beam thickness is 32 to 46 m. This implies the upper limit of the transition zone is $[224.4 \text{ m} - (32 \text{ to } 46 \text{ m})] / 2.9 \text{ m} = 66$ to 61 times the mined thickness.

Old Ben No. 21 Mine

Longwall mining of face No. 6 started June 9, 1969, and stopped on April 1, 1970, because of serious ground control problems (32, 40, 61). This location was 67 m from the TDR cable location. The panel was completed using high-extraction retreat mining, and the cable was undermined May 24, 1970. The TDR cable was installed in the same hole as an inclinometer-extensometer, which showed localized horizontal displacements at depths of 41, 50, 61, 78, 91.5, 104, 124, and 148 m over the period from June 2 to 5, 1970. The casing was pinched off at a depth of 104 m on June 5. The TDR records are shown in figure A-2B. TDR reflections developed at depths of 76, 70, 66, 62, 59, 56, and 25 m. The cable was sheared off at 76 m on June 7 and then failed in tension at 25 m on June 9. The most probable beam thickness is 18 to 29 m. This implies

the upper limit of the transition zone is $[199.6 \text{ m} - (18 \text{ to } 29 \text{ m})] / 2.1 \text{ m} = 87$ to 81 times the mined thickness.

Old Ben No. 24 Mine—Panel 1 and 2

Longwall mining of panel 1 began September 3, 1976, and was completed May 5, 1977 (40, 87). The TDR cable was undermined on October 11, 1976, records are shown in figure A-3B. TDR reflections developed at depths of 17.5, 21.5, 30, 64, 138, and 141 m. The most probable beam thickness is 28 to 38 m. This implies the upper limit of the transition zone is $[188.7 \text{ m} - (28 \text{ to } 38 \text{ m})] / 2.4 \text{ m} = 67$ to 63 times the mined thickness.

Longwall mining of panel 2 began in August 1977 and was completed in December 1978. The mining was interrupted for a period from December 6, 1977, to April 2, 1978, because of a labor strike. The face was 76 m from the TDR cable at that time. The cable was undermined on May 15, 1978, records are shown in figure A-4B. TDR reflections developed at 108.5, 895, 79, 73, 57.6, 44, 40, 32.6, 30, 28, and 25 m. The most probable beam thickness is 30 m to 40 m. This implies the upper limit of the transition zone is $[188.4 \text{ m} - (30 \text{ to } 40 \text{ m})] / 2.4 \text{ m} = 66$ to 62 times the mined thickness.

Old Ben No. 24 Mine—North Marcum Branch

Longwall mining started in November 1991 and was completed in June 1992. The adjacent panel had been mined previously. The TDR cable was undermined on May 21, 1992 (67), records are shown in figure A-5B. TDR reflections developed at the depths of 28.7, 44.0, 55.7, 61.7, 71.4, 77.3, and 103.0 m. The most probable beam thickness is 70 m to 100 m, but this is a supercritical panel. This implies the upper limit of the transition zone is $[181.4 \text{ m} - (70 \text{ to } 100 \text{ m})] / 1.83 \text{ m} = 61$ to 45 times the mined thickness.

Old Ben No. 25 Mine—Heron Road

Two adjacent longwall panels were instrumented. The south panel was mined from June 1989 to May 1990, and the north panel was mined from August 1990 to June 1991 (24). The TDR cable was installed over the north panel and was undermined on June 12, 1990 (22). TDR records are shown in figure A-6B. TDR reflections developed at depths of 41.0, 43, 46, 49, 51.9, 54.3, 56.9, 61.4, 62.9, 66.5, and 115.4 m. The most probable beam thickness is 50 m to 72 m, but this is a supercritical panel. This implies the upper limit of the transition zone is $[159.1 \text{ m} - (50 \text{ to } 72 \text{ m})] / 1.8 \text{ m} = 61$ to 48 times the mined thickness.

Kerr-McGee Calatia Mine

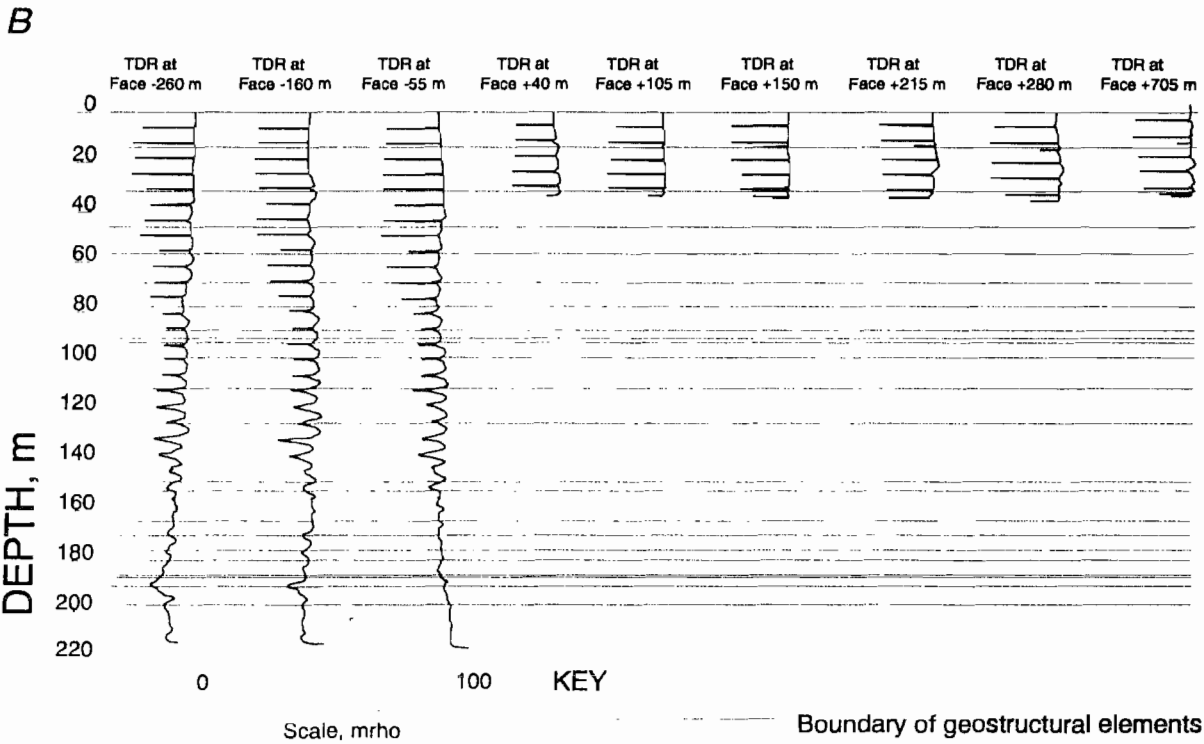
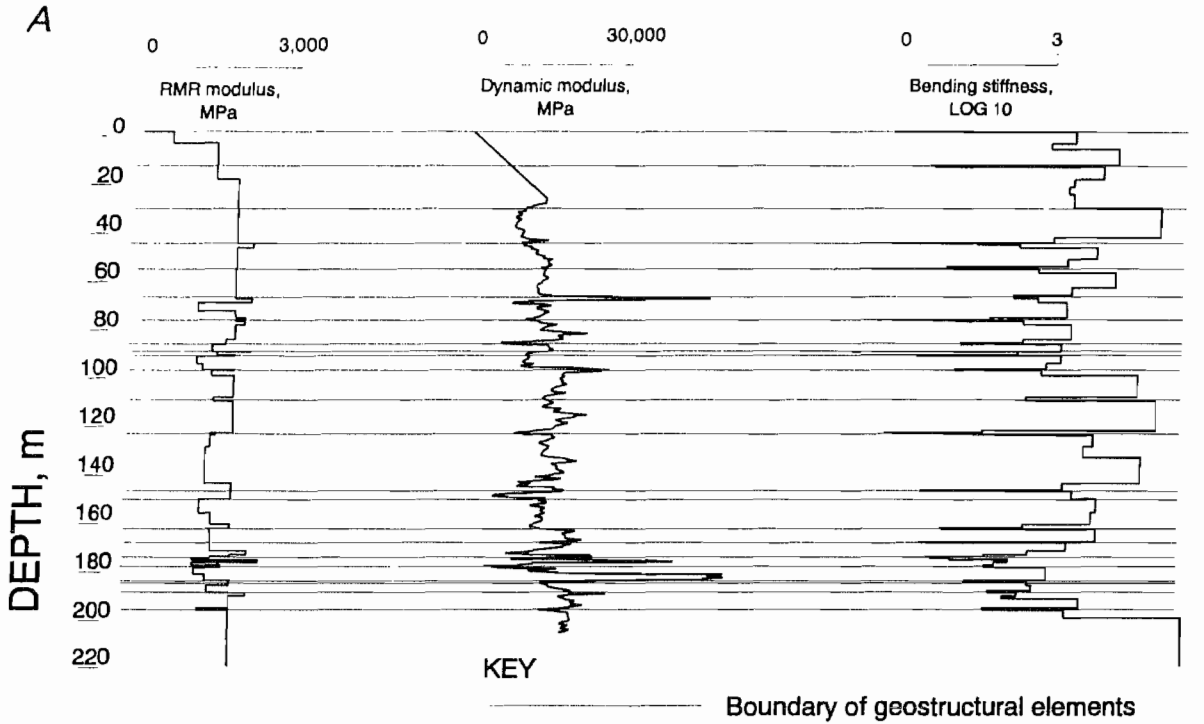
Longwall mining of panel 2 was done in 1990, and panel 1 was previously mined (21, 85). The TDR cable was undermined on September 21, 1990, records are shown in figure A-7B. TDR reflections developed at depths of 52.9, 46.3, 37.9, 31.5, and 26.2 m. In addition to the TDR installation, multi-anchor extensometers and an inclinometer were installed. Based on an analysis of surface curvature and inclinometer data, Van Roosendaal and others (85) estimated that a near-surface beam 24 m thick had developed. Based on the plot in figure A-7E, the most probable laminated beam thickness required to support itself with only fixed end supports would be 38 to 50 m. This implies the upper limit of the transition zone is $[122.5 \text{ m} - (38 \text{ to } 50 \text{ m})] / 1.8 \text{ m} = 47 \text{ to } 40$ times the mined thickness. This is a supercritical panel so a smaller beam thickness can be supported by the caved strata. Based on

the extensometer data, it was concluded that there were no large differential displacements within the overburden to within 6 m of the mine roof. It was also concluded that the overburden subsided as a contiguous rock mass at the panel centerline.

Freeman Orient No. 4 Mine

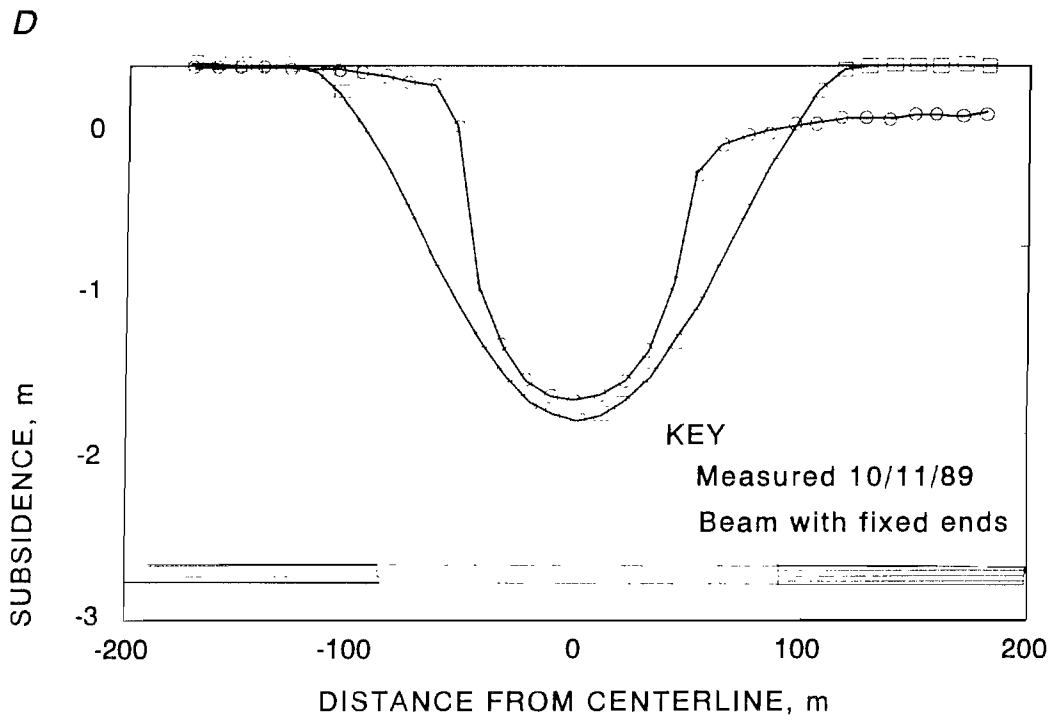
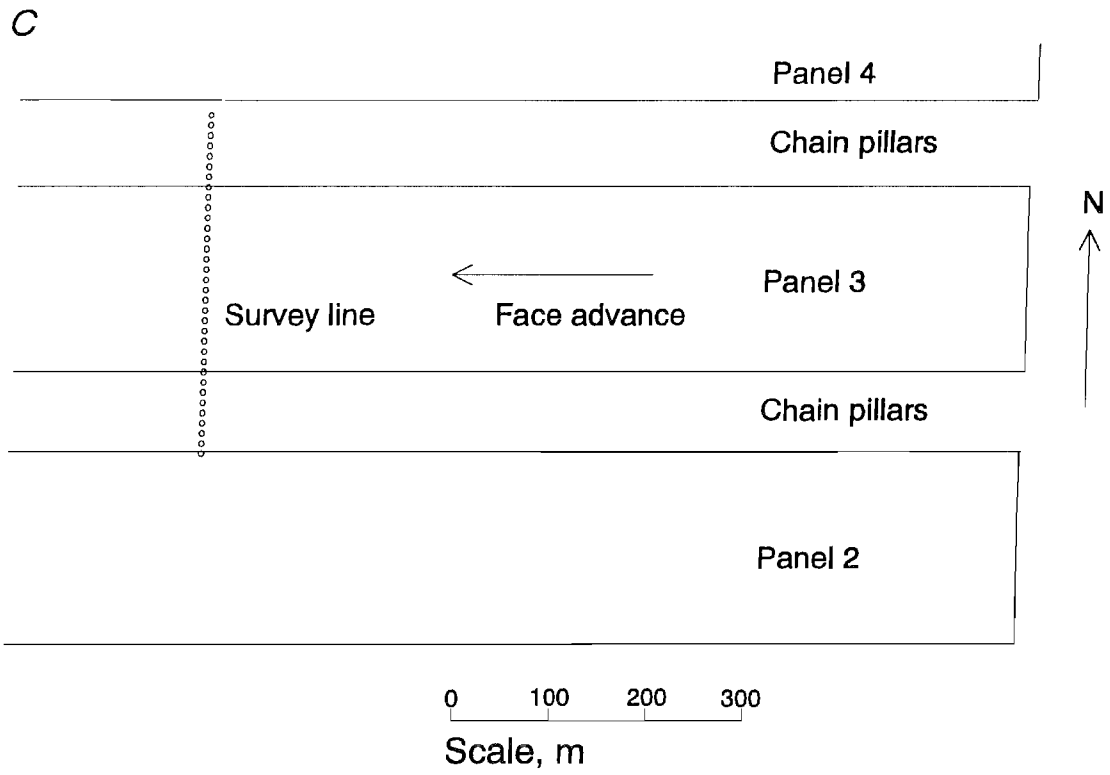
Retreat mining of panel 23 East began in early 1987, and operations ceased May 18, 1987; after the panel had progressed 275 m, the mine was closed because of market conditions (49). The TDR cable was undermined in March 1987, records are shown in figure A-8B. TDR reflections developed at depths of 62, 50, 25, 15, 11, and 5 m. The most probable beam thickness is 15 to 20 m. This implies the upper limit of the transition zone is $[75.7 \text{ m} - (15 \text{ to } 20 \text{ m})] / 1.8 \text{ m} = 34 \text{ to } 31$ times the mined thickness.

Figure A-1



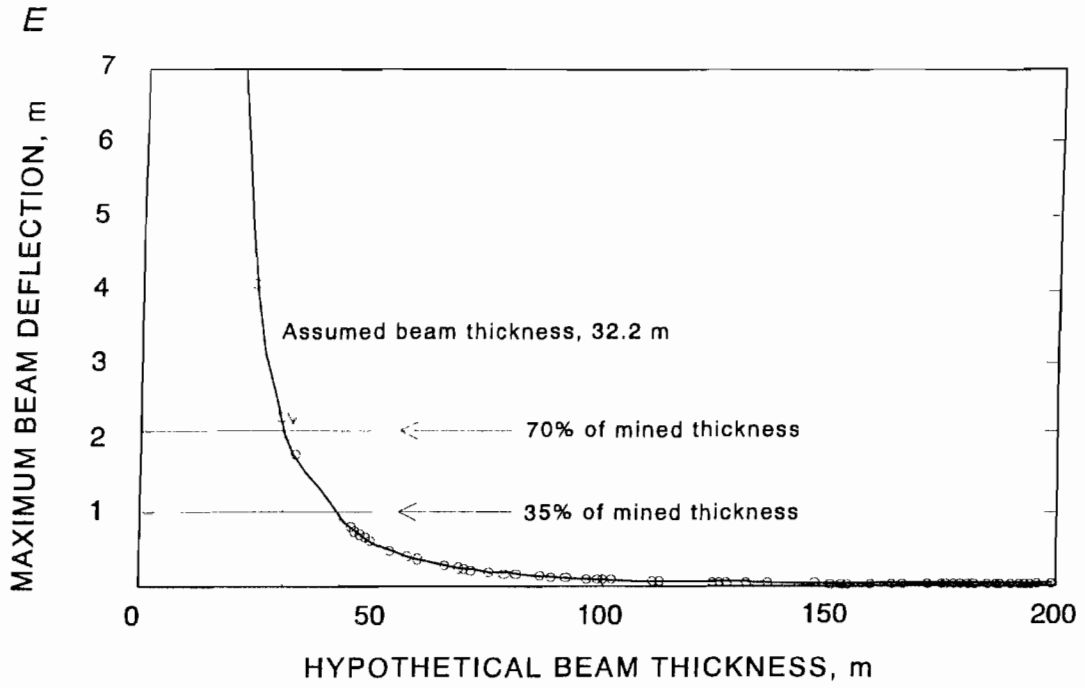
Consol Rend Lake Mine. A, Bending stiffness profile. B, TDR signatures.

Figure A-1—Continued



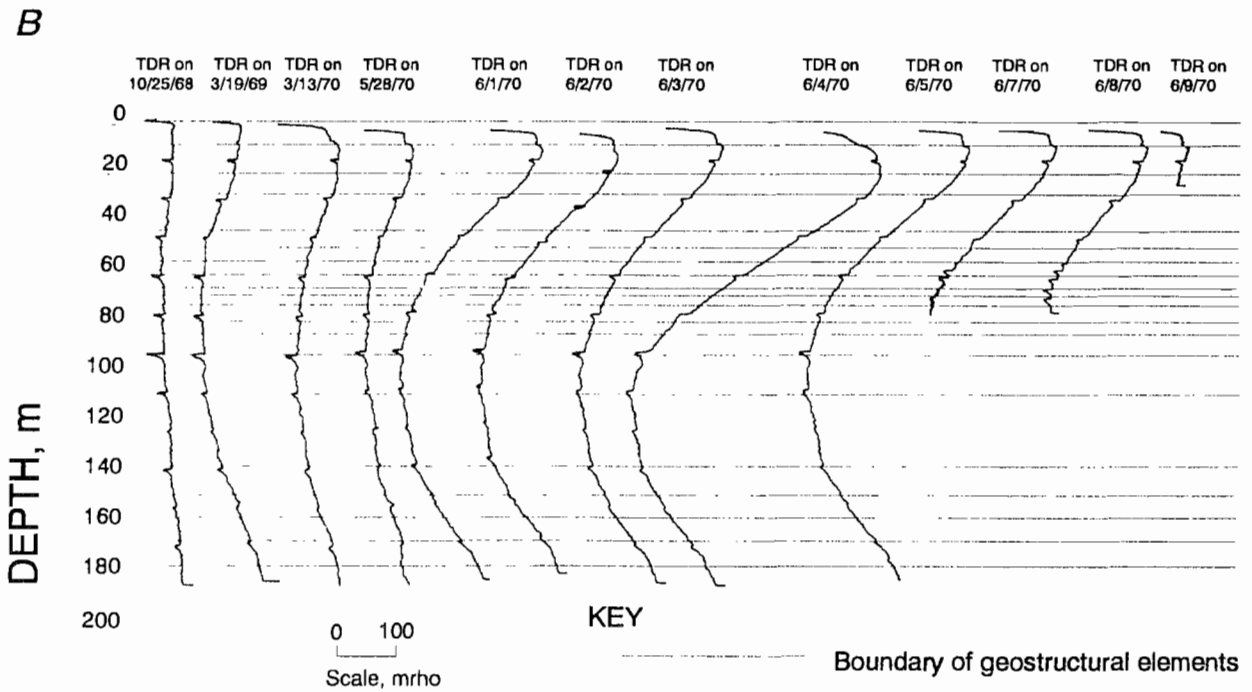
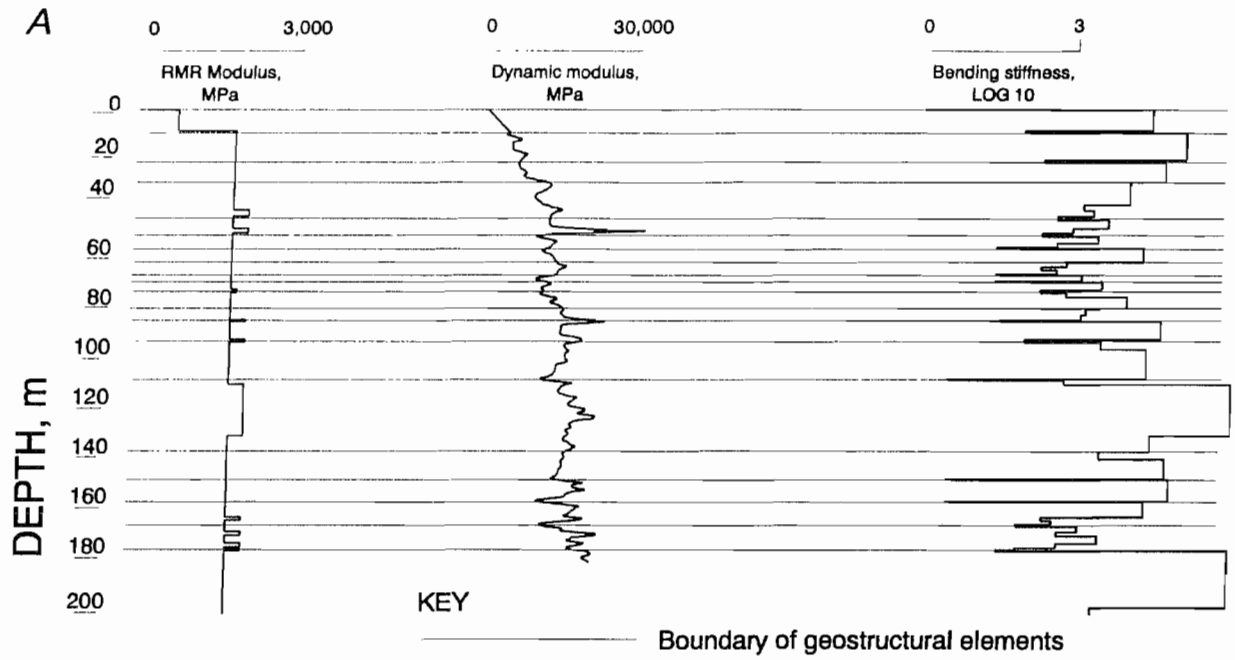
C, Mine map. D, Deflection profile.

Figure A-1—Continued



E, Beam thickness versus deflection.

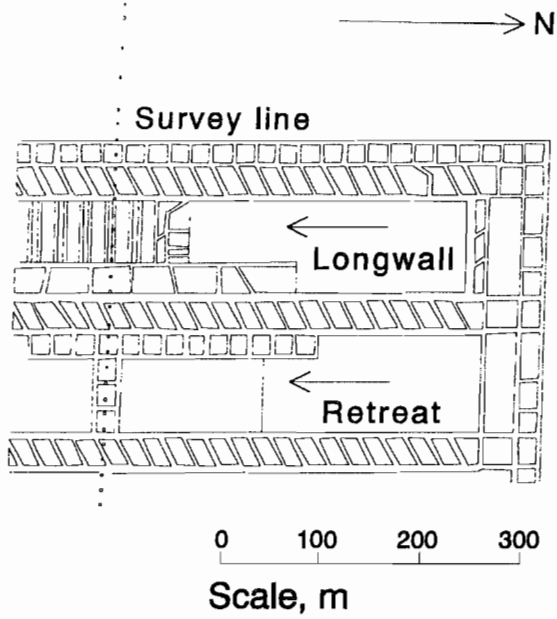
Figure A-2



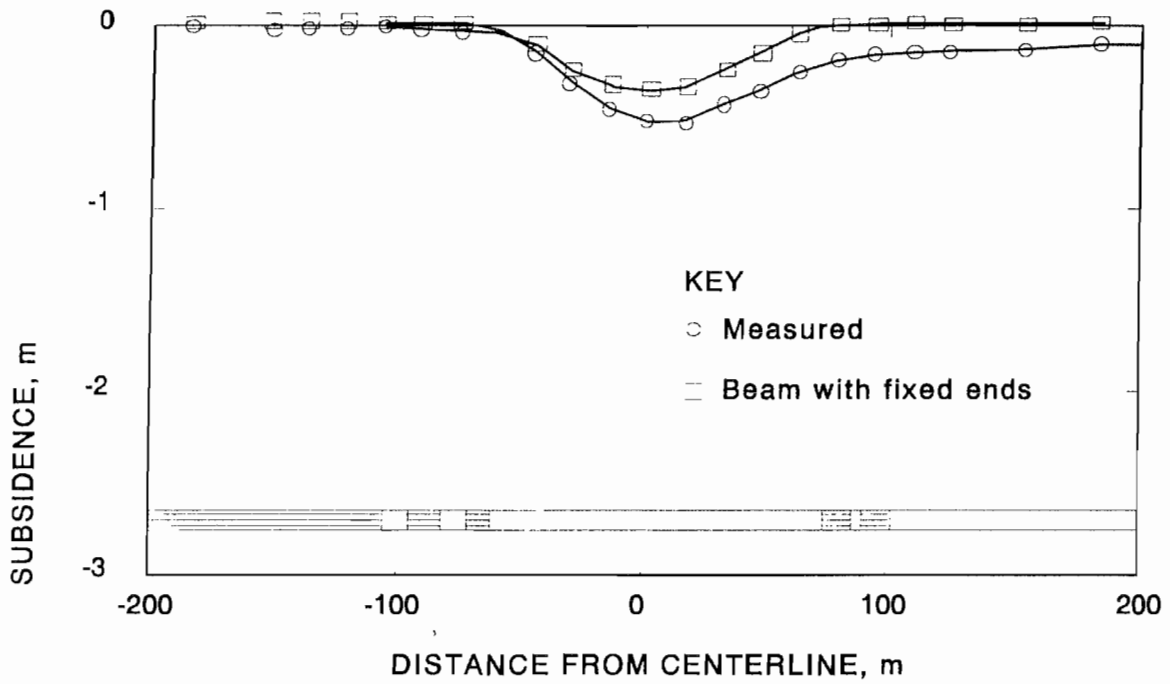
Old Ben No. 21 Mine. A, Bending stiffness profile. B, TDR signatures.

Figure A-2—Continued

C



D



C, Mine map. D, Deflection profile.

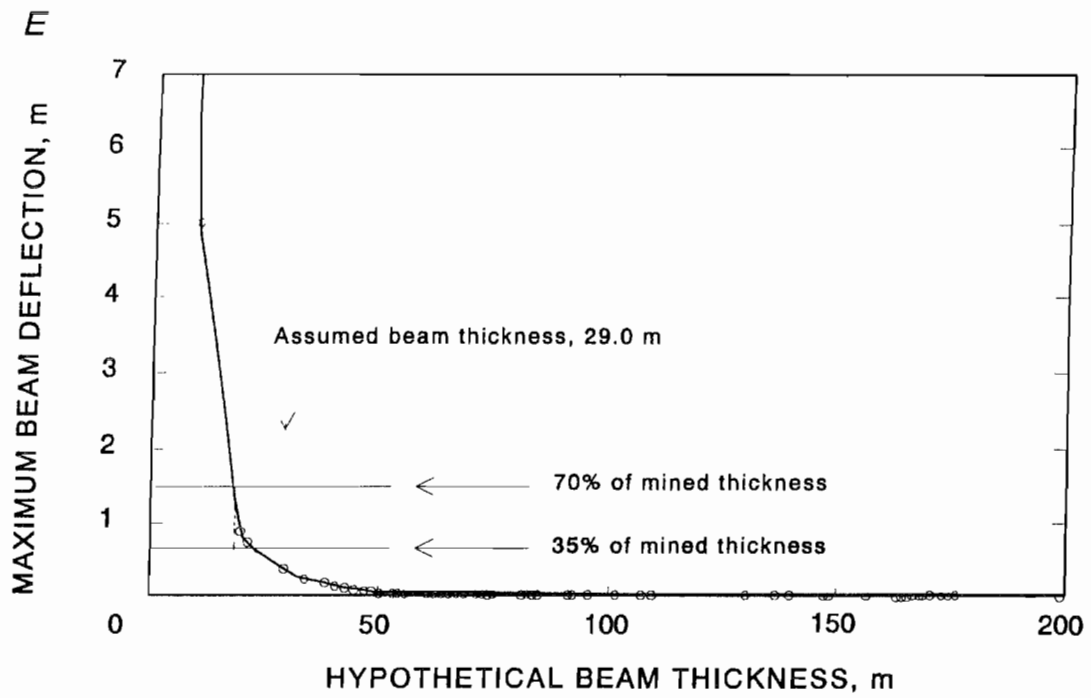
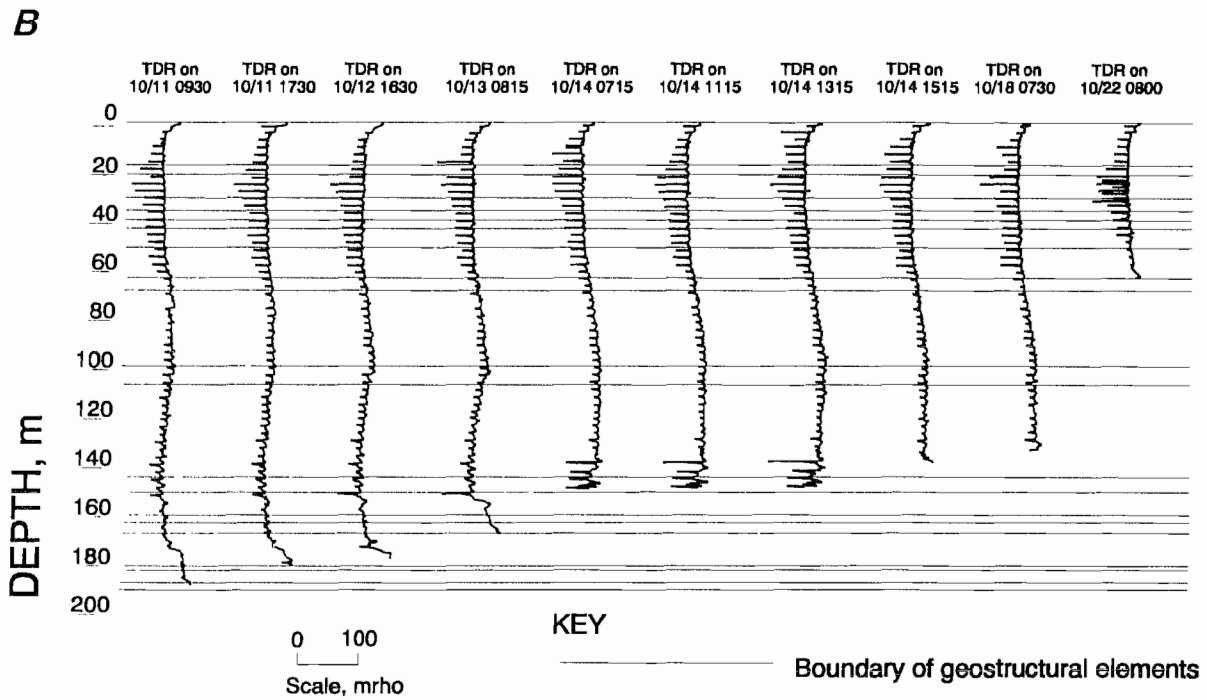
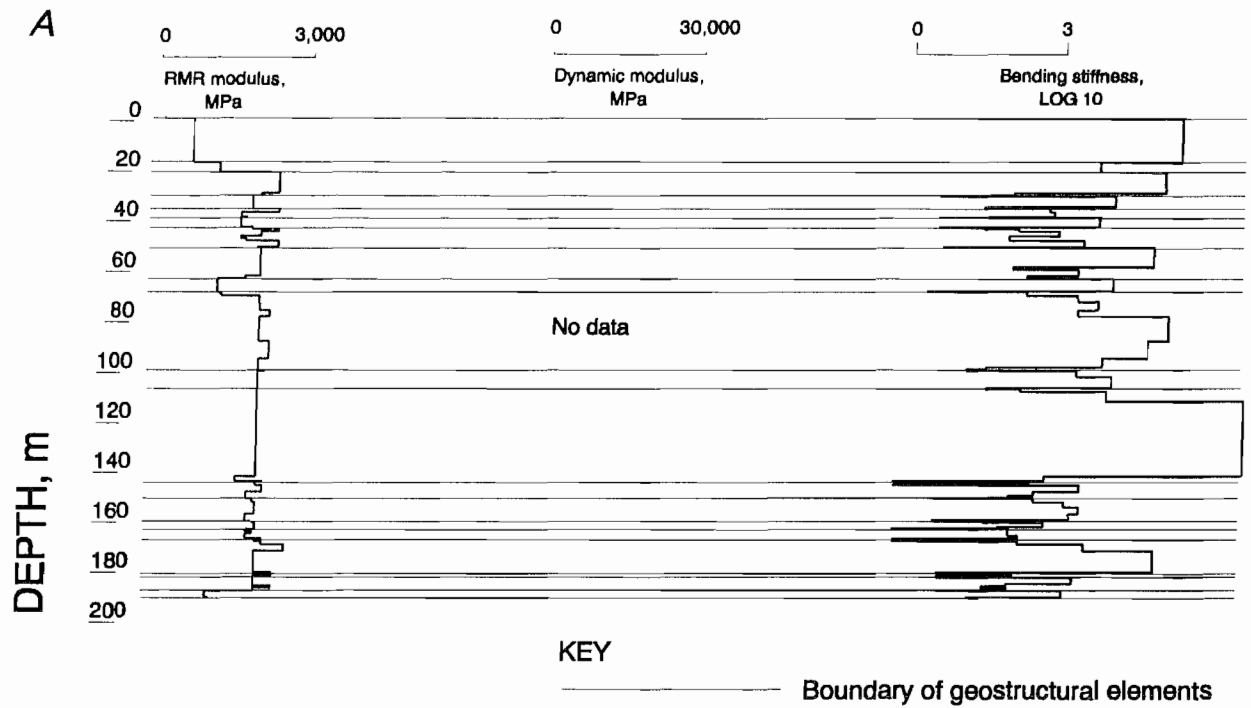
Figure A-2—Continued*E, Beam thickness versus deflection.*

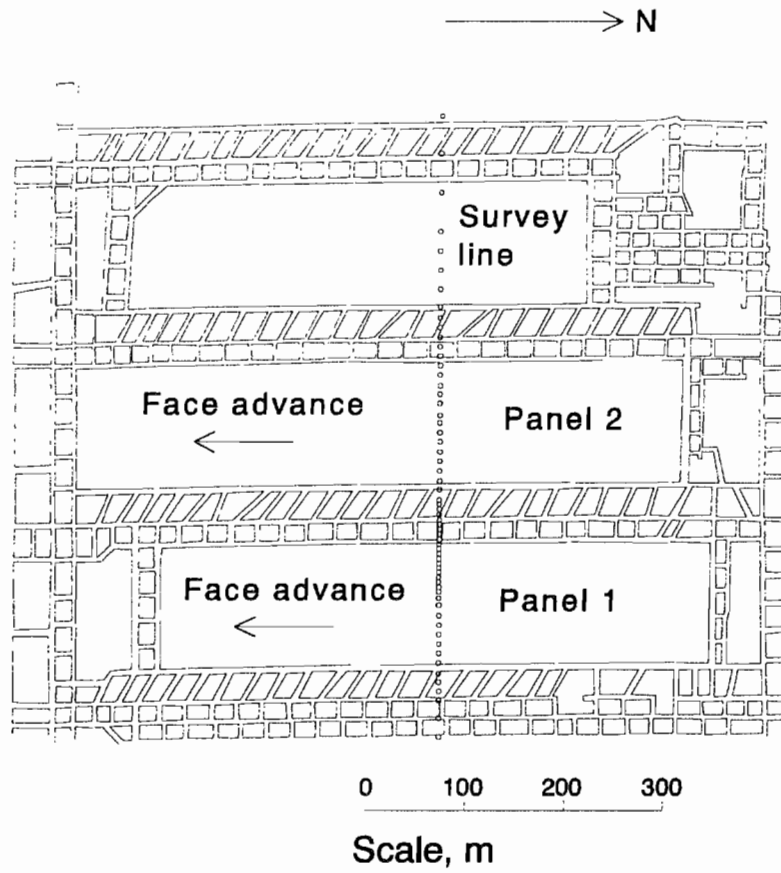
Figure A-3



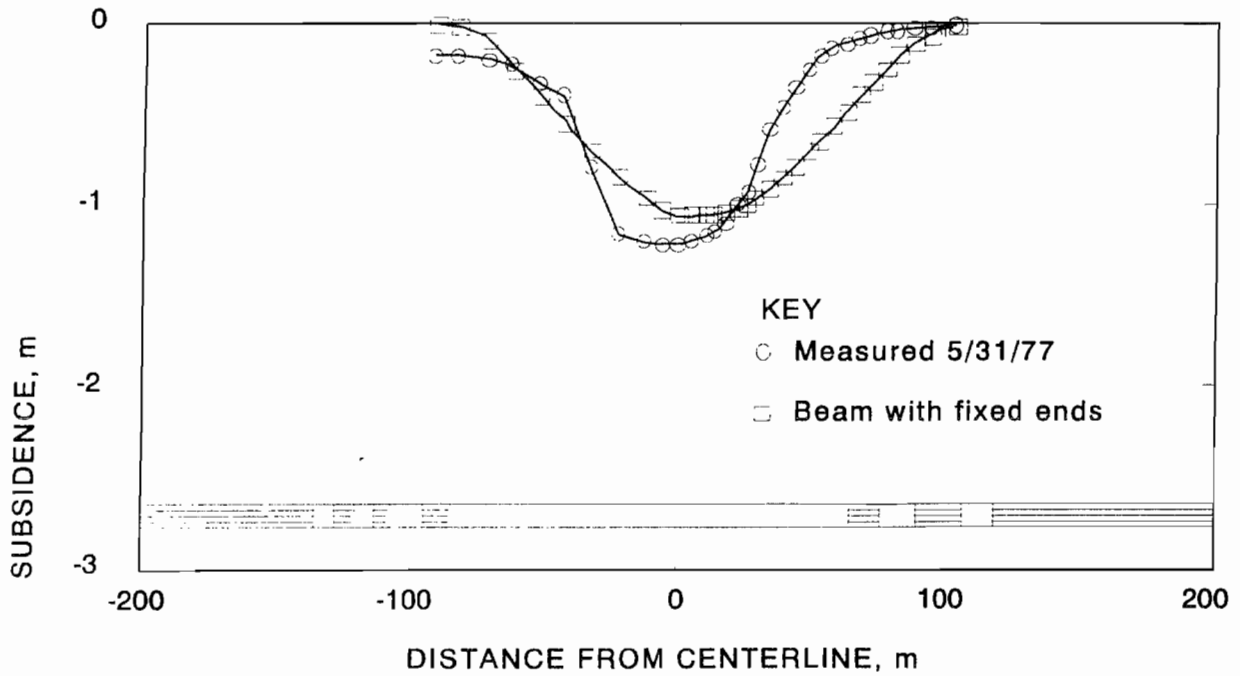
Old Ben No. 24 Mine panel 1 site. A, Bending stiffness profile. B, TDR signatures.

Figure A-3—Continued

C



D



C, Mine map. D, Deflection profile.

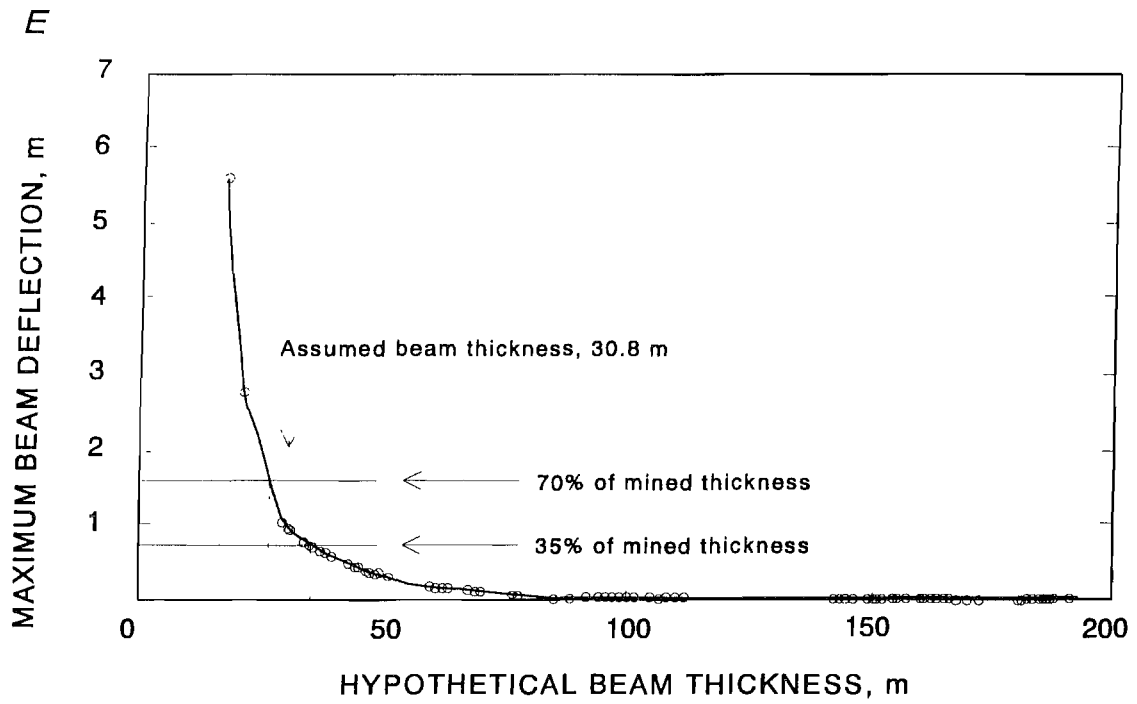
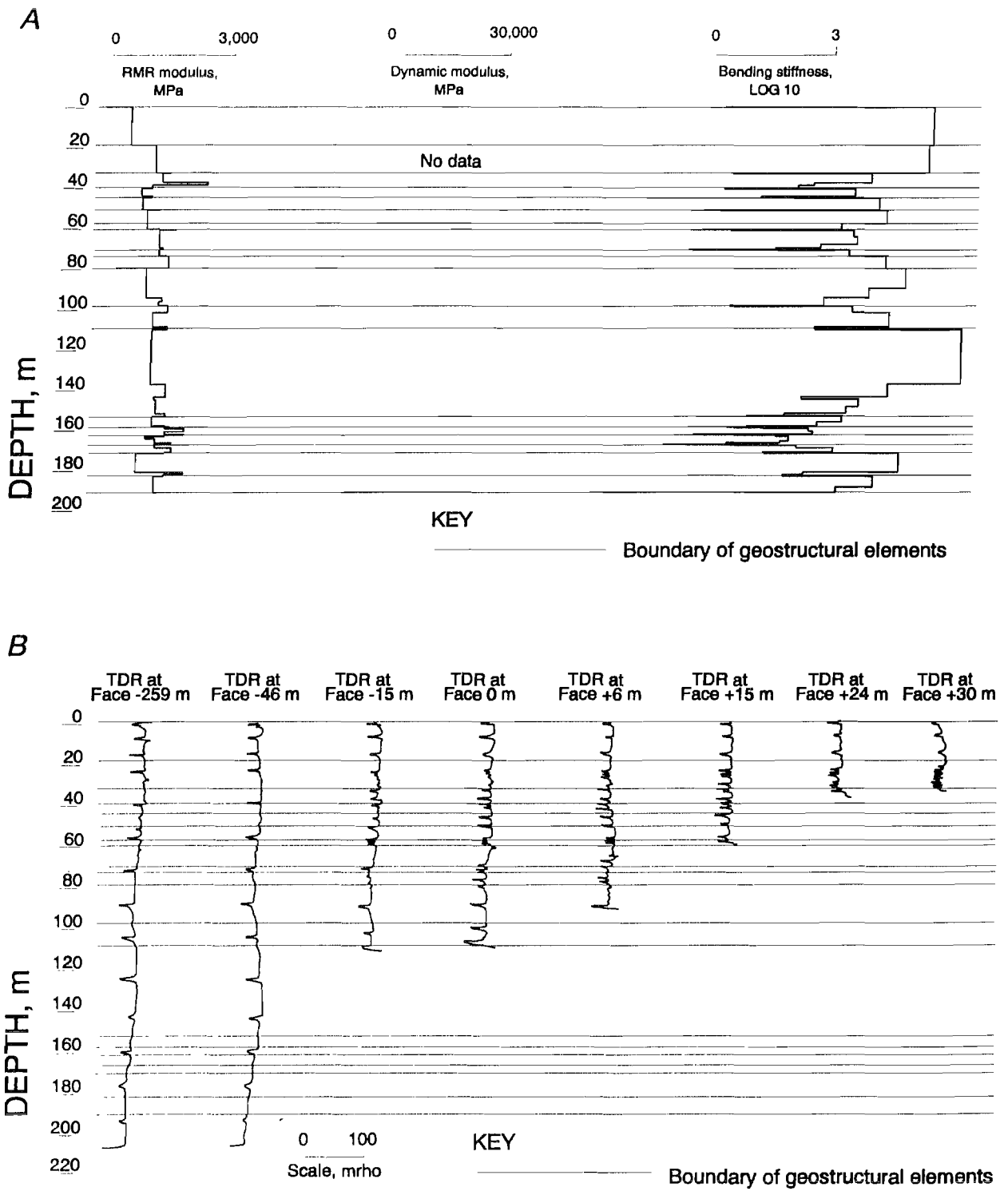
Figure A-3—Continued*E, Beam thickness versus deflection.*

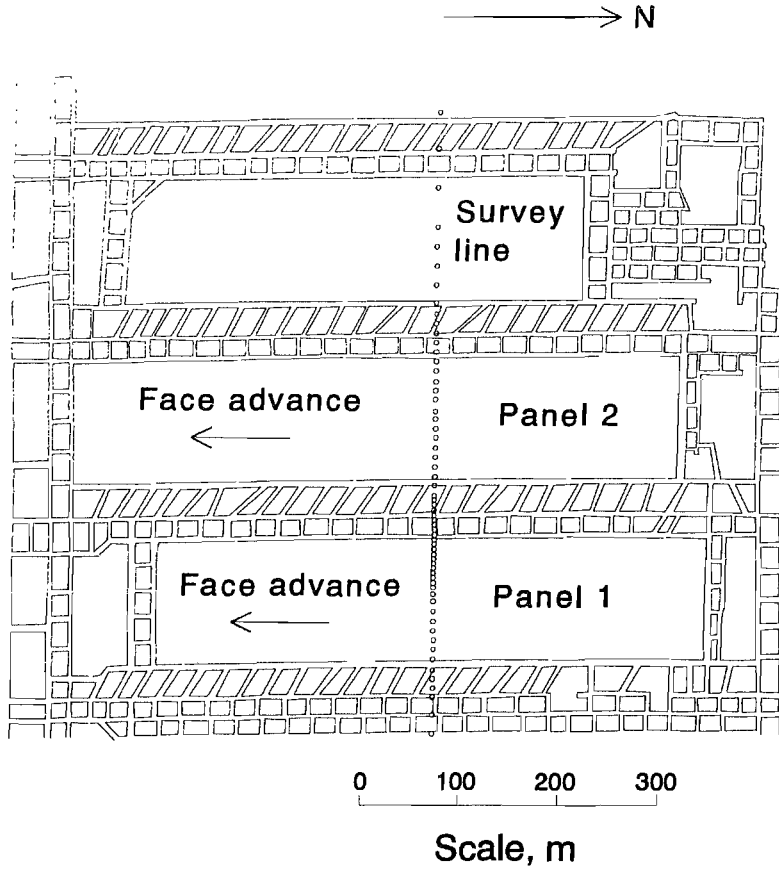
Figure A-4



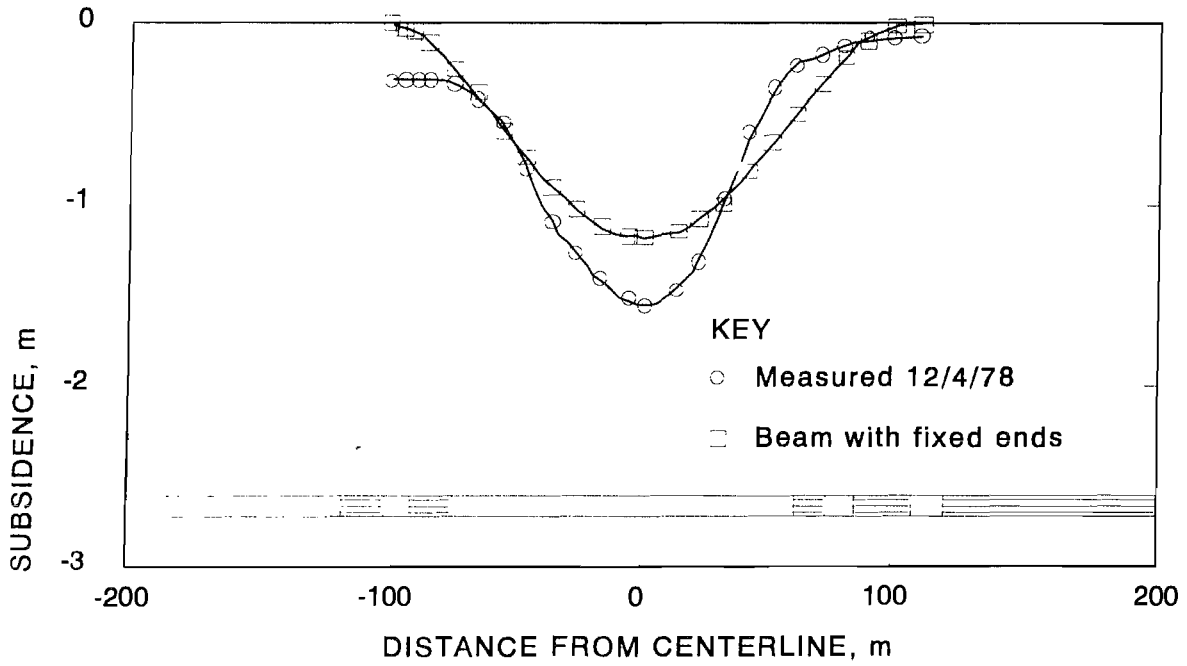
Old Ben No. 24 Mine panel 2 site. A, Bending stiffness profile. B, TDR signatures.

Figure A-4—Continued

C

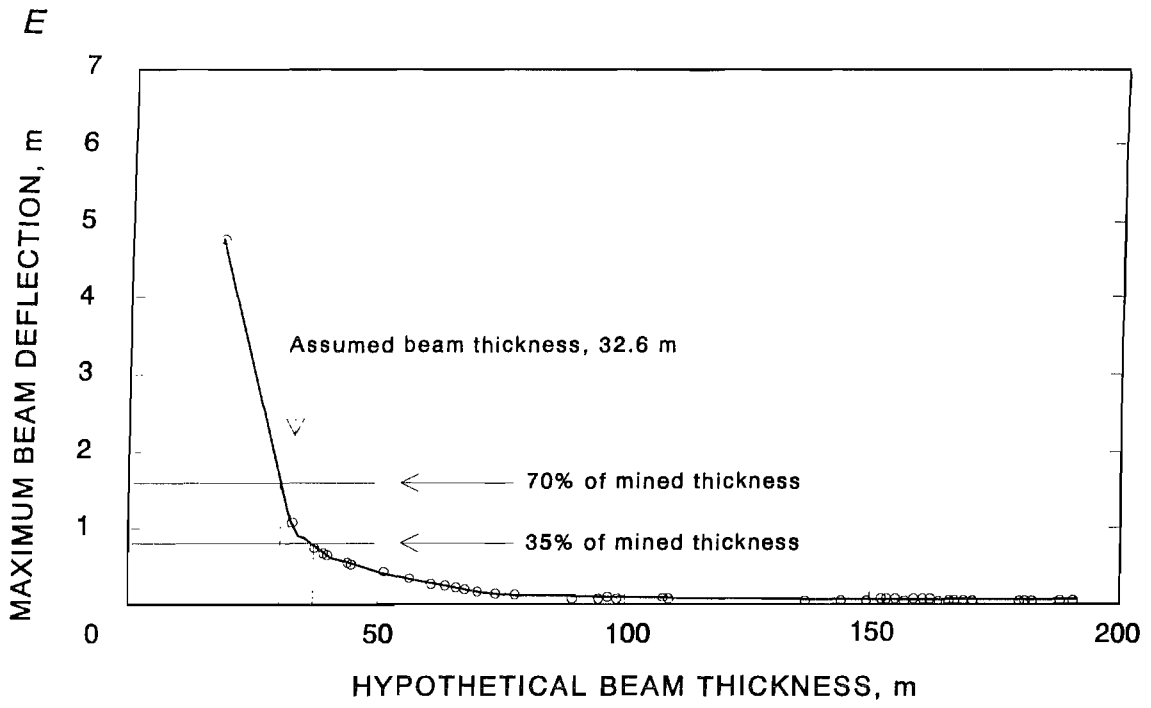


D



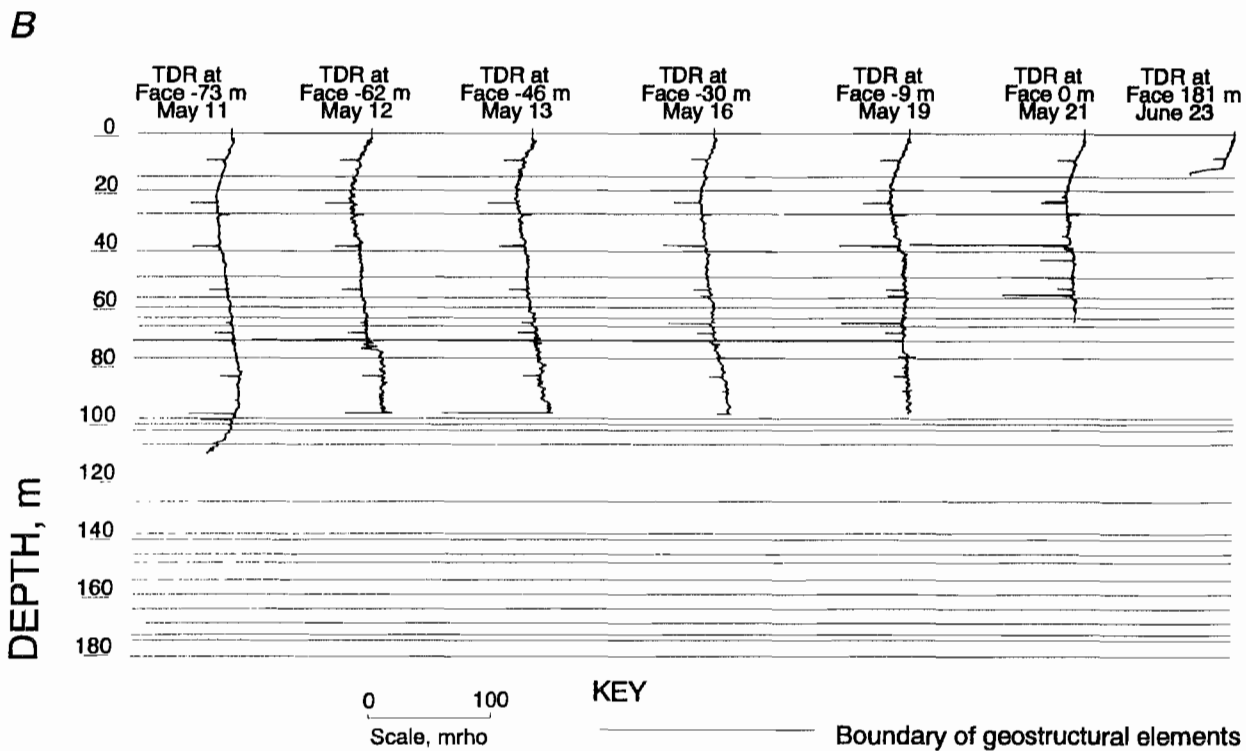
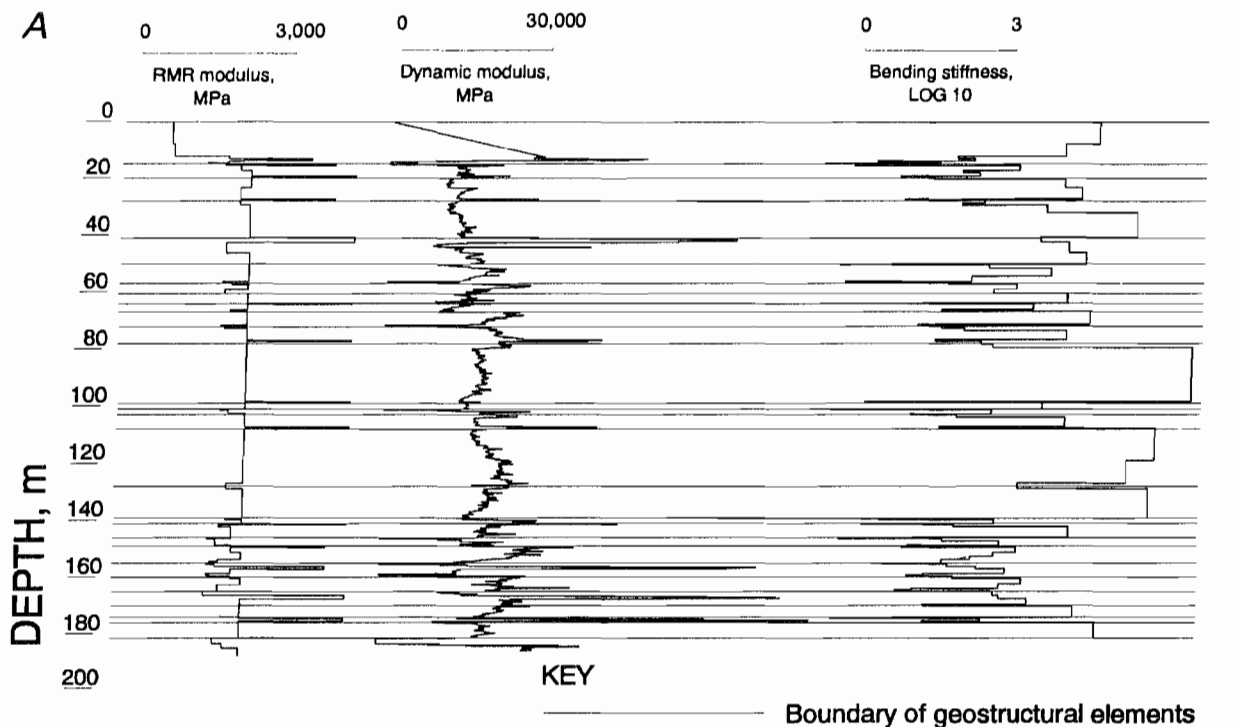
C, Mine map. D, Deflection profile.

Figure A-4—Continued



E, Beam thickness versus deflection.

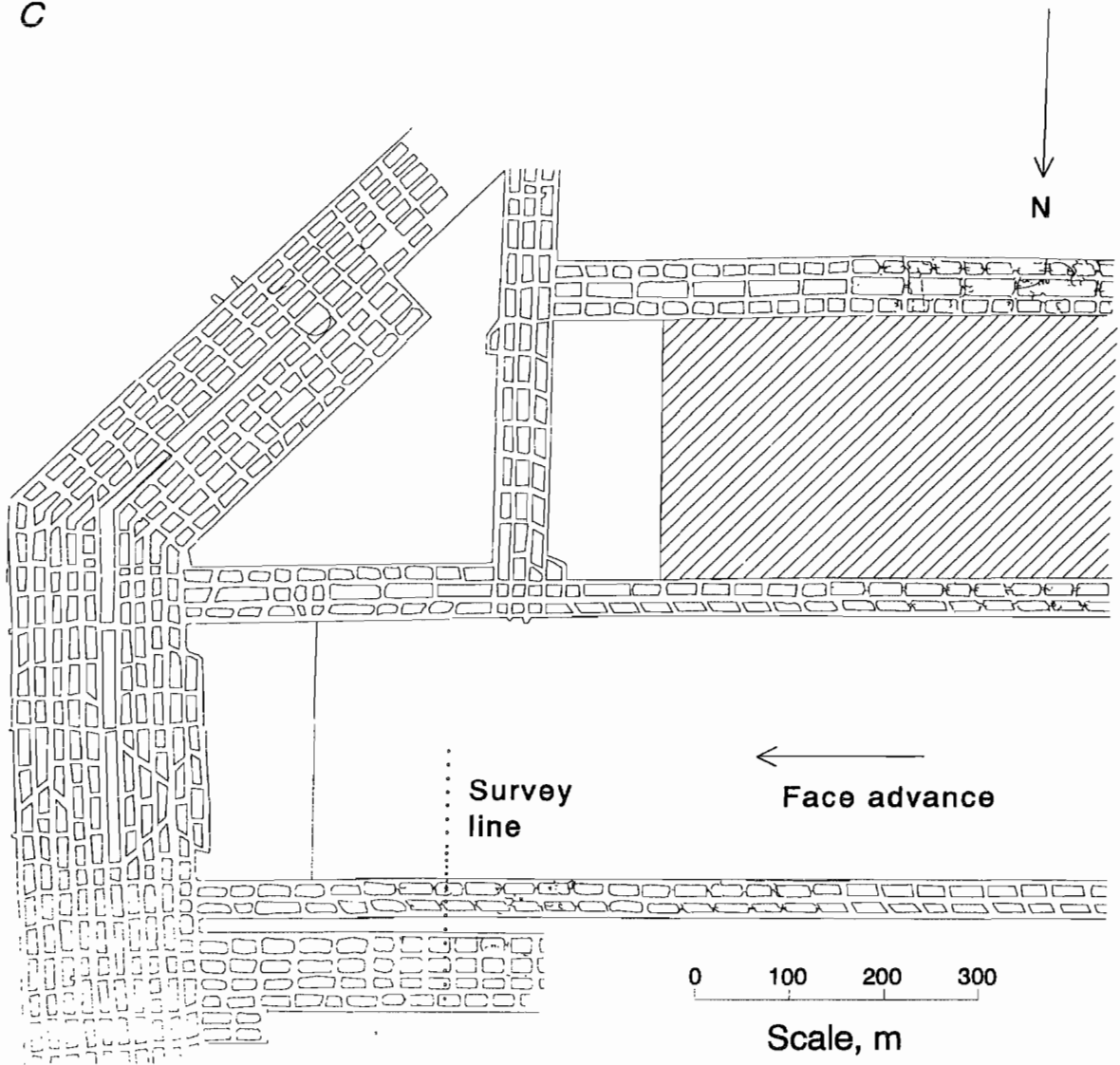
Figure A-5



Old Ben No. 24 Mine North Marcum site. A, Bending stiffness profile. B, TDR signatures.

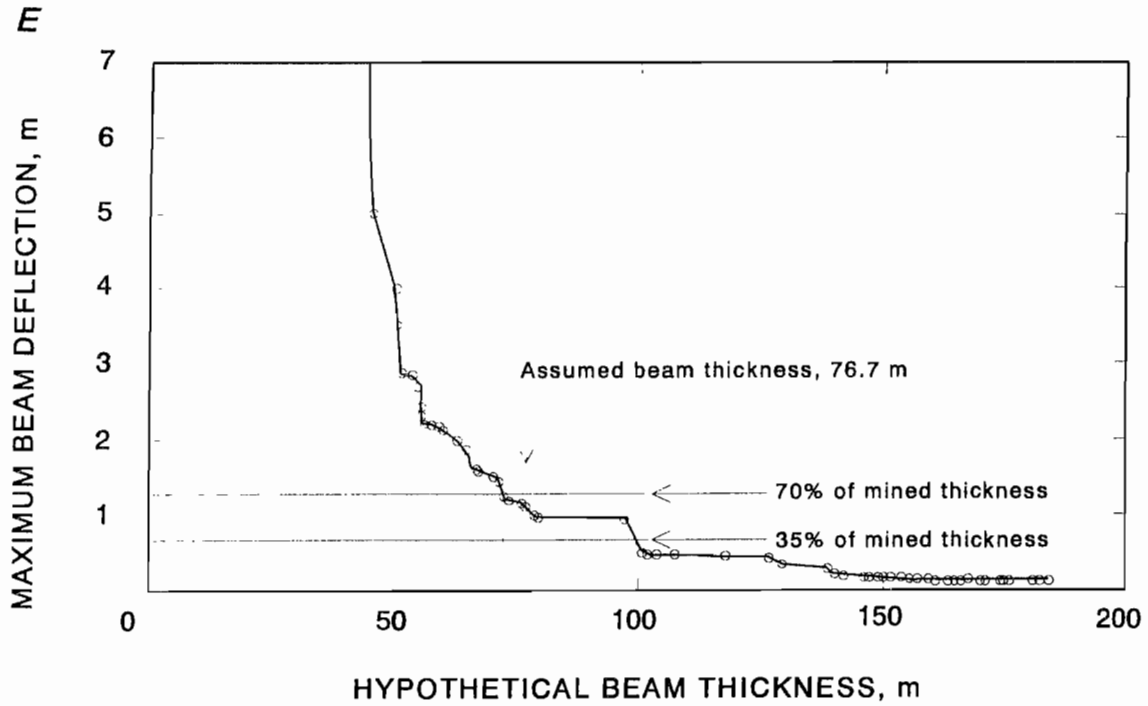
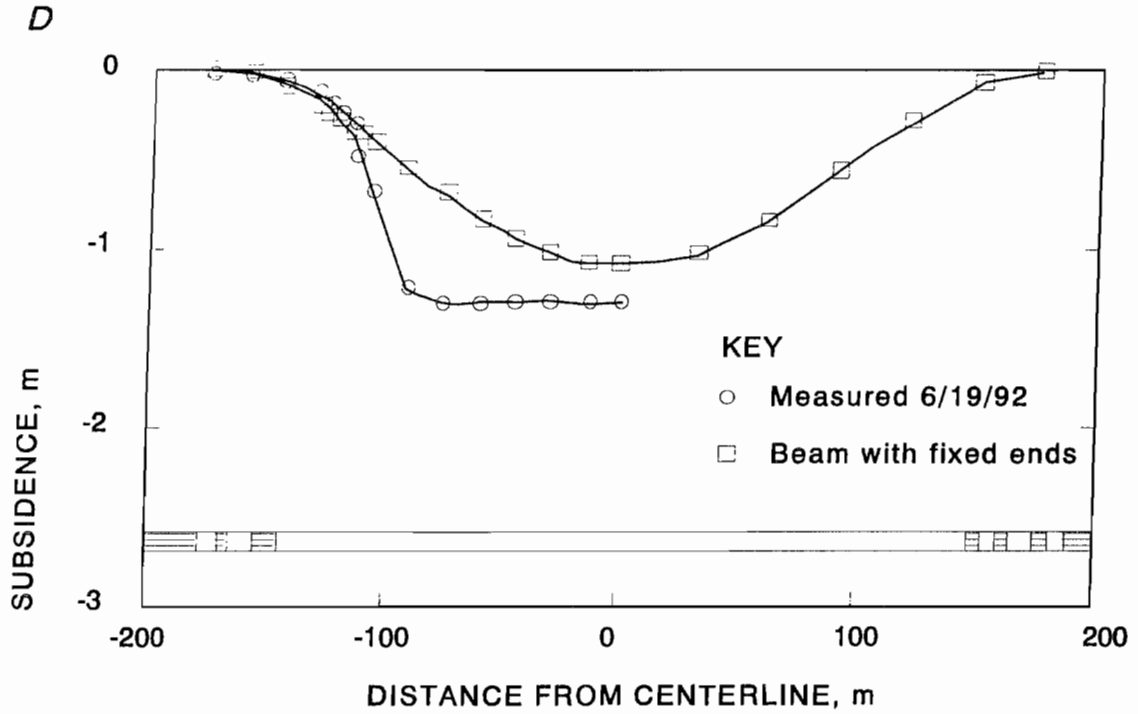
Figure A-5—Continued

C



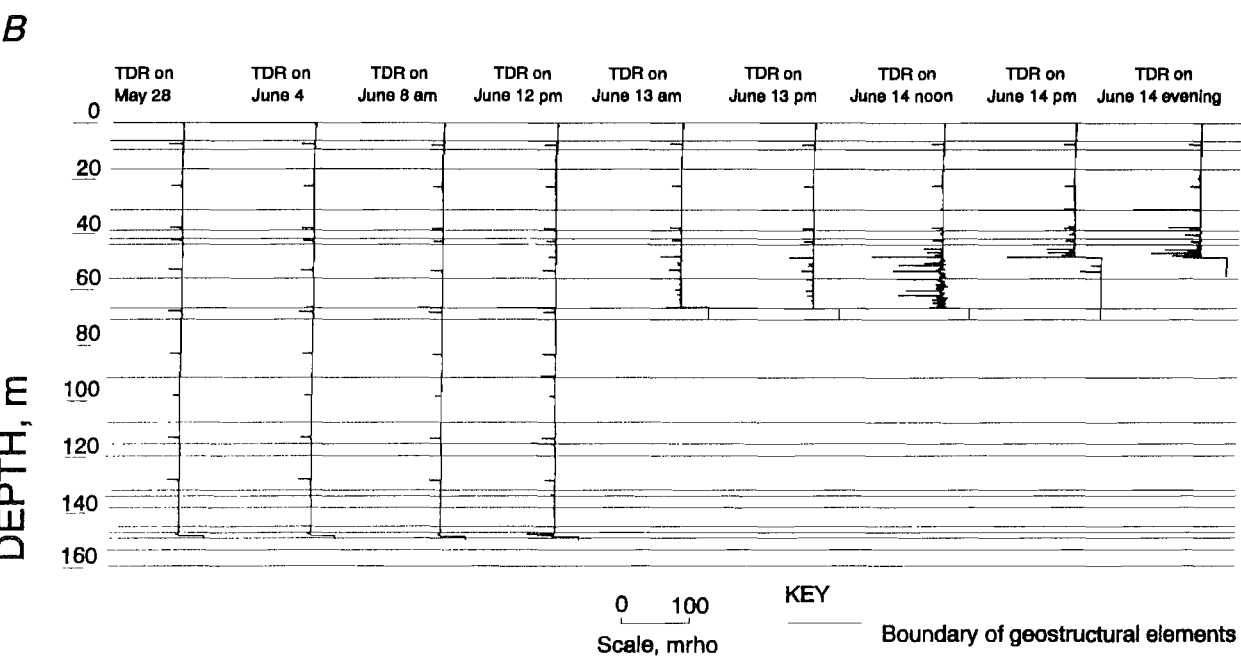
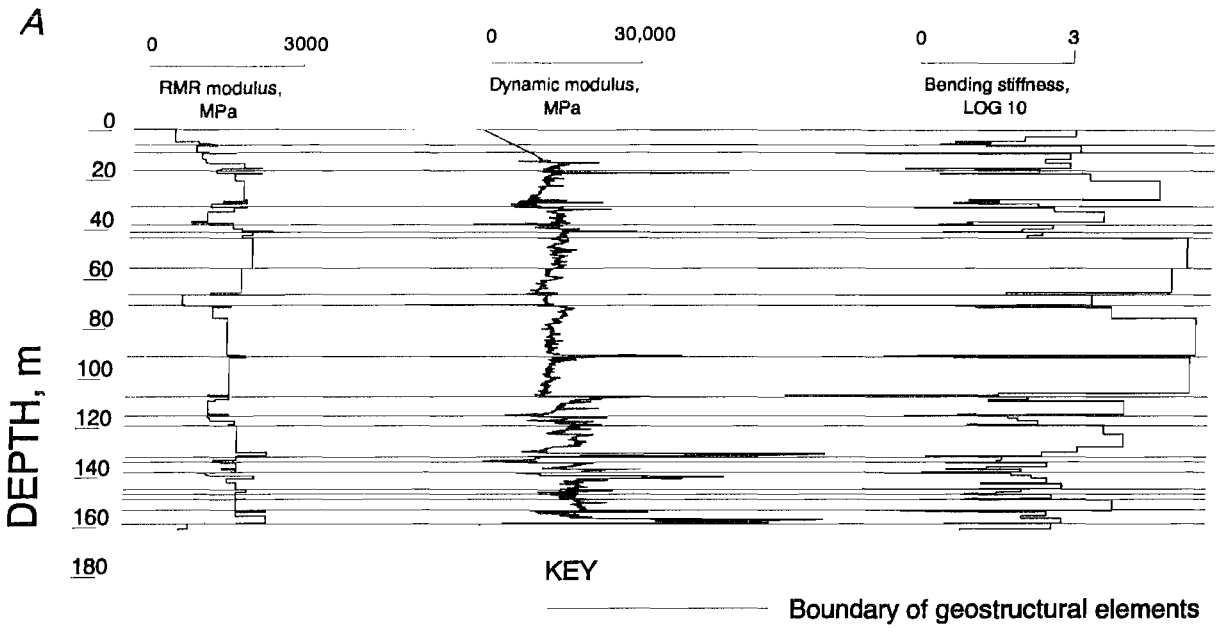
C, Mine map.

Figure A-5—Continued



D, Deflection profile. E, Beam thickness versus deflection.

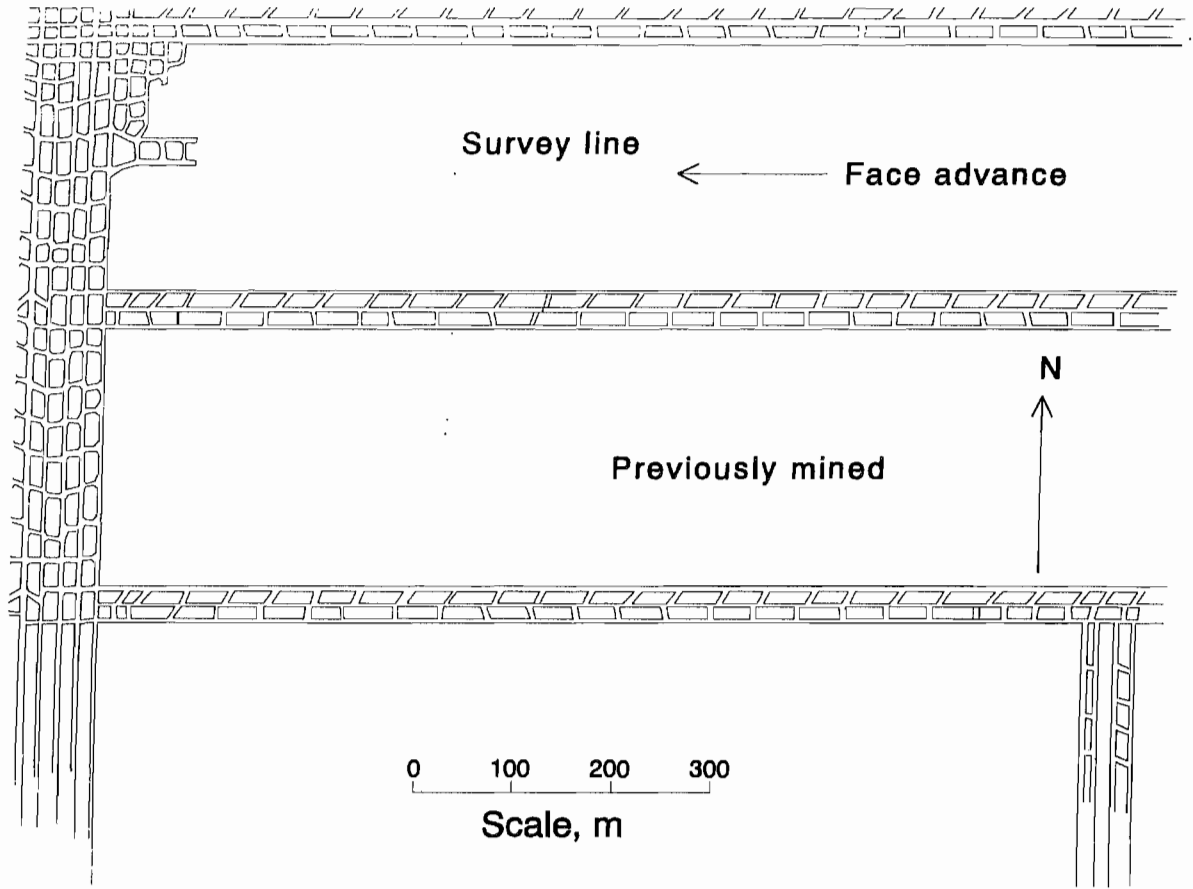
Figure A-6



Old Ben No. 25 Mine. A, Bending stiffness profile. B, TDR signature.

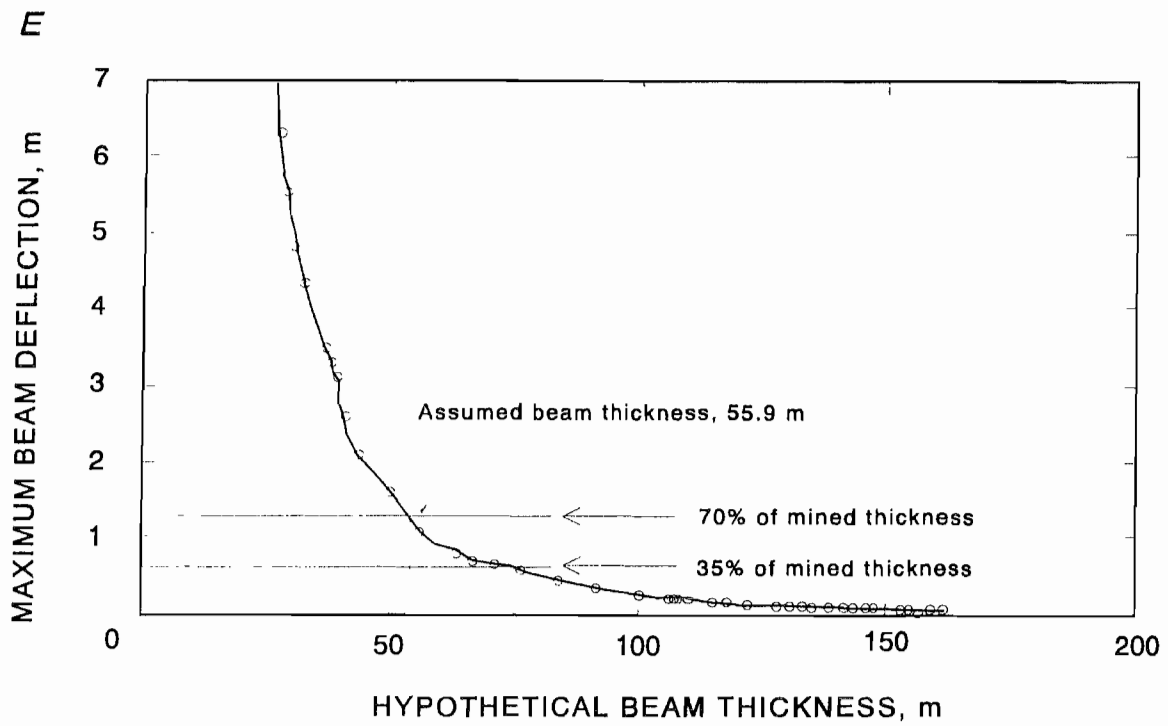
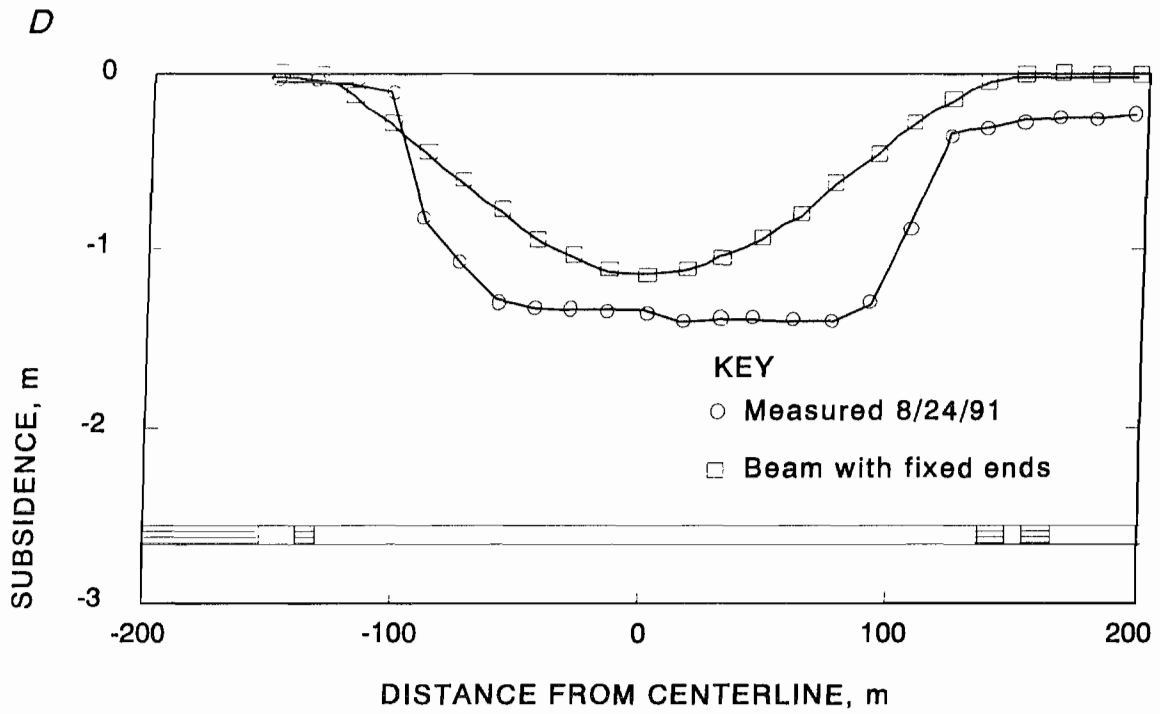
Figure A-6—Continued

C



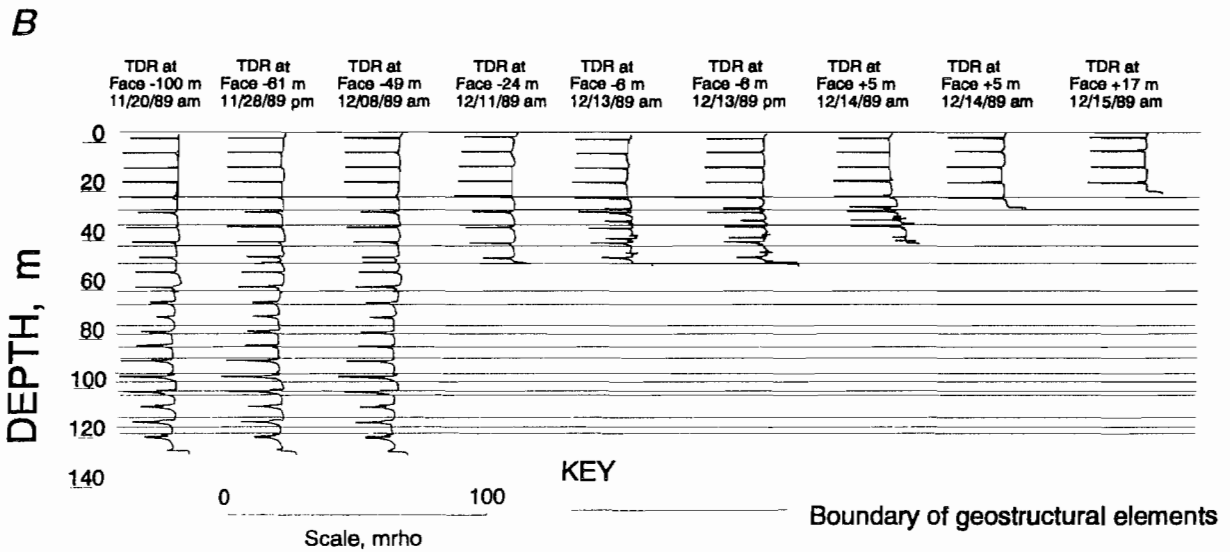
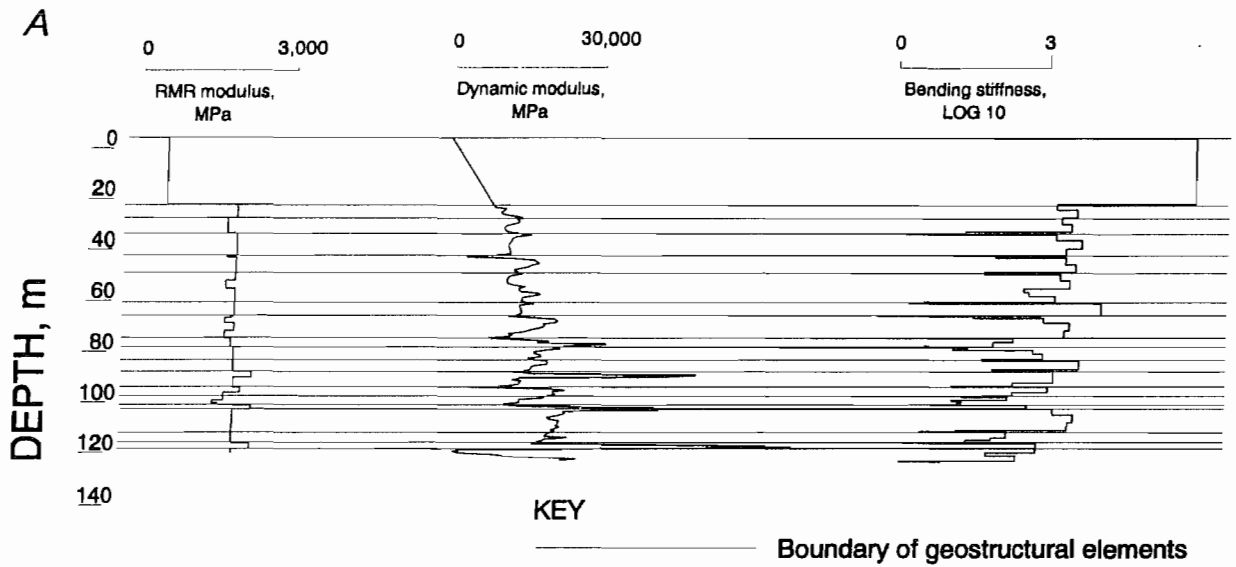
C, Mine map.

Figure A-6—Continued



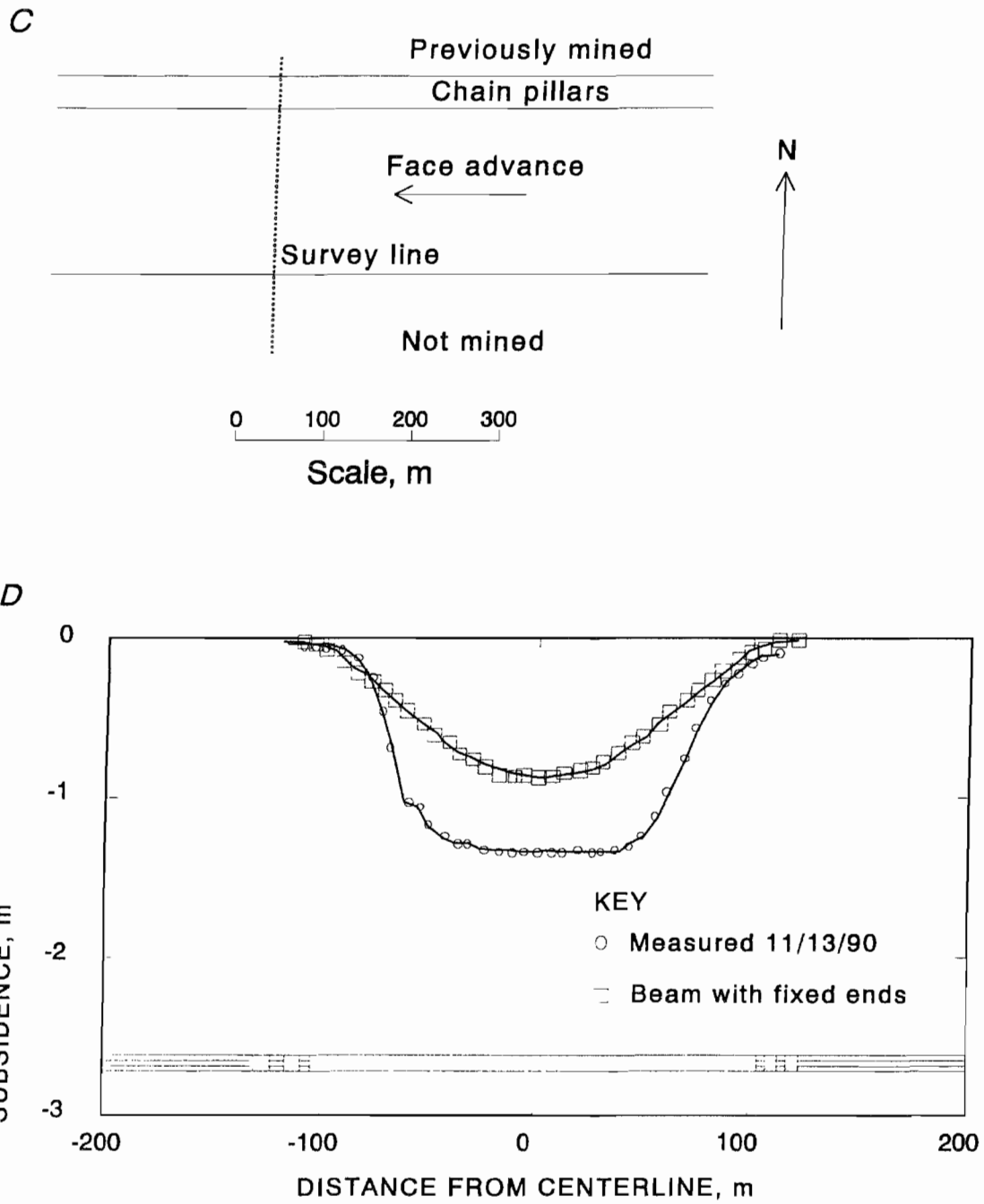
D, Deflection profile. E, Beam thickness versus deflection.

Figure A-7



Galatia Mine. A, Bending stiffness profile. B, TDR signature.

Figure A-7—Continued



C, Mine map. D, Deflection profile.

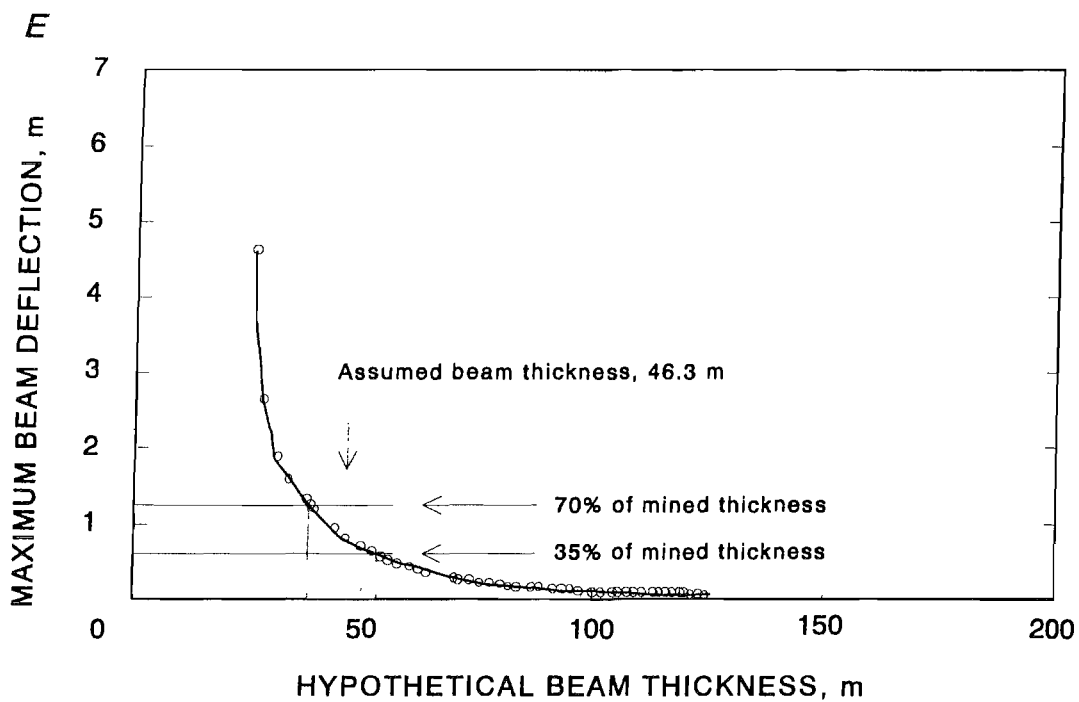
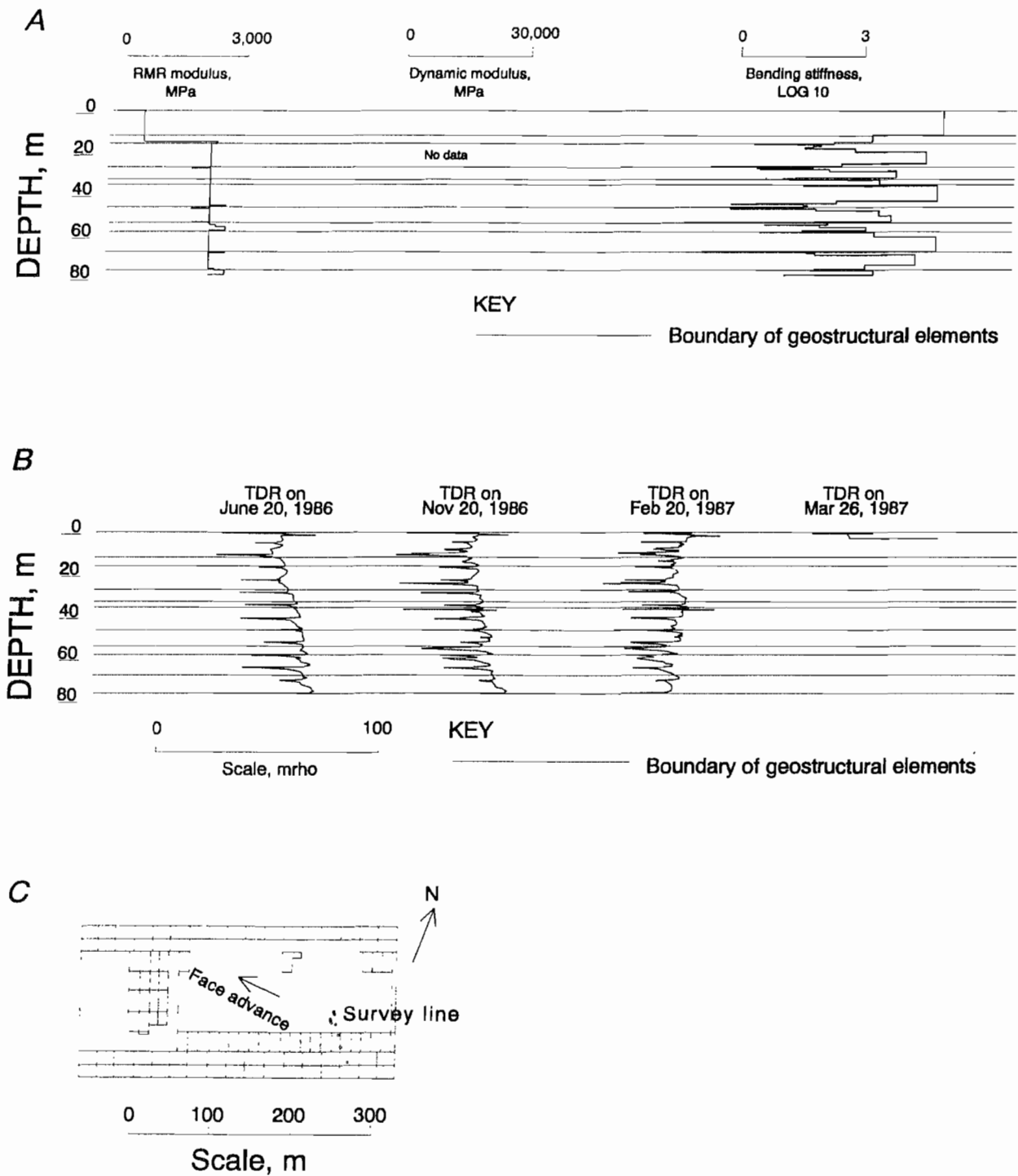
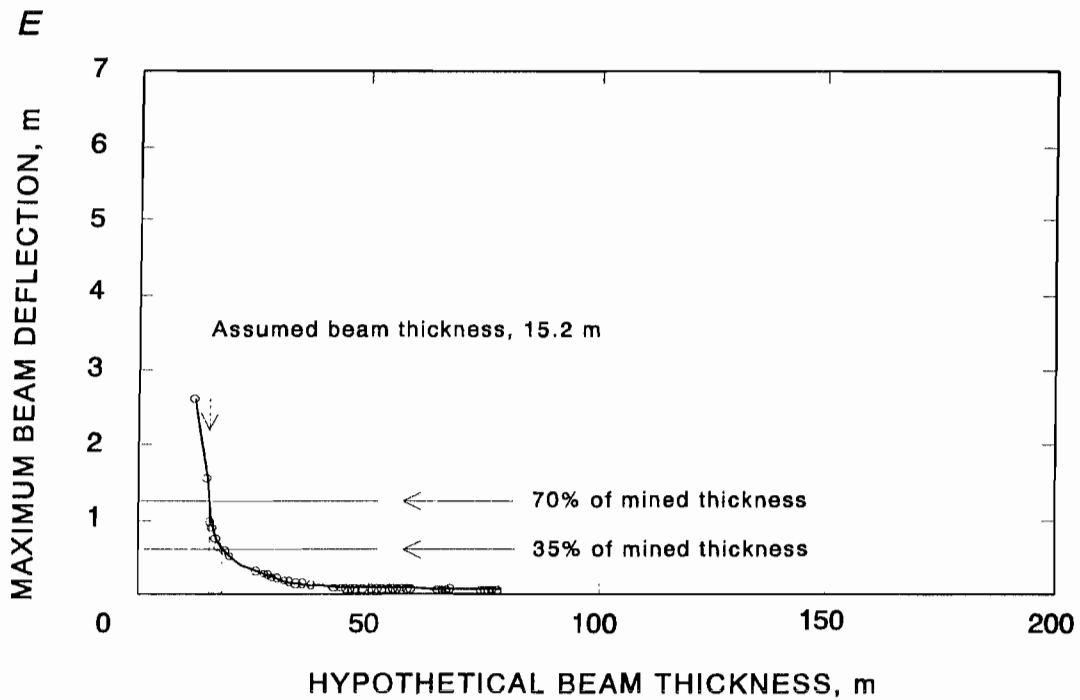
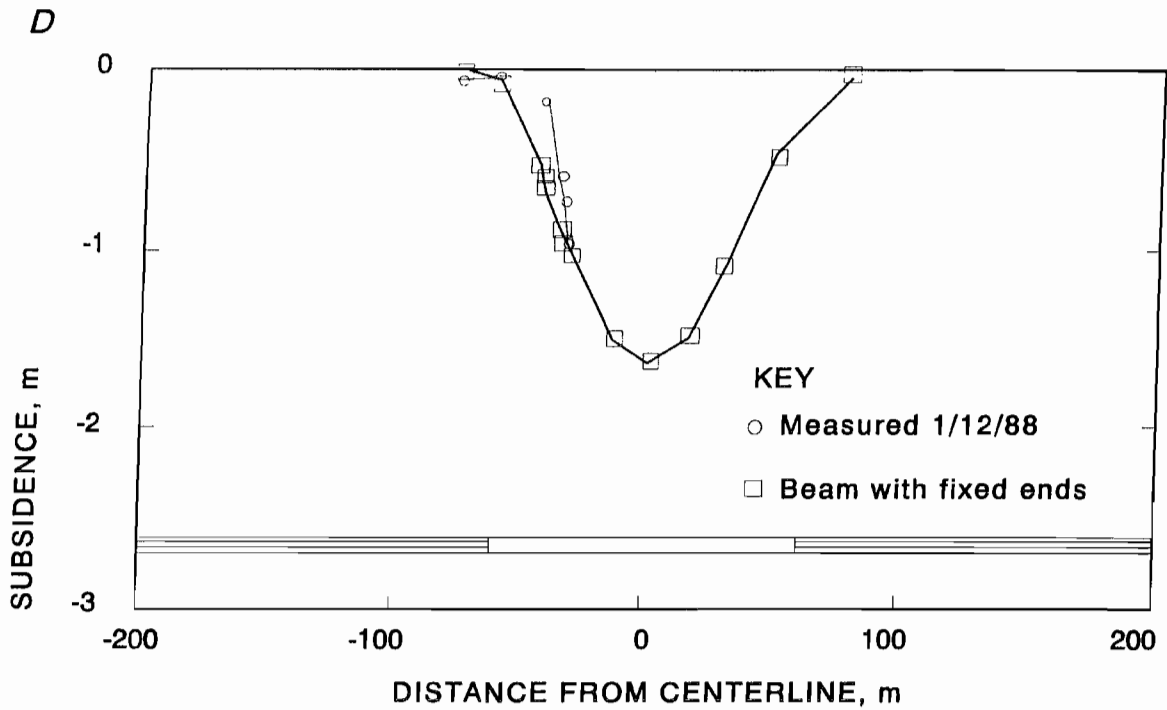
Figure A-7--Continued*E, Beam thickness versus deflection.*

Figure A-8



Freeman Orient Mine. A, Bending stiffness profile. B, TDR signatures. C, Mine map.

Figure A-8—Continued



D, Deflection profile. E, Beam thickness versus deflection.

APPENDIX B.—RATIONALE FOR UTILIZING A SIMPLE BEAM MODEL IN SPREADSHEET

The deflection of a laminated beam is computed in the spreadsheet using a simple beam model. Let us consider the validity of this model by comparing it with more general cases progressing from a simple beam supported only at its ends to an elastic beam supported by an elastic foundation. The objective is to consider the error introduced by ignoring support provided by underlying caved material.

SIMPLE BEAM WITH UNIFORM LOADING OVER ENTIRE SPAN

Consider a prismatic beam of rectangular cross section subjected to a uniform load (figure B-1A). The equation for deflection as position x of a beam pinned at both ends is (3)

$$\Delta(x) = \frac{-wx}{24EI} (L^3 - 2Lx^2 + x^3), \quad (\text{B-1})$$

and for a beam fixed at both ends (figure B-1B) the equation is

$$\Delta(x) = \frac{-wx^2}{24EI} (L - x)^2. \quad (\text{B-2})$$

For these two cases the maximum deflection occurs at midspan ($x = L/2$), so

$$\Delta_{\max} = \frac{-wL^4}{KEI}, \quad (\text{B-3})$$

where K is $384/5 = 77$ for a beam pinned at both ends and 384 for a beam fixed at both ends.

SIMPLE BEAM WITH UNIFORM LOADING OVER A PORTION OF ITS SPAN

Consider the possibility that only a portion of a near-surface laminated beam would have to support its weight. This would approximate the case in which a portion of the beam is supported by chain pillars along the edge of a high-extraction panel. This also approximates the intensity field proposed by Triplett and Yurchak (80).

When the beam is fixed at both ends it is necessary to determine the reaction forces and end moments (figure B-1C) as follows (31):

$$R1 = \frac{w}{4L^2} \left[12d^2 - 8 \left[\frac{d^3}{L} \right] + 2 \left[\frac{be^2}{L} \right] - \frac{e^3}{L} - e^2 \right], \quad (\text{B-4})$$

$$R2 = we - R1, \quad (\text{B-5})$$

$$M_1 = \frac{1}{24} \left[\frac{we}{L} \right] \left[24 \left[\frac{d^3}{L} \right] - 6 \left[\frac{be^2}{L} \right] + 3 \left[\frac{e^3}{L} \right] 11 + 4e^2 - 24d^2 \right], \quad (\text{B-6})$$

and

$$M2 = M1 - \frac{1}{24} \left[\frac{we}{L} \right] (2e^2 + 24d^2 - 24dL). \quad (\text{B-7})$$

The equation for deflection of a beam fixed at both ends is

$$\Delta_{AB11}(x) = \frac{-1}{6EI} (R1x^3 - 3M1x^2), \quad (\text{B-8})$$

$$\Delta_{BC}(x) = \frac{-1}{6EI} \left[R1x^3 - 3M1x^2 - \frac{we}{4} \left(\frac{x-a}{e} \right)^4 \right], \quad (\text{B-9})$$

and

$$\Delta_{CD}(x) = \frac{-1}{6EI} (R1(L-x)^3 - 3M2(L-x)^2). \quad (\text{B-10})$$

ELASTIC BEAM SUPPORTED ON WINKLER FOUNDATION

An analytical solution for the problem of an elastic beam supported on an elastic foundation (figure B-2) was developed by Hetényi (36) using series solutions. This technique is presented in Scott (64) using a slightly different approach and the original Winkler differential equation is satisfied by the analytical functions.

The strain energy for deflection of a prismatic beam of length L , width b , and height h is

$$U_{\text{beam}} = \frac{1}{2} \int_0^L \int_0^b \int_0^h \sigma_x \epsilon_x \, dx \, dy \, dz, \quad (\text{B-11})$$

so

$$U_{\text{beam}} = \frac{1}{2} \int_0^L \int_0^b \int_0^h \frac{1}{E} \left[\frac{My}{I} \right]^2 \, dx \, dy \, dz, \quad (\text{B-12})$$

which reduces to

$$U_{\text{beam}} = \frac{1}{2} \int_0^L EI \left[\frac{d^2 \Delta}{dx^2} \right]^2 dx \quad (\text{B-13})$$

where Δ is the vertical deflection of the beam, σ is stress, and ϵ is strain.

The strain energy for deflection of a subgrade, modeled as a series of springs, is

$$U_{\text{subgrade}} = \frac{1}{2} \int_0^L F \Delta dx, \quad (\text{B-14})$$

where F is the force required to compress a spring and is converted to displacement using the spring stiffness, k ,

$$U_{\text{subgrade}} = \frac{1}{2} \int_0^L k \Delta^2 dx. \quad (\text{B-15})$$

So, the total strain energy

$$U_V = U_{\text{beam}} + U_{\text{subgrade}} \quad (\text{B-16})$$

is

$$U_V = \frac{1}{2} \int_0^L EI \left[\frac{d^2 \Delta}{dx^2} \right]^2 dx + \frac{1}{2} \int_0^L k \Delta^2 dx. \quad (\text{B-17})$$

If a uniform load $w(x)$ is acting on the beam between the locations $x = a$ and $x = b$, the work done by the distributed load is

$$W = \int_a^b w(x) \Delta(x) dx. \quad (\text{B-18})$$

The expression for the potential energy of the entire beam will be formed from the difference between the stored strain energy and the external work done

$$\Pi = U_V - W, \quad (\text{B-19})$$

so

$$\begin{aligned} \Pi = & \frac{1}{2} \int_0^L EI \left[\frac{d^2 \Delta}{dx^2} \right]^2 dx + \frac{1}{2} \int_0^L k \Delta^2 dx \\ & - \int_a^b w(x) \Delta(x) dx. \end{aligned} \quad (\text{B-20})$$

The solution to the problem consists in finding an equation for the beam deflection, $\Delta(x)$, which minimizes the potential energy. Hetényi (36) proposed to represent the deflection by the series

$$\Delta(x) = \sum_{n=1}^{\infty} X_n(x), \quad (\text{B-21})$$

and to represent the X_n using the functions

$$\begin{aligned} X_n(x) = & C_{1n} \left[\cos r_n \frac{x}{L} + \cosh r_n \frac{x}{L} \right] \\ & + C_{2n} \left[\cos r_n \frac{x}{L} - \cosh r_n \frac{x}{L} \right] \\ & + C_{3n} \left[\sin r_n \frac{x}{L} + \sinh r_n \frac{x}{L} \right] \\ & + C_{4n} \left[\sin r_n \frac{x}{L} - \sinh r_n \frac{x}{L} \right]. \end{aligned} \quad (\text{B-22})$$

ELASTIC BEAM SUPPORTED ON ELASTIC FOUNDATION

Fekete (27) presents a technique and computer program for modeling an elastic beam supported on an elastic half-space rather than a series of springs. The foundation is characterized by an elastic modulus, E , and Poisson's ratio, ν .

Let $\Delta(r, z)$ be the deflection of a half-space caused by the concentrated force F acting at the surface (figure B-3A). If the deflections are integrated over the entire half-space and we assume that $\Delta(r, \infty) = 0$, then

$$\Delta_{\infty}(r, z) = \frac{1 - \nu^2}{\pi E} F \left[\frac{1}{L} + \frac{z^2}{2(1 - \nu)L^3} \right], \quad (\text{B-23})$$

and so the deflection at the surface is

$$\Delta_{\infty}(r, 0) = \frac{1 - \nu^2}{\pi E} \frac{F}{r}. \quad (\text{B-24})$$

The deflections occurring at great depth are negligible compared with those on the surface so it is sufficient to consider the deflection down to a given depth, the so-called limit depth, h_s . The deflection found by integrating to this depth is

$$\Delta_s(r) = \Delta_{\infty}(r, 0) - \Delta_{\infty}(r, h_s), \quad (\text{B-25})$$

so,

$$\Delta_s(r) = \frac{1-\nu^2}{\pi E} F \left[\frac{1}{r} - \frac{1}{r_L} - \frac{h_s^2}{2(1-\nu)r_L^3} \right] \quad (B-26)$$

Let us place a distributed load $w(x,y)$ on an elastic foundation over a surface area, Γ (figures B-3B,C). Based on the elastic half-space model, the deflection of point (x,y) can be given by the integral

$$\Delta_s(x,y) = - \int_{\Gamma} \int_{\Gamma} A_s(x,y,\xi,\eta) w(\xi,\eta) d\xi d\eta, \quad (B-27)$$

where

$$A_s(x,y,\xi,\eta) = \frac{1-\nu^2}{\pi E_s} \left[\frac{1}{r} - \frac{1}{r_L} - \frac{h_s^2}{2(1-\nu)r_L^3} \right], \quad (B-28)$$

$$r = \sqrt{(x-\xi)^2 + (y-\eta)^2}, \quad (B-29)$$

and

$$r_L = \sqrt{r^2 + h_s^2}. \quad (B-30)$$

In order to solve these equations numerically, Fekete (27) discretizes the beam into n even pieces and interprets the functions at the center of each piece by a staged function and the distributed loads as concentrated loads. This procedure is implemented in the Elastic Beam on Elastic Soil (EBESS) program.

COMPARISON OF BEAM DEFLECTION PROFILES

It should be apparent from the above discussion that as you progress from a model of a simple unsupported beam to an elastic beam supported by an elastic foundation, the complexity increases from a simple analytical expression with few variables to a complex expression that contains several poorly defined variables and must be solved numerically. The tradeoff is between reduced accuracy of the solution if a simple model is used and the need for more detailed information, which may be unavailable, if the more complex model is used. The former may be acceptable when the only objective is to provide an index of rock mass behavior.

To quantify the differences among the models, examples were used. The model parameter values are listed as follows:

Simple elastic beam, fixed both ends

Beam:

Length, L	500 m.
Width, b	1 m.
Thickness, t	78 m.
Moment of inertia, I	39,546 m ⁴ .
Bending stiffness, EI	5.90 × 10 ⁷ MPa·m ⁴ /m.

Load:

Unit weight, w	1.71 × 10 ⁶ (N/m)/m.
Full load example	Loaded entire span.
Partial load example	Loaded span 100 to 400 m from left end.

Elastic beam supported on Winkler foundation

Beam:

Length, L	500 m.
Width, b	1 m.
Thickness, t	78 m.
Moment of inertia, I	39,546 m ⁴ .
Bending stiffness, EI	5.90 × 10 ⁷ MPa·m ⁴ /m.

Foundation:

Spring stiffness constant, k	0.354 MN/m.
------------------------------------	-------------

Load:

Unit weight, w	1.71 × 10 ⁶ (N/m)/m.
Partial load	Loaded span 100 to 400 m from left end.

*Elastic beam on elastic foundation*Beam:

Length, L	500 m.
Width, b	1 m.
Thickness, t	78 m.
Moment of inertia, I_b	$39,546 \text{ m}^4$.
Modulus, E_b	$1.492 \times 10^3 \text{ MPa}$.
Bending stiffness, $E_b I_b$	$5.90 \times 10^7 \text{ MPa}\cdot\text{m}^4/\text{m}$.

Foundation:

Modulus, E_s	$1.0 \times 10^7 \text{ MPa}$.
Poisson's ratio, ν	0.3.
Limit depth, h_s	500 m (numerical convenience).

Load:

Divide beam into 20 segments.

Segment length = $500 \text{ m} / 20 = 25 \text{ m}$.

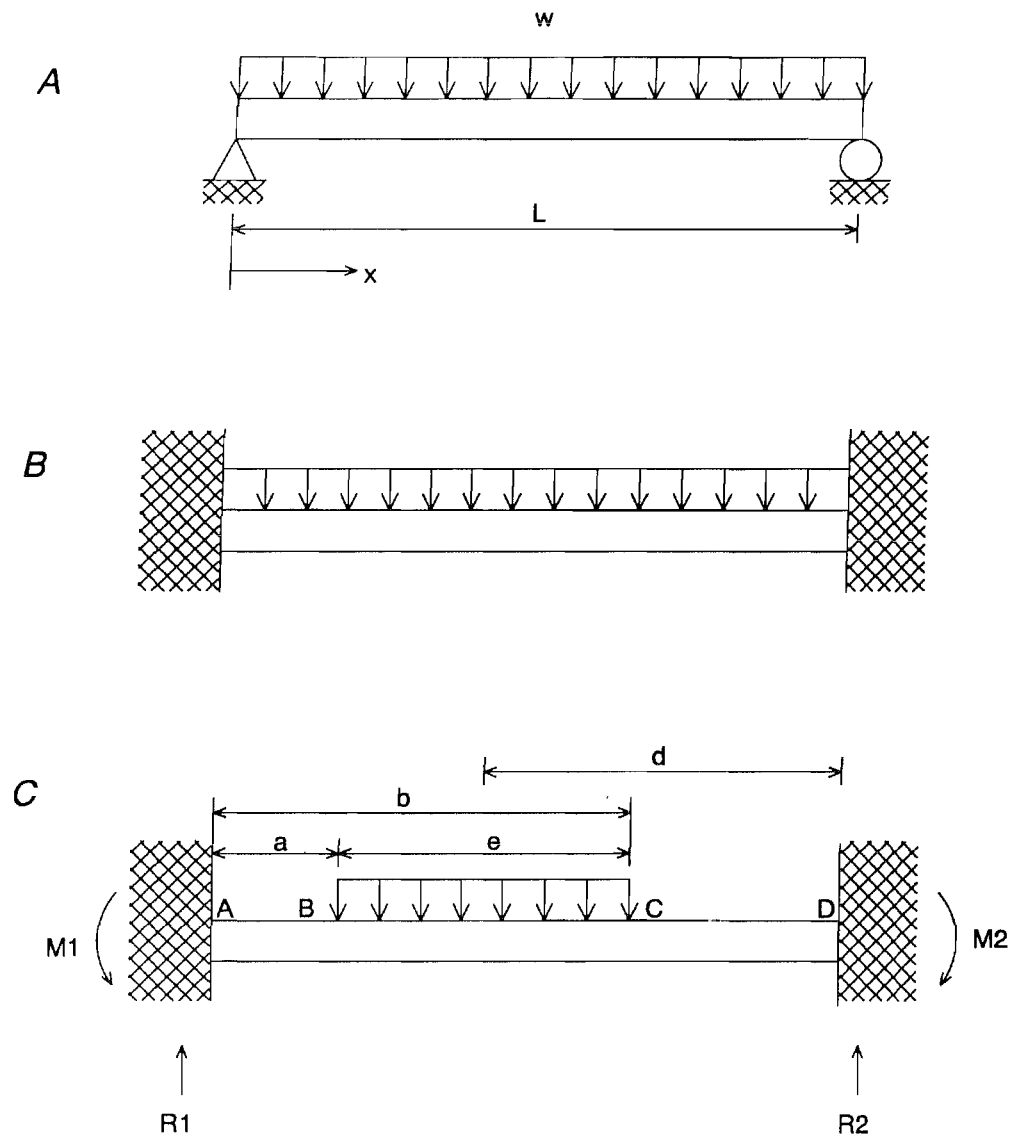
Concentrated force applied to segments 5 through 16.

Load per segment, $F = (1.71 \times 10^6 \text{ MN/m})(25 \text{ m}) = 4.28 \times 10^7 \text{ N}$.

Support stiffness values for the Winkler foundation and elastic foundation were selected so that the maximum deflection would be in the range of 3.5 to 4.5 m (figure B-4). Consequently, the magnitude of deflection is not pertinent since support stiffness can be changed to get any desired value (this is not true for the beam stiffness, which was computed using the spreadsheet macro). This is also the approach commonly adopted in finite-element modeling of subsidence (69, 72). A major justification for using the simple beam model in the spreadsheet is the feature of not needing to input a support stiffness.

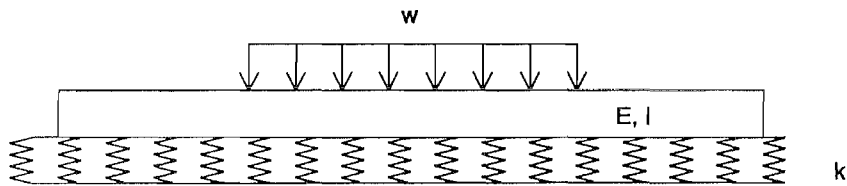
The most obvious difference in deflection profiles (figure B-4) is at the end points. End point deflection for the beams on Winkler and elastic foundations is approximately 25% of the maximum deflection. This type of end deflection is important for high-extraction mining when considering subsidence over chain pillars. However, the objective of the spreadsheet is to provide a simple index of the rock mass properties and the influence of a variable mine configuration.

Figure B-1



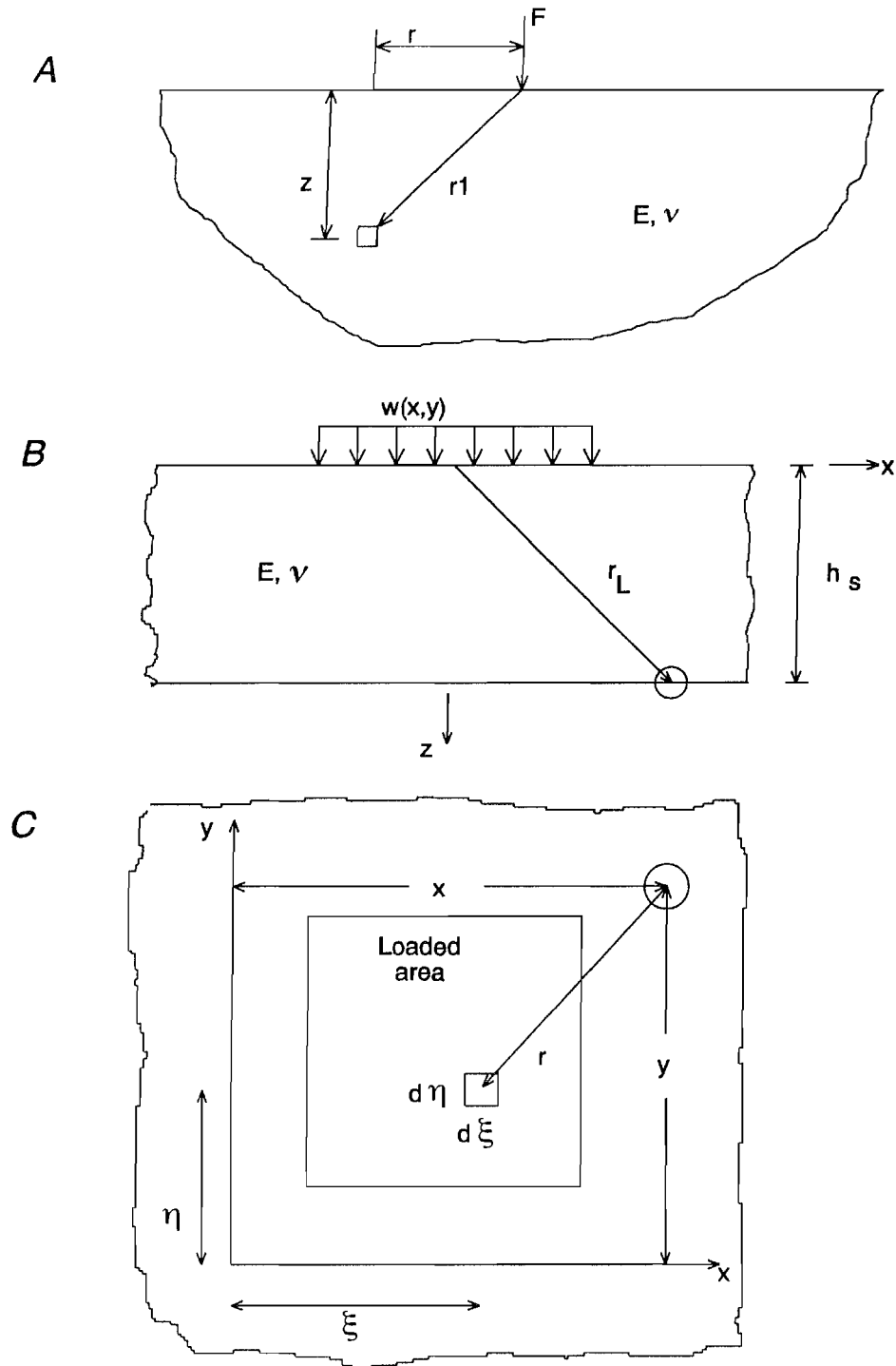
Elastic beam with (A) uniform load and pinned ends; (B) uniform load and fixed ends; (C) partial load and fixed ends.

Figure B-2



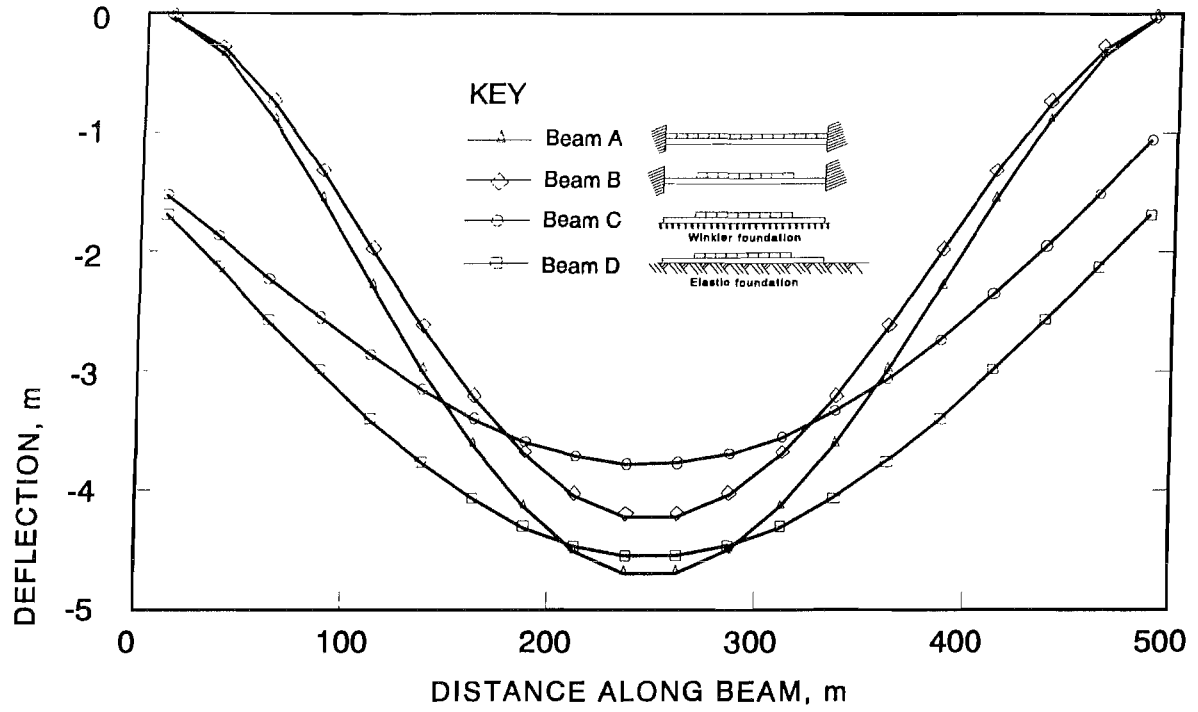
Elastic beam on Winkler foundation.

Figure B-3



Elastic half-space. A, Profile view of concentrated force. B, Profile view of distributed load. C, Plan view of distributed load.

Figure B-4



Comparison of beam deflection profiles.

APPENDIX C.—SYMBOLS USED IN THE REPORT

b	width of beam, m
d	distance from the neutral axis to the midpoint of the lithologic bed, m
E	deformation modulus of the lithologic bed, MPa
E*	deformation modulus of the transformed section, MPa
EI	bending stiffness of the lithologic bed, MPa·m ⁴
E*I*	bending stiffness of the transformed section, MPa·m ⁴
F	force to compress a spring, N
g	gravitational acceleration, m/s ²
h	height or depth, m
I	moment of inertia of the lithologic bed, m ⁴
I*	moment of inertia of the transformed section, m ⁴
K	constant determined from end conditions
k	spring stiffness constant, N/m
L	effective span of the transformed section, m; length of beam
M	bending moment at end of elastic beam, MN·m
n	number of lithologic beds in the transformed section
na	neutral axis
R	reaction at end of elastic beam, N
r	distance from location of applied force to location for which deflection is desired, m
t	thickness of the lithologic bed or beam, m
U	strain energy, N·m
W	work done, N·m
w	weight per unit width of the transformed section, N/m
x	distance from left end of beam, m
y	distance from midpoint of lithologic bed to top of transformed section, m
y*	distance from neutral axis of transformed section to top of transformed section, m
Γ	surface area over which a distributed band is applied, m ²
Δ	deflection, m
ε	strain, m/m
η	distance along y-axis from origin to subelement of area Γ, m
ν	Poisson's ratio
ξ	distance along x-axis from origin to subelement of area Γ, m
ρ	mass density of the lithologic bed, kg/m ³
σ	stress, MPa